Power Loss Estimation of PV Modules Through IV-characteristics and Image Analysis

Modelling uniform and partial snow cover situations using an IV-curve based model, in combination with an image analysis method to estimate power losses due to snow.

ØYVIND BJØRGUM

SUPERVISOR

Anne Gerd Imenes
Mari Øgaard

University of Agder, 2022

Faculty of Engineering and Science

Power loss estimation of PV modules through IV-characteristics
and image analysis

Abstract

In this thesis a methodology utilizing IV-characteristics and image analysis to model power losses due to snow cover is presented. The objective of this dissertation is to investigate the performance of PV modules under different snow cover conditions by simulating and analyzing IV-curves. Additionally, investigating if image analysis could be useful in estimating snow cover, and could improve the modelled IV-curve power loss estimations. An IV-characteristics model in MATLAB Simulink was used to model situations with uniform and partial snow cover for different irradiance and snow depth conditions. The image analysis method was used to estimate PV module snow cover and used in combination with the IV-curve model to improve power loss estimations. It was concluded that the IV-curve model proved capable of estimating power losses due to uniform snow covers, but less effective in some partial snow cover situations. Including image analysis improved the power loss estimations in some cases, however, to improve the model accuracy additional factors must be included. The numerous model uncertainties that were identified has a certain impact on the model accuracy which should be investigated further. For further research it is recommended that the model is developed further to include and account for significant snow characteristics.

Preface

Background and motivation

I am a 28-year-old male from Valle municipality in Setesdal, Norway. I have formerly obtained a bachelor's degree in Renewable Energy, Engineering from the Norwegian University of Science and Technology, and a MSc in Renewable Energy and Environmental Modelling from the University of Dundee, Scotland. My inspiration for writing this dissertation was to investigate further the effects snow has on PV modules and their IV-characteristics, which is a probable challenge to encounter as PV technology develops further and becomes more widespread throughout the world.

The intended target group of this thesis is people wanting to get a better understanding of some of the challenges PV systems has related to snowfall, and how significant the negative consequences can be.

Acknowledgements

I would like to express my gratitude to my supervisor, Anne Gerd Imenes for supplying me with data required to perform simulations, educational discussions, and providing continuous and constructive feedback through regular meetings. Additionally, my sincere thanks to my co-supervisor Mari Øgaard at IFE for helpful guidance, providing relevant literature, and for putting me in contact with one of her colleagues at IFE. Thanks to Bjørn Aarseth at IFE for his helpfulness and recommendations related to the modelling of IV-characteristics.

Individual/group Mandatory Declaration

The individual student or group of students is responsible for the use of legal tools, guidelines for using these and rules on source usage. The statement will make the students aware of their responsibilities and the consequences of cheating. Missing statement does not release students from their responsibility.

1.	I/We hereby declare that my/our report is my/our own work and that I/We have not used any other sources or have received any other help than mentioned in the thesis.	☒
2.	I/we further declare that this thesis: - has not been used for another exam at another department/university/university college in Norway or abroad; - does not refer to the work of others without it being stated; - does not refer to own previous work without it being stated; - have all the references given in the literature list; - is not a copy, duplicate or copy of another's work or manuscript.	☒
3.	I/we am/are aware that violation of the above is regarded as cheating and may result in cancellation of exams and exclusion from universities and colleges in Norway, see Universitets- og høgskoleloven §§4-7 og 4-8 og Forskrift om eksamen §§ 31.	☒
4.	I/we am/are aware that all submitted theses may be checked for plagiarism.	☒
5.	I/we am/are aware that the University of Agder will deal with all cases where there is suspicion of cheating according to the university's guidelines for dealing with cases of cheating.	☒
6.	I/we have incorporated the rules and guidelines in the use of sources and references on the library's web pages.	☒

Publishing Agreement

Authorization for electronic publishing of the thesis.

Author(s) have copyrights of the thesis. This means, among other things, the exclusive right to make the work available to the general public (Åndsverkloven. §2).

All theses that fulfill the criteria will be registered and published in Brage Aura and on UiA's web pages with author's approval.

Theses that are not public or are confidential will not be published.

I hereby give the University of Agder a free right to

make the task available for electronic publishing: ☒JA ☐NEI

Is the thesis confidential? ☐JA ☒NEI

 (confidential agreement must be completed and signed by the Head of the Department)

   - If yes:

Can the thesis be published when the confidentiality period is over? ☐JA ☐NEI

Is the task except for public disclosure? ☐JA ☐NEI

(contains confidential information. see Offl. §13/Fvl. §13)

Publishing Agreement

Table of Contents

List of Figures

List of Tables

Nomenclature

Abbreviations

c-Si	Crystalline Silicon
DC	Direct Current
HSV	Hue Saturated Value
IPT	Image Processing Toolbox
IRA	Image Region Analyser
IRT	Infrared Thermography
IS	Image Segmentation
I-V	Current - Voltage
MMP	Maximum Power Point
pc-Si/mc-Si	Poly/multicrystalline Silicon
PV	(Solar) Photovoltaic
P-V	Power - Voltage
RMS	Root Mean Square
STC	Standard Test Conditions
TMY	Typical Meteorological Year
UiA	University of Agder
UV	Ultraviolet

Constants

k	Boltzmann Constant	$1.3805*10^{-23}$ J/K
q	Electron Charge	$1.609*10^{-19}$ C
$\mathbf{T_{C,STC}}$	Cell Temperature at STC	25°C

Parameters

$\mathbf{I_D}$	Diode Current	I
$\mathbf{AM_{STC}}$	Air Mass at STC	1.5
DHI	Diffuse Horizontal Irradiance	W/m^2
DNI	Direct Normal Irradiance	W/m^2
GHI	Global Horizontal Irradiance	W/m^2
$\mathbf{G_{STC}}$	Irradiance at STC	1000 W/m^2
GVI	Global Vertical Irradiance	W/m^2

I	Current	I
I_0	Dark Saturation Current	I
I_{MP}	Current at Maximum Power Point	I
I_P	Shunt Current	I
I_{PH}	Photocurrent	I
I_{SC}	Short-Circuit Current	I
n	Ideality factor	
P	Power	W
P_{MPP}	Maximum Power Point	W
R_{IR}	Internal Resistance	Ω
R_S	Series Resistance	Ω
R_{SH}	Shunt Resistance	Ω
T	Absolute Temperature	K
TGI	Tilted Global Irradiance	W/m^2
V_F	Forward Voltage	V
V_{MP}	Voltage at Maximum Power Point	V
V_{OC}	Open-Circuit Voltage	V
V_T	Thermal Voltage	V
α	Temperature Coefficient of Current	%/K
β	Temperature Coefficient of Voltage	%/K

1. Introduction

This master's thesis is written as part of the master's degree in Renewable Energy at the University of Agder. It aims to investigate the impact different types of snow cover has on the power output of a PV module and its IV-curve, which is accomplished by modelling IV-characteristics and using an image analysis method.

This dissertation is a further work for ENE503 Energy Research Project "The Effects of Snow on IV-curves and PV Module Performance" [1] written by the author. The research question proposed in this thesis can be seen as a continuation of the work conducted in ENE503.

1.1 Background

The use of photovoltaic (PV) systems has become increasingly more popular in the last decades with a strong focus on utilizing renewable energy sources that eventually can replace conventional energy sources and end the age of oil. Along with other renewable energy sources the price of PV panels has seen a significant price drop, which has resulted in a rapid growth of the PV installations worldwide.

As electricity production from PV systems are dependent on the available solar resources in a particular area they are normally found in areas with favourable solar conditions. For instance, countries located closer to the equator have some of the best solar resources in the world, at least in terms of high solar irradiance. However, there are also other factors that impact PV system performance, such as temperature, among other things [2, 3]. Globally, the installed PV capacity has seen substantial growth, which is expected to increase by 17% annually and reach 200 GW of new installed capacity in 2026. Utility-scale solar PV installations are responsible for 60% of new renewable energy capacity and is the cheapest form of adding new electricity generation capacity [4]. Furthermore, in Europe, Germany in particular is responsible for spearheading the development of solar PV in the 2000s, and in 2020 the total installed capacity reached 54 GW_P [5].

For a country located in the northern hemisphere like Norway, precipitation in the form of snow is not uncommon to encounter. Operating PV systems in colder climates does have a positive impact on energy production, on the other hand should snow cover the panels, the power output is reduced substantially [6]. Therefore, it is beneficial that PV installations in areas with a high probability of snowfall implement measures that can help minimize the power losses [6].

There are studies and research papers that have investigated the effects of snow on PV system performance, although it is not a widely researched area [7-11]. Additionally, it is not easy to create models that can accurately predict the output from a PV system affected by snow

cover. Snowfall events have proven to be challenging to identify in power generation datasets since it is difficult to distinguish the effects of snowfall from PV faults [12]. Moreover, snow on PV modules is rarely measured, likely due to the complex behavior of snow which is challenging to model.

In this thesis the effects of snow on PV module performance are going to be investigated through the modelling and measurement of IV-characteristics, and image analysis. Previously recorded IV-curves are used to validate the modelling results. The modelled and measured results will then be used to assess the impact of snow cover on PV module output and the losses associated with it. This is for a fixed system with PV modules installed in a rack on the UiA roof with a 45° tilt angle facing south. However, the methodology presented is thought to be applicable for a wider range of PV system configurations and locations. This is primarily because the results, for instance how snow cover impacts IV-curves, is assumed to be applicable to other PV systems.

Additionally, as there is a considerable number of images of the PV modules available, an image analysis will be conducted to get a better understanding of how power losses are affected by the actual PV module area covered by snow. This is to be done through automatic detection of individual PV modules from images, followed by the detection of snow on the module surface. Similarly, to the modelling of IV-curves the objective here is also to use this to estimate the power losses from PV modules associated with snow cover.

Consequently, the thesis sets out to investigate how snow affects IV-curves and PV module performance and uses the modelling of IV-curves to estimate power loss caused by different types of snow cover. In addition, an image analysis methodology is introduced to investigate if it could contribute to more accurate power loss estimations.

To make accurate snow loss predictions, we need to understand the effect of snow on PV modules, which is challenging since predicting the behaviour of snow is complicated. Furthermore, more irregular weather events are likely to occur frequently in the future as a direct result of global warming [13]. As a result, increasing the necessity for reliable snow loss models. Several different snow loss models have been proposed in the existing literature based on various input parameters [9-11]. The results proved to be inconsistent with some models showing unreasonably low estimated losses [8].

1.2 Thesis structure and scope

The main work in form of the methodology, results, discussion, and conclusion are new, while the following sections: chapter 1, parts of subchapter 1.1, parts of chapter 3, chapter 4, subchapter 4.1, and parts of subchapters 4.2-4.5, is based on work conducted in the ENE503 Energy Research Project course taken in 2021 at UiA. Parts of sections written in this thesis is taken from the report "The Effects of Snow on IV-curves and PV Module Performance" written by the author [1].

First, this thesis presents a brief introduction to PV and how the performance is related to irradiance, temperature, and meteorological factors, such as snow. A brief overview of existing research on areas related to PV systems with regards to snow is presented, and possible research gaps are identified. Furthermore, the type of data available from UiA PV system is also presented. Then the thesis subject and research questions that the thesis attempts to answer are presented along with methods that will be used to accomplish this. Secondly, a literature review on PV systems and the effects of shading, challenges with snow cover, module orientation, mechanical loads and snow, IV-curve simulations, and snow loss models is presented.

Thirdly, a theory part is included to provide some background information relevant to the project. It includes an explanation of the PV module structure, IV-curves, effects of temperature, shading and bypass diodes, and the electrical circuit diagram for a solar cell. Moreover, the methodology chapter explains the goal and scope of the thesis and introduces the UiA PV research system, along with the necessary correction factors due to the system design. The datasheet values for each relevant PV module used throughout the thesis is also included here. Then the IV-characteristics model in MATLAB Simulink used to perform IV-curve simulations is explained and validated to assess its accuracy. Based on this model the methods for simulating cases with uniform and partial snow cover is introduced, along with an investigation of the correlation between irradiance and snow depth. Lastly, the image analysis methodology is explained.

The results chapter shows the modelling results of the IV-curves for different irradiance, module temperatures, and snow depths for uniform and partial snow cover. In addition, to the IV-curves simulated using the results from the image analysis. The next chapter includes discussion about things and factors impacting the results, such as irradiance and temperature measurements. Besides talk about the inclination angle, comparing modelled and recorded IV-curves, and discussing the relationship between P_{MPP} (maximum power point) reduction and snow depth. Finally, a conclusion is drawn based on the work conducted throughout the thesis, together with the findings from the results and discussion chapters. A recommendation for further work is also included, along with the used references.

The scope of this thesis is limited by the available data from the UiA PV system, which does not include any data related to transmittance, although this is an important factor when trying to model snow cover. Furthermore, in the available data there is a limited number of dates where PV modules have snow cover, which reduces the availability of situations to analyse.

The dissertation utilizes a wide range of sources, such as PV textbooks and online resources, research articles from various journals, and published reports.

2. Research Question

The purpose of this master's thesis is to investigate how precipitation in the form of snow, and accumulation of snow on PV modules would impact their performance and how this can be estimated from modeling and imaging tools. This is assessed by doing power loss estimations of different PV modules that are part of the UiA PV research system. More specifically, the research question is investigated through modelled and measured of IV-characteristics, and image analysis using the historical data available from the PV system. Based on this, the thesis aims to answer the following research questions:

1. How does different degrees of snow cover affect the performance of PV modules and their IV-characteristics?
2. Is it possible to accurately predict power losses associated with a specific snow cover on a PV module through the modelling of IV-curves?
3. Can image analysis be used to quantify the uniform/partial snow cover on the surface of PV modules, and can this in combination with the modelling of IV-curves improve the estimation of power losses?

To answer these research questions the following methods are used:

1. Analysis of measured data from the UiA PV research system and modelling of IV-characteristics.
2. An image analysis is conducted by implementing simple MATLAB code to process raw images of the PV modules and using the tools available in the Image Processing Toolbox in MATLAB to identify partial snow cover.

3. Literature Review

The purpose of a PV system is to generate electricity and although this is achieved most of the time it is inevitable that faults and problems can curtail this production. There are several things that can cause power losses, for instance, faults such as hot spots created because of shaded or damaged cells [14]. Furthermore, current mismatching will reduce power output and can lead to the development of hot spots. This can occur if the manufactured solar cells have different characteristics [15]. Problems with shading are usually due to trees or objects covering parts of a module, however snow build-up on PV modules will have the same negative effect [16].

There are several research papers that consider the effects of snow on PV systems. Because the effects of snow are like that of shading, they are often compared. We often distinguish between two different types of shading, soft and hard shading. Soft shading is typically caused by distant obstacles, such as clouds. This type of shading is normally considered to be uniform, meaning it is distributed equally throughout the entire module area and will therefore not result in local hot spots. It results in lower irradiance and lower power output, and is also

uncontrollable [14]. On the other hand, there is hard shading or partial shading which is often caused by physical objects blocking the irradiance on parts of a module. Shading caused by trees, bird droppings, dirt, antennas, etc. are some examples of hard shading [14]. Hard shading can produce hot spots and have drastic effects on the power output of a PV system [17, 18].

The power losses caused by snow is strongly dependent on the climatical conditions at the location and the PV system design [6]. For instance, one study by Powers et al. [10] conducted in Truckee, California, tried to estimate the power losses caused by snow throughout the winter. They concluded that for different module tilt angles of 0°, 24°, and 39°, the estimated annual power output losses were 18%, 15%, 12%, respectively. The location received on average amounts of precipitation, which is around 500 cm of snow annually, although in this case it was slightly below the average of 500 cm [10]. Another study done by Becker et al. [19] investigated the effects of snow on a 1 MW_p grid connected PV system (28° tilt) in Munich, Germany. For a five-year period, their results showed annual losses of 0.3-2.7% during the winter months. However, the number of days with snow covering PV modules was only 5-17 days each year, with snow heights of 40 cm and 20 cm in January and March, respectively [19]. Hence, the much lower power loss reported by [19] could be due to much less snow compared to [10].

A study published by Marion et al. [9] compared measured and modelled energy losses for several PV systems in Colorado and Wisconsin. These systems were modelled for a duration of two-years. In some cases, measurements showed that monthly losses due to snow reached as high as 90%, although annually they varied between 1-12% with average annual snowfalls of 137 cm and 98 cm for Colorado and Wisconsin, respectively. They also suggest a snow loss model with promising results for long term modelling. The model results deviated less than 2% from the measured losses, although short term modelled losses were less accurate and could deviate by over 10% [9]. Summing up these studies, annual losses are highly dependent on which type of climate the PV systems are found in, and the accuracy of the snow loss model being used determines the correlation between measured and modelled energy losses.

The accumulation of snow greatly impacts the total power production. A large portion of the incoming solar radiation is reflected because of the high reflective properties (albedo) of snow [8, 11]. However, even a small layer of snow accumulated on a PV module surface can have significant negative effects on the power production. For instance, a study published by Perovich [20] investigated the effects of reflection and transmission of light by snow. They found that for thin layers of snow, the albedo is heavily reliant on snow depth. For example, a snow depth of only 5 cm resulted in an albedo equal to 0.9, meaning there is very little transmittance through the snow layer as most of it gets reflected. Furthermore, a snow cover of 10 cm only allowed less than 5% and 1%, of visible and near-infrared transmittance, respectively [20].

Moreover, the type of snow is also an important factor, which can influence the transmittance and the shedding time of snow on a PV module surface [7, 12]. One of the advantages of PV modules is that they require little maintenance, compared to other ways of generating electricity, which typically involves many moving parts. However, heavy loads of densely packed snow, can, if left unattended, cause structural damage to the modules themselves [7, 21]. In addition, if snow is allowed to freeze on the surface, removing it can be difficult without causing damage [22]. Different types of coatings (hydrophobic) have been developed to enhance the surface to make water droplets slide off. Icephobic coatings that prevent or halt the creation of ice are also being researched [7]. Another solution to reduce snow build-up is to run a current through the modules to effectively melt the snow. The Norwegian company Innos have created a system able to do this, named "Weight watchers", which depends on a certain snow weight limit to start snow melting [23, 24].

The orientation of PV modules should be taken into consideration when trying to minimize power losses from potential snow build-up. Portrait and landscape orientation meaning that the long side of the module is facing east-west and north-south, respectively. Several studies have looked at how module orientation can impact power losses, both regarding natural removal of snow, but also systems with active snow removal features [25]. Different types of orientation on the modules will also have an impact on power losses. Especially, if the module contains bypass diodes that are series connected, and with strings of series connected cells parallel to the long side of the module [7]. Articles published by Andenæs et al. [7] and Andrews et al. [8] argue that power losses due to snow cover will be higher for modules with portrait orientation compared to landscape orientation [7, 8]. However, another study found that modules installed in portrait orientation resulted in quicker module snow clearing [26].

In general, due to gravity it is obvious that a greater module tilt angle can allow for better sliding conditions and potentially reduce the build-up of snow. However, this also depends on the climatic conditions. For example, in colder climates snow is less likely to melt and slide off the modules [8]. In a research article published by Jelle [25], snow was observed on modules installed at tilt angles of 70° degrees without sliding, even under cold climatic conditions [25]. These conditions should be considered in design of the system, when increasing the module angle is expected to provide better snow clearing abilities, although sacrificing some power output. Building integrated photovoltaics (BIPV) mounted on building facades can be beneficial in areas with frequent snowfall. The increase in albedo because of snow around a PV system can result in higher yields, especially for systems with high tilt angles [8].

A challenge with snowfall is that from power generation datasets it is not easily detectable and separated from what could be common PV faults. A study by Øgaard et al. [12] stated that production data recorded for modules with complete snow cover resembled that of a damaged inverter. The modelling of PV systems that utilize statistical models or machine learning algorithms can result in lower accuracy when parts of a training data set include snow events, unless thousands of snow events exist in the data, which the model is trained to recognize

[27]. However, a paper published by Schill et al. [28] concluded that the effects of soiling were clearly mirrored in the form of the IV-curves, but challenging to differentiate from a PV fault. In this case soil had accumulated at the bottom of modules that were mounted in portrait orientation. Schill et al. [28] observed similar results on IV-curves for modules with partial snow cover located in the alpine region.

In literature there are several articles that consider the power output losses related to snow cover on PV modules, but different methods are used for this estimation. Creating accurate snow loss models is essential to properly predict PV system yields, especially as weather patterns are likely to get more sporadic because of climate change [13]. However, creating accurate models is a challenge, particularly considering the complexities of snow and its behavior. The performance of different snow loss models varies greatly. For instance, one study by Andrews et al. [8] found the snow loss estimates to be unrealistically low.

Furthermore, in the article by Andrews et al. [8] a model was created that considered different PV module types at various fixed angles. The short-circuit current (I_{sc}) and back temperature were monitored, where I_{sc} was used to determine the performance because of its close correlation with irradiance and as temperature has relatively small impacts on I_{sc}. To have a basis of comparison it is necessary to establish a baseline for the performance of the PV system. The predicted and actual values were then to be compared to give an idea of how snowfall would impact the output. The I_{sc} was predicted based on meteorological data [11]. To account for snow clearance from PV modules a filtering algorithm was implemented.

Additionally, images of the modules were also taken frequently to identify accumulation and clearing of snow [8]. Results showed that snow shedding is hard to predict from meteorological data, and that with an increase in module angle snow losses were reduced because of better snow shedding. Overall, the predicted loss was lower than the actual loss.

The study from Truckee, California published by Powers et al. [10] considered an empirical model based on meteorological data from The National Renewable Energy Laboratory (NREL) using the 30-year TMY (typical meteorological year) database. This included daily data for snow depths and number of days since last snowfall, but also hourly solar and weather data [29]. Based on these datasets an analytical model was created, which estimated annual snow losses to 2-5%. Furthermore, a generalized relationship between module tilt angle, snowfall, and losses was observed. A simple relationship of annual % snow losses was presented and is given by multiplying a factor of 0.1 with snowfall (inches) and $\cos^2$(tilt angle). It proved to be satisfactory, however, there was an RMS (root-mean-square) error margin of +/- 2%. Moreover, the relationship only proved to be decent for tilt angles below 45 degrees [10].

Moreover, a study published by Marion et al. [9] developed a model that utilized a combination of several meteorological variables. This includes the daily snow depths to recognize fresh snow, predicting the occurrence of snow sliding by using a relationship

between hourly global horizontal irradiance (GHI) and air temperature, predicting the snow sliding length by using the array tilt angle, and the degree of energy output losses related to array snow coverage. The snow losses were determined by using the measured daily electrical energy generated and subtracting it from an estimated value for each day. The electrical energy generated without snow was estimated based on an equation that considers module DC (direct-current) power, performance ratio, temperature effects and irradiance. In general, the model performed well. Modelled annual energy losses were within 0.5% and 1.5% of measured losses for the non-residential and residential systems, respectively. The residential systems had a module tilt angle of 18.4° and 22.5°, while the non-residential systems had a module tilt angle of 15°, 26°, 30°, and 35°. Nonetheless, for shorter time periods (months) a larger difference between modelled and measured annual energy loss was observed. It was concluded that additional studies could help improve the model, particularly studies related to temperature and snow loads, but also a wider range of PV systems setups [9].

One study by Øgaard et al. [12] compared four different snow loss models utilizing five years of PV system data from an installation Norway. Three of these models utilize empirical relationships in combination with several meteorological factors, these are the models used by Andrews et al. [11], Powers et al. [10], and Townsend et al. [30], while the last model by Marion et al. [9] estimates snow losses based on a snow cover estimate. The results showed variable performance of the models. Overall, the completely empirical models performed the worst, which are models where PV system and weather data is used directly to approximate power loss. On the other hand, the Marion snow loss model, which relied on empirical correlations, proved more flexible and performed better. This model had separated different consequences resulting in snow clearing/coverage and modelled them separately. The improved Marion model proposed in this paper resulted in more accurate modelled snow losses and the authors suggest that it could potentially be used to separate snow loss events from other events impacting PV production, such as faults [12]. Further testing of the model is still necessary, so a possibility to improve this model could be done by comparing it to a model using a combination of IV-curves and images to verify its accuracy.

Besides these models there are also alternative methodologies proposed in other studies that involve utilizing MATLAB Simulink to model IV-curves to estimate power losses related to snow or shading [12, 31, 32]. For example, a study published by Øgaard et al. [12] compared the actual recorded PV data with modelled data that were to represent no snow conditions. The model of the IV-curves was based on the single diode model [33], which is an electrical circuit representation of a solar cell. The results showed similar trends in voltage, current and power losses, although the measured current losses take longer to reach a steady level compared to the simulated values, as the snow cover gradually decreases. An explanation for this trend is thought to be related to the uneven distribution of snow coverage and thickness on the PV module surface that occurs during snow melting [12]. However, although the study did model IV-curves it did not compare them with actual IV-curves recorded under snow conditions in real-time. Therefore, it will be beneficial to model IV-curves based on the

specifications in the module datasheet and compare these results with actual IV-curves recorded for modules under partial and total snow cover.

Furthermore, another study by Aarseth et al. [34] utilized IV-curves to simulate defective PV modules and compared them to infrared thermography (IRT). Based on the IRT images, the IV-curves of defective modules are modelled and compared to field IV measurements of the same modules. As a result, power losses related to different module defects could be identified [34]. Other studies have used the modelling of IV-curves to investigate the effects of shading, for which the IV-curve has similar characteristics to snow coverage. For instance, Bazzi et al. [32] proposed a new method for detecting P_{MPP} under partial shading conditions. Results showed that the proposed model is capable of simulating IV-curves that match the experimental results from real PV modules. However, for two different modules under partial shading conditions the P_{MPP} values did include an error margin between 5-7% and 11-13%, respectively [32]. This shows that it can be difficult to accurately model IV-curves under partial shading conditions.

Several studies have looked at alternative ways of estimating power losses associated with snow cover on PV module area [6-9, 11, 12, 35]. In a study by Andrews et al. [8] image analysis was used to identify snow on the PV module surface by analyzing time series of images to determine where snow typically accumulated over time. Furthermore, in a study by Braid et al. [35] images were used to determine snow shedding rates from the PV modules. In addition, performance metrics, such as, start/finish show shedding, power production start time, and timeslot for 90% power production were also identified. None of these studies utilize image analysis single handedly to estimate power loss due to snow cover, but both studies use it as part of a more comprehensive methodology. This type of image analysis is an effective way to identify the behavior of snow on PV module surfaces, however beyond that there are some limitations.

4. Theory

4.1 Solar module structure

Photovoltaics cells, or commonly known as solar cells, utilize the photovoltaic effect to convert the energy in sunlight directly into electrical energy. The cells are typically made from crystalline silicon (c-Si), either mono or poly/multi-Si (pc-Si/mc-Si) [36, 37]. Several solar cells are mounted together in a framework to create a module. The PV module is built up in a sandwich structure which includes different layers, each with their own purpose. This structure is illustrated in Figure 4.1. The solar cell layer is in the middle, enclosed by a layer of special plastic on each side. This encapsulant's function is to prevent moisture and soil from entering, which can reduce panel lifetime and performance. The front of the solar module is enclosed in a glass sheet which protects it from the elements [38]. The glass typically has an anti-reflection layer on the backside, which minimizes reflection losses and

improves transmittance. An aluminium frame is used to protect the edges and improve the overall structural integrity. The back sheet consists of different layers designed to withstand UV radiation over time, humidity, mechanical load and provide insulation (electric) [39]. The electrical conductors from each solar cell string are interconnected in the junction box, together with bypass diodes, see Figure 4.8. The junction box is mounted on the back sheet and must be weather-resistant [40].
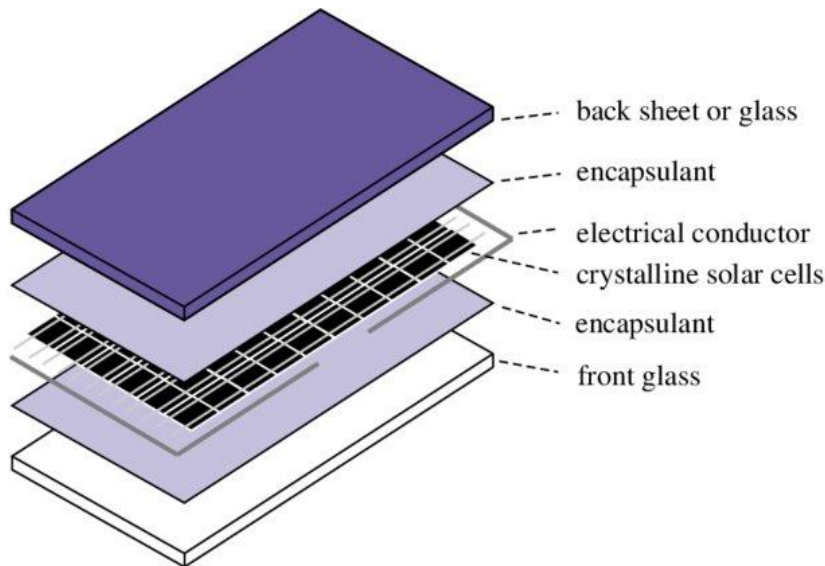
Figure 4.1 – Structure of a typical solar module. Source: [41].

The performance of PV modules is typically tested under standard test conditions (STC), which is the industry standard that ensures equal and fair comparison between different solar PV modules. It is specified with a cell temperature of 25°C, irradiance of 1000 W/m^2, and air mass 1.5 (AM1.5) [42].

4.2 Solar cell IV-characteristics

The IV-characteristics of a solar cell is based on the principle of a photodiode, a component that changes properties when illuminated [16]. The current passing through this diode is represented by the equation known as the ideal diode law equation, given as a function of voltage [43]. The expression is given in Equation (1),

$$I = I_0 \left[\exp\left(\frac{qV}{kT}\right) - 1 \right] \tag{1}$$

where I_0 is the dark saturation current, k is the Boltzmann constant, q is the electron charge value, V is the voltage, and T is the absolute temperature (K).

When the solar cell is illuminated it shifts the IV-curve from the first quadrant down into the fourth quadrant to allow for the extraction of power [44]. Figure 4.2 shows a simplified equivalent circuit diagram of a solar cell. In addition, Figure 4.2 illustrates how the IV-curve is shifted from the first quadrant down into the fourth quadrant as the light intensity increases.
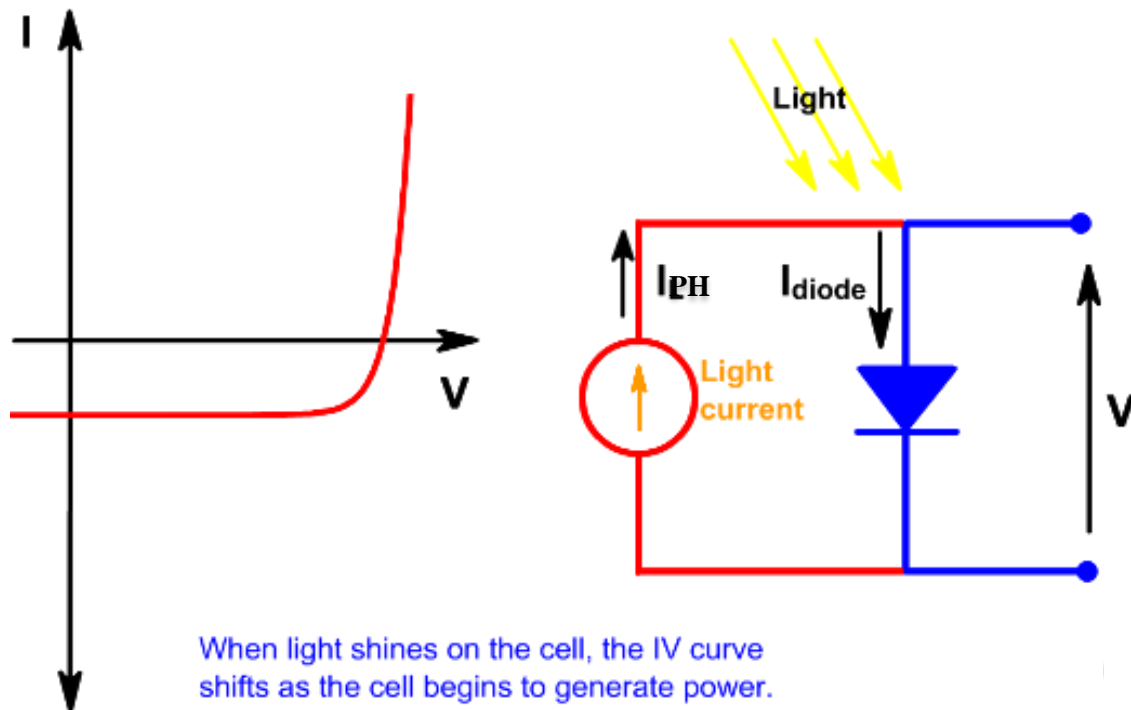
Figure 4.2 – Illustration of how the intensity of light affects and shifts the IV-characteristics, and a simplified equivalent circuit diagram of a solar cell. Source: PVEducation [44].

The equation for the IV-characteristics in the first quadrant is given by the following expression in Equation (*2*):

$$I = I_{PH} - I_0[\exp\left(\frac{qV}{nkT}\right) - 1]$$

(2)

Where I_{PH} is the light generated current and n is the ideality factor.

Usually, the -1 term in Equation (*2*) is neglected as the exponential expression often is much larger than 1, however this is not the case at low voltages. Under illumination the I_{PH} term is superior to the I_0 term making it negligible [44].

By rearranging Equation (*2*) an expression can be found for the voltage in terms of current, shown in Equation (*3*):

$$V = \frac{nkT}{q} \ln\left(\frac{I_{PH} - I}{I_0} + 1\right)$$

(3)

Figure 4.3 shows an example of an IV-characteristics of a single solar cell for different irradiance levels, and that I_{SC} is proportional to the irradiance.
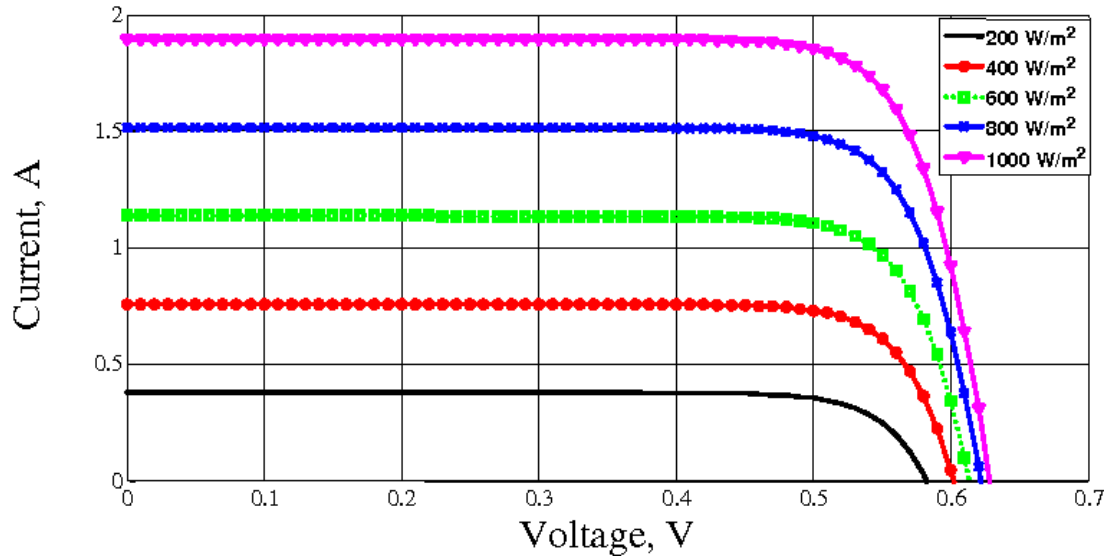
Figure 4.3 – Example of an IV-characteristics of a single solar cell at different irradiance levels and 25°C. Source: [45].

Figure 4.4 shows a typical IV-curve and power curve for a solar cell. The short circuit current (I_{SC}) and open-circuit voltage (V_{OC}) can be determined from IV-curve, they are denoted by green points on the y-axis and x-axis, respectively. The maximum voltage point (V_{MPP}) and maximum current point (I_{MPP}) are also marked on the IV-curve. The electrical power equation states that current multiplied with voltage equals power. The product of V_{MPP} and I_{MPP}, the maximum power point (P_{MPP}), can be seen on the blue line graph, which represents the power curve [44].
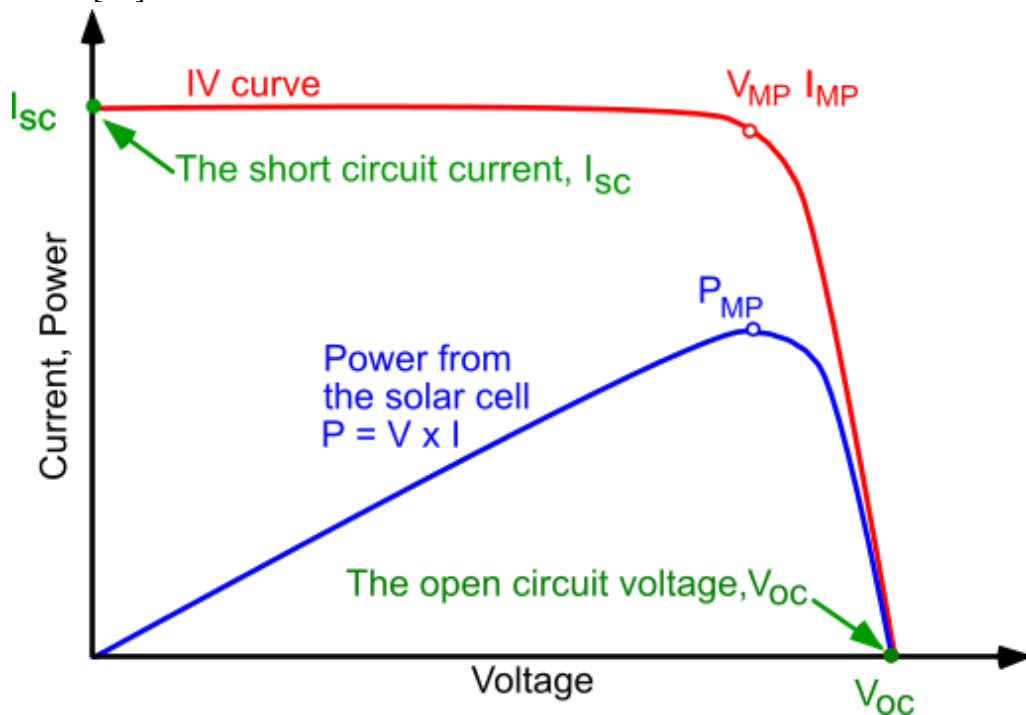
Figure 4.4 – Current/Power vs Voltage curve for a solar cell. Maximum power point denoted as P_{MP}. Source: [44].

4.3 Solar cell standard equivalent circuit diagram

The solar cell is often represented by a circuit diagram, more specifically called the standard model or single-diode model. This is because the IV-characteristics of a solar cell can be represented by an electrical component, such as a diode. It is used to explain the behaviour of a solar cell as accurately as possible. Figure 4.5 shows the standard equivalent circuit of a solar cell. The photocurrent I_{PH} represents the current generated from the solar cell. Ideally, the goal is to pass the generated current to our load at the terminals, however because of the physical limitations the diode is not ideal. Moreover, the equivalent circuit also includes I_D and I_P, representing the diode current and parallel (shunt) current, respectively.
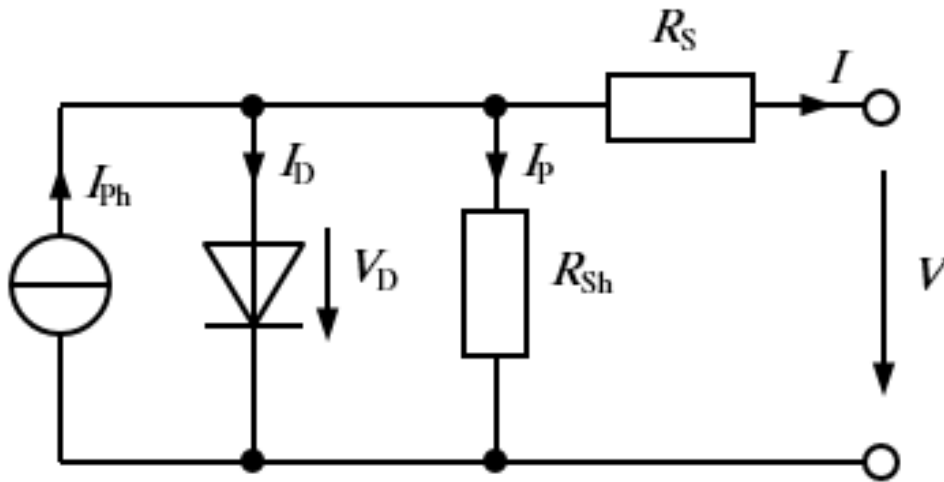
Figure 4.5 – Standard equivalent circuit diagram of a solar cell. Source: Mertens, K. [46].

The electrical circuit includes the series resistance R_S, which is composed of the ohmic losses (losses due to voltage drop) at the front contacts of the solar cell, the resistance from the semiconductor material and metal electrodes, and the contact resistance between semiconductor and metal contacts [46, 47]. Figure 4.6 illustrates how increasing the series resistance R_S results in the IV-characteristics curve losing its traditional shape, which leads to a reduction in the fill-factor of the solar cell.
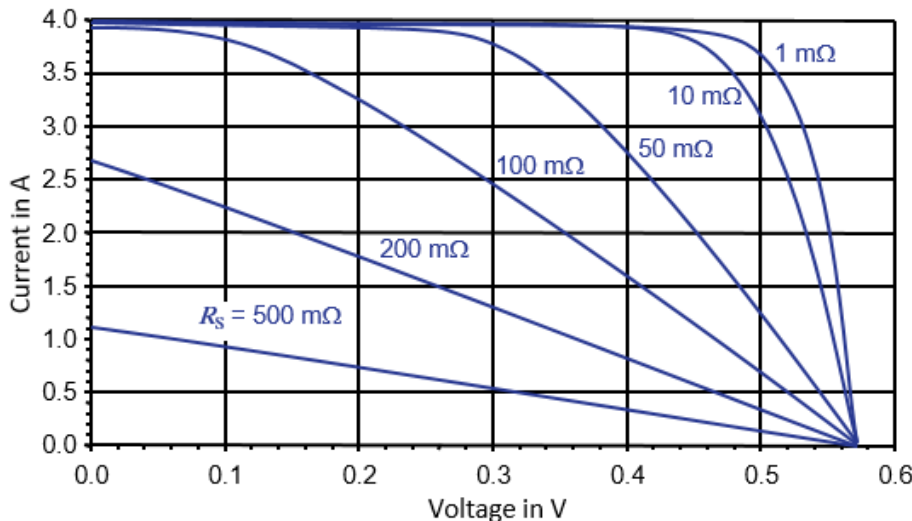
Figure 4.6 – Effects of series resistance R_S on the IV-characteristics curve. Source: Mertens, K. [46].

In addition to the series resistance R_S another resistance is included in the circuit diagram, the shunt resistance **R_{SH}**. The decrease of shunt resistance is mainly due to defects in the solar cell created during the manufacturing process or as a result of degradation processes. These defects can result in alternative ways for the light-generated current to flow, resulting in power losses in the solar cell. Consequently, an increase in the shunt resistance leads to a more optimal curve and a higher fill-factor, which is visible from the IV-characteristics in Figure 4.7.
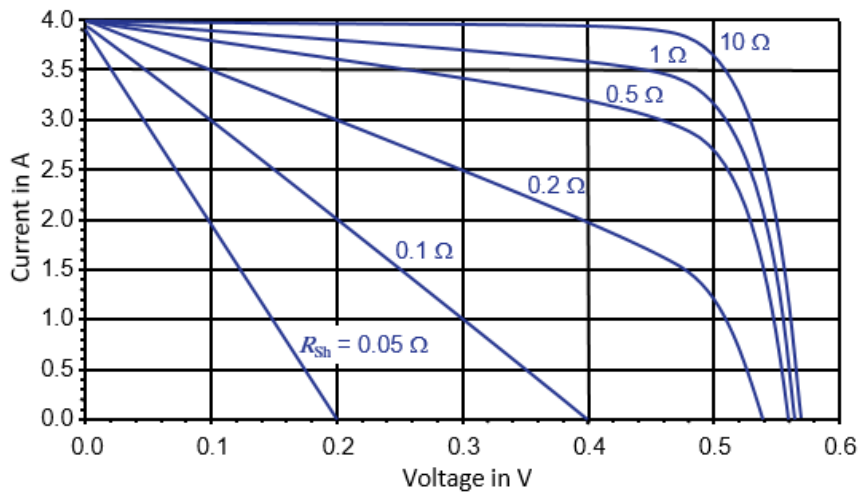
Figure 4.7 – Effects of shunt resistance R_{SH} on the IV-characteristics curve. Source: Mertens, K. [46].

Furthermore, it is generally agreed upon in published literature that the increase in shunt resistance R_{SH} is seen as a direct result of lower irradiance conditions [48, 49]. The single diode equation is widely used as an electrical circuit representation of a solar cell, although some weaknesses in certain situations has been identified, especially when trying to model IV-curves in low irradiance conditions [49]. In addition, a paper by Grunow et al. [50] mentions the importance of R_{SH} and its influence as a substantial loss mechanism at low irradiance levels. However, throughout the years low light conditions is taken into account by manufacturers, simply by considering a large enough R_{SH} [51].

Apart from the resistances, although not included in the circuit diagram another variable is the ideality factor **n** which is used to denote how closely a solar cell is able to follow the ideal diode equation. From Figure 4.5 the current **I** is given by Equation (4), which shows the characteristics curve equation for the standard model.

$$I = I_{PH} - I_s * \left(e^{\frac{V + I*R_S}{n*V_T}} - 1 \right) - \frac{V + I * R_S}{R_{SH}} \tag{4}$$

The shunt current I_P is then given in Equation (5).

$$I_P = \frac{V_D}{R_{SH}} = \frac{V + I * R_S}{R_{SH}} \tag{5}$$

The equation can be used to model the IV-characteristics of a solar cell, although it is only solvable using numerical methods [46].

4.4 Bypass diodes and PV module faults

There are typically either 36, 60 or 72 series connected solar cells in a PV module. Therefore, as they are connected in series, the voltage of all the cells is added up together. Additionally, there are usually three bypass diodes for the typical crystalline silicon modules [16]. A module with 60 series connected cells, including three bypass diodes are shown in Figure 4.8. The function of a bypass diode is closely related to its name. The performance of the module is limited by the worst performing cell in the series connection which can end up being a bottleneck. For instance, if a single cell in a string is shaded, and as the current through a series connection is the same, the current through the string of cells reduces to the current level of the shaded cell [52]. Furthermore, the excess current produced by the good cells will (forward bias) the good cells. Therefore, if this string of cells is short circuited, then this (forward bias across all good cells) reverse biases the shaded cell. Thus, this is causing heat to be dissipated in the bad cell, which can result in overheating (hot spots) in some areas [16, 53]. As a result, to circumvent this problem bypass diodes allow the current to flow in an external circuit.
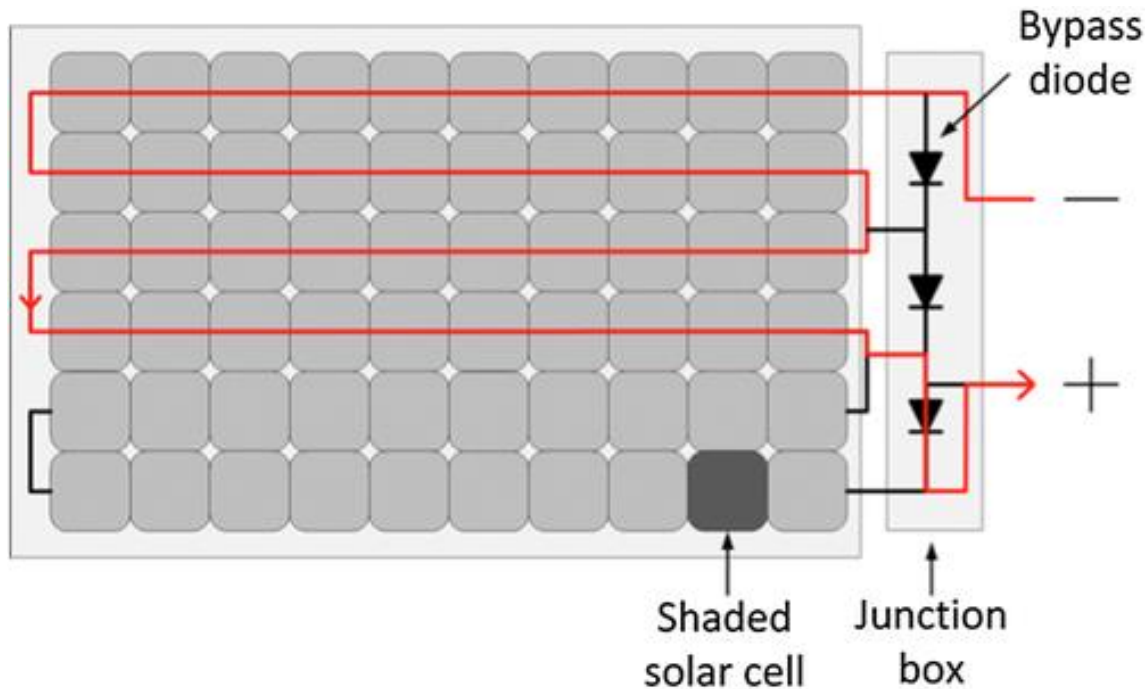
Figure 4.8 – Structure of a PV module with 60 series connected cells and three bypass diodes, and illustration of six solar cell strings or three sub-strings. Source: [54].

Figure 4.9 shows the IV-curve of a solar cell both with and without a bypass diode. The bypass diode will only become active when there is a reverse bias and starts to conduct when it passes the threshold voltage (around 0.6 - 0.7 V). Looking at the IV-curve in Figure 4.9 we see this occurring as the voltage reaches V_d and the current increases, which reduces the energy loss in the cell [53].
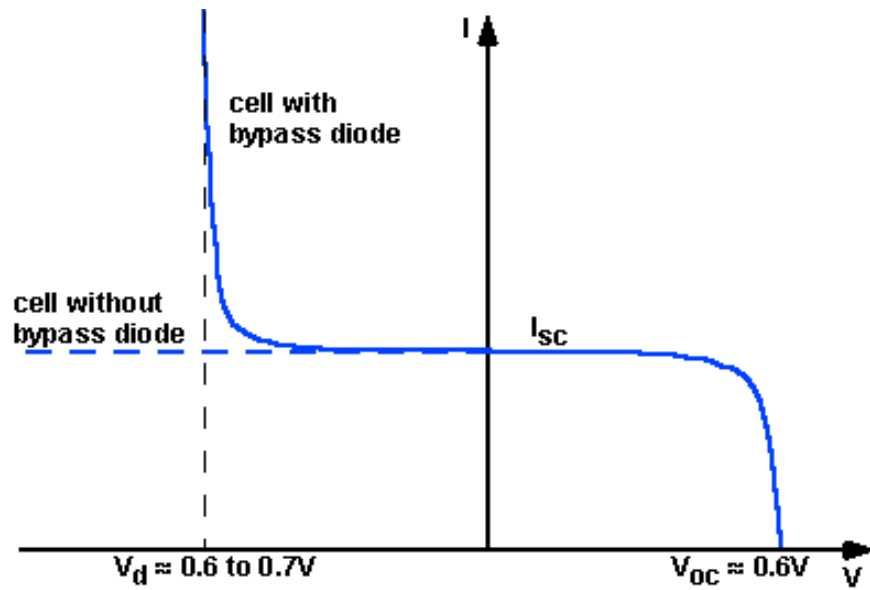
Figure 4.9 – IV-curve of solar cell with and without bypass diode. Source: PVEducation [53].

There are several faults that typically can occur throughout the lifetime of a PV module, and that can be detected on the IV-curve. Some of these faults is cell breakage, glass corrosion, defect bypass diode, short-circuited cells, and broken cell interconnections, to mention some [55]. These faults have different effects on the IV-curve. Figure 4.10 shows an example of an IV-curve for a PV module with different faults.
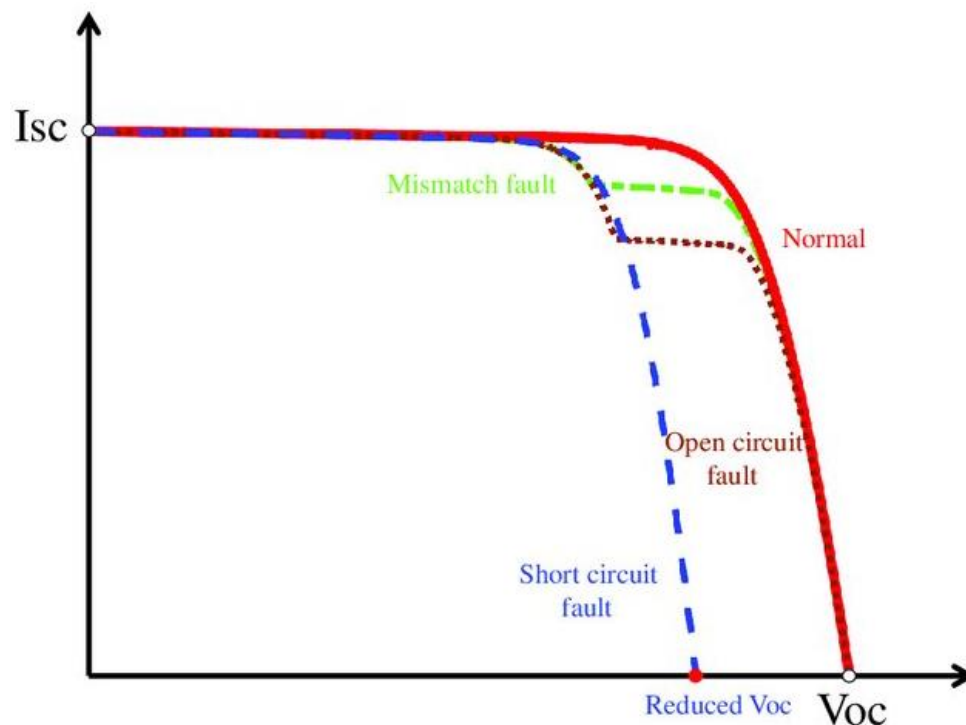
Figure 4.10 – IV-characteristics for different PV faults. Source: Dong et al. [56].

A mismatching fault, where the individual solar cells in the module can have slightly different characteristics, results in a reduction in I_{MP} as seen by the green curve in Figure 4.10. Similarly, an open-circuit fault has an identical effect on the IV-characteristics, but I_{SC} is reduced further compared to a mismatch fault. This is due to an entire string of solar cells

being disconnected with an open-circuit fault, so the current from these cells is effectively lost. An open-circuit fault can occur if the electrical circuit is damaged because of broken wires or fuses. The reduction in open-circuit voltage V_{OC} can typically be caused by short-circuit faults where there is failure in individual cells or bypass diodes [55]. Such faults can occur both in a series connected string, but also between two individual strings. The difference between open-circuit faults and short-circuit faults is that in one case I_{SC} is greatly reduced and V_{OC} in the other.

4.5 Shading and snow cover

Snow cover on a PV module will affect the IV-characteristics, but the impact could be more drastic as compared to the effects of faults seen in Figure 4.10. The presence of snow reduces the sunlight hitting the module surface, and thus reducing the current substantially. Figure 4.11 shows the comparison of the IV-characteristics for a PV module both completely covered by snow (blue curve) and without snow (orange curve). It is clearly visible from Figure 4.11 that the current from the module without snow is almost thrice the value of the current from the snow-covered module. Additionally, there is another drop in current just before the voltage reaches 10 V, likely due bypass diode activation. However, the two example IV-characteristics represents data for the same timeslot, but with an interval of a day between them. The weather was overcast on both days with available irradiance levels of 129 W/m^2 and 65 W/m^2 for the day with and without snow cover, respectively. Figure 4.11 clearly illustrates how the current is reduced when the entire module area is covered by snow.
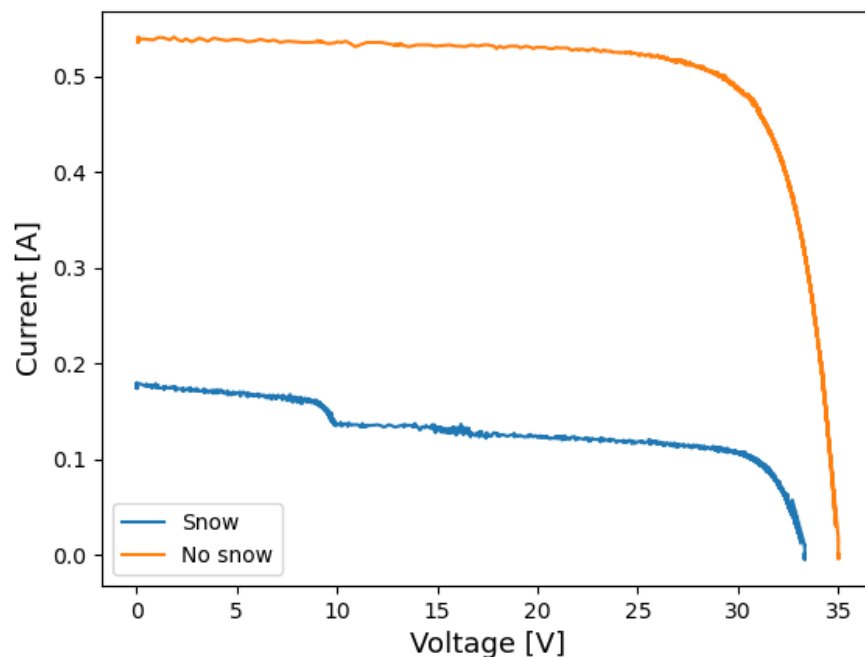
Figure 4.11 – IV-characteristics for a PV module with and without complete snow cover. Source: Data from UiA PV System 2016. Figure created by author.

The effects of snow have been discussed earlier and it can be closely resembled by shading a cell. Figure 4.12 illustrates the effects of shading 50% of the 60 series connected cells in a module without a bypass diode. As expected, the current is reduced to half of its original value, because of its close connection with irradiance, although the voltage is not [52].
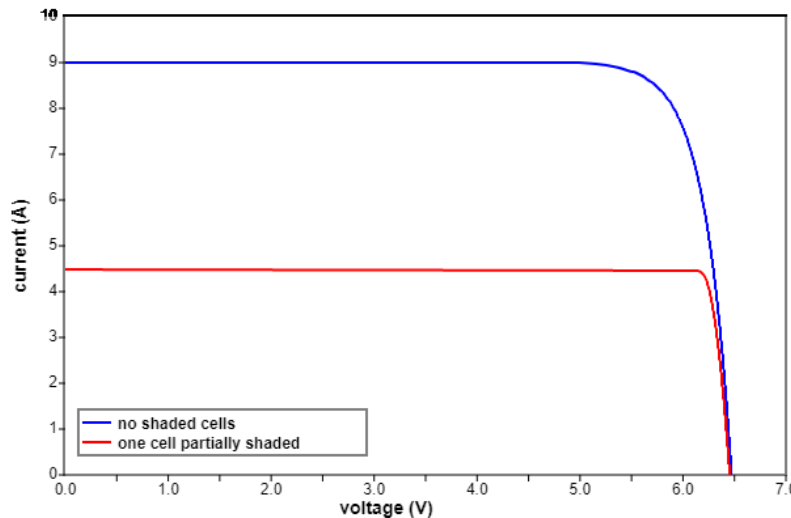
Figure 4.12 – Effects of shading a single cell in a module. Source: PVEducation [52].

A similar occurrence can happen with snow covering parts of a module, although when snow melting occurs the covered area is likely to vary greatly resulting in a non-uniform shaded area [8]. In addition, snow cover will also have a cooling effect on the modules, which is positive for the power output [57]. Nevertheless, this beneficial cooling effect does not exceed the power output lost because of snow cover. The effects of covering parts of a cell were illustrated in Figure 4.12, but this was without any bypass diodes. Figure 4.13 displays what an IV-curve looks like for a module with different faults and with bypass diodes included. We observe that there is a noticeable drop in current before the bypass diodes are activated in case number (4) and (5). However, with bypass diodes the current is not reduced any further, hence the power output is increased relative to a module without bypass diodes [53].
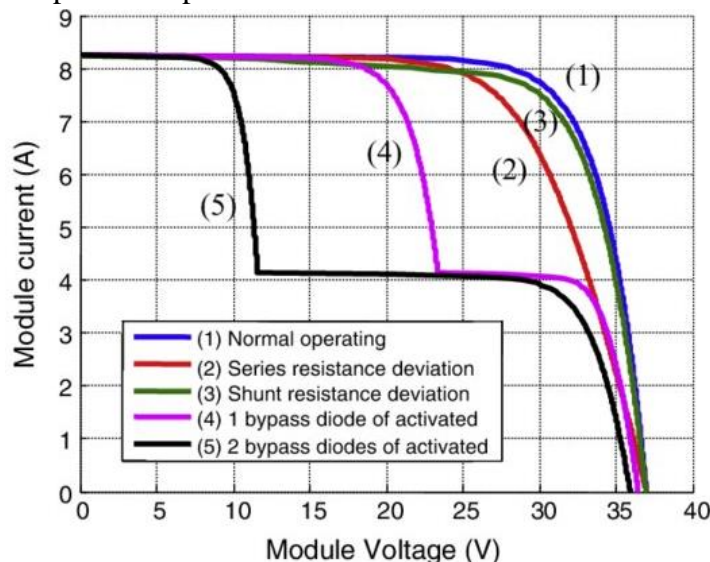
Figure 4.13 – Effects of different faults on the IV-curve of a PV module with bypass diodes. Source: [58].

Figure 4.14 shows an IV-curve for a PV module which is subject to partial snow cover and is the result of snow covering parts of each module substring. This leads to the activation of each of the three bypass diodes connections found in the junction box. As a result, the active bypass diodes are visible on the IV-curve as three noticeable kinks since the voltage levels of the module is reduced as one module substring is bypassed. Furthermore, as the product of

current and voltage represents the power this leads to the creation of numerous local MPP on the curve, and where the inverter should find the global MPP as the operating point. However, without the bypass diodes the IV-curve would be more like the blue IV-curve illustrated in Figure 4.11, resulting in a lower current and therefore reduced power output.
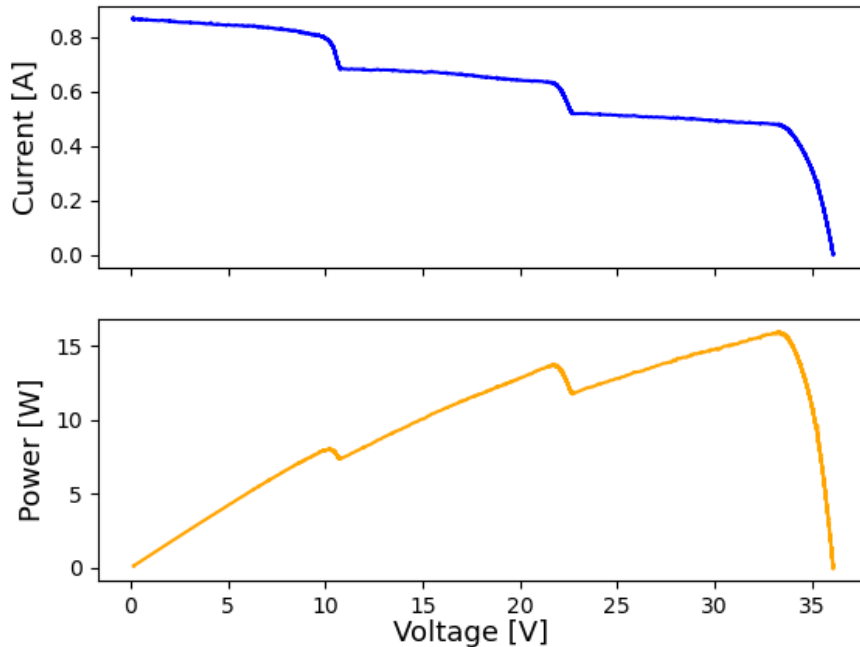
Figure 4.14 – Top figure: IV-characteristics with three active bypass diodes. Bottom figure: PV-characteristics with three active bypass diodes. Source: UiA PV System 2016. Figure created by author.

4.6 Effects of temperature

Besides shading there are other phenomena that impact solar cells in a negative way. Solar cells utilize the photovoltaic effect to convert the energy in incoming sunlight directly to electricity. However, only approximately 15-20% of this sunlight is successfully converted to electricity, as much of it is transformed into heat [59]. This heat is undesirable since an increase in module temperature has negative effects on the performance of the PV module. Typically, a change in module temperature by 1 Kelvin results in a decrease/increase in power output of around 0.5% [3, 60]. This is because the open circuit voltage is reduced gradually with an increase in module temperature. Figure 4.15 illustrates this effect. At the same time the short circuit current increases slightly, but this is not enough to counter the voltage drop. Consequently, the power output will decrease [2, 16].
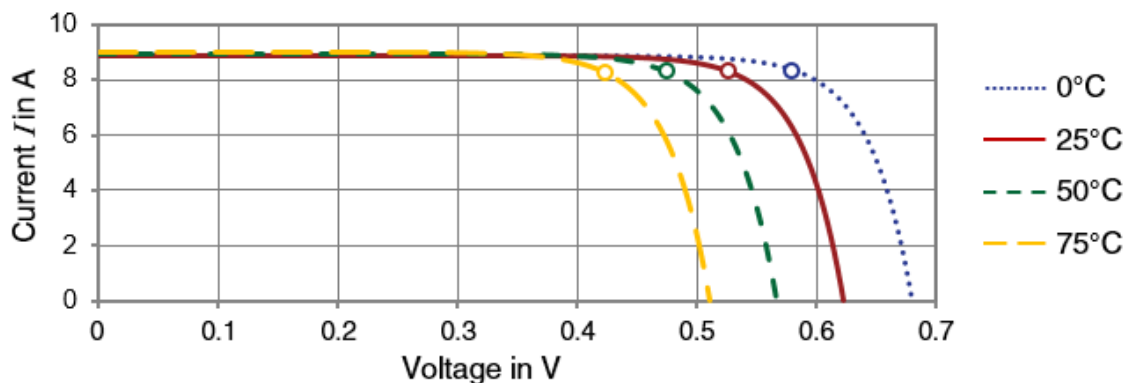
Figure 4.15 – Temperature dependency of a silicon solar cell. Source: [16].

5. Methodology

5.1 Goal and scope

This thesis proposes a methodology that is set to utilize a large quantity of available data consisting of both recorded IV-curves, images, irradiance, and PV module temperature data. The main objectives are to investigate if using an IV-characteristics model can be effective to perform power loss estimations on uniformly and partially snow-covered PV modules. The overall shape of the modelled IV-curves and the P_{MPP} deviation is compared against the recorded IV-curves available from the UiA PV research system to assess the accuracy of the power loss estimations. The IV-characteristics model uses irradiance and module temperature as input data. Module images and recorded snow depths from SeNorge [61] is used to make an initial assumption on the irradiance reduction due to a specific snow cover. Based on the results from the first IV-curve simulation the irradiance reduction is adjusted with a trial-and-error approach to achieve the best possible IV-curve fit between the modelled and recorded IV-curves. The snow depths are not used directly as input in the model, but only to get an idea of what power losses could be expected for different snow depths and snow covers under various irradiance conditions.

Furthermore, the work also aims to investigate if an image analysis method can be used to identify snow covered module areas and be incorporated into the IV-curve model to improve power loss estimations for partial snow cover situations. This methodology uses module images as input, and the results, the calculated partial module snow coverages are used as input to the IV-characteristics model. The calculated partial module snow coverage replaces the trial-and-error approach described in the previous section. The methodology proposed is tested on different types of PV module snow coverages to evaluate the accuracy of the modelled power loss estimations under various irradiance conditions.

The first part of this methodology focuses on trying to simulate IV-curves based on a set of predefined parameters based on datasheet values for the relevant PV module. This is done to estimate the expected output of the modules with and without snow cover which is compared with measured IV-curves. These five parameters are estimated, based on the datasheet values, by a set of built-in equations in MATLAB, which is then used as input in the single diode equation to perform the simulations. These parameters include the dark saturation current (I_0), light current (I_L), series resistance (R_S), shunt resistance (R_{SH}), and the diode ideality factor (n). In addition, the temperature coefficients of V_{OC} (β) and I_{SC} (α) are also necessary as input to account for how the open-circuit voltage and short-circuit current will react to a change in cell temperature. However, it is also necessary to make some assumptions for the PV module being considered, such as each individual cell being identical, constant irradiance and temperature levels for all the cells. Moreover, by utilizing a PV model available in MATLAB Simulink, these five parameters are calculated automatically when the PV datasheet values are used as input. Additionally, the bypass diodes included in the PV model also have parameters

that needs to be specified. This includes the forward voltage (V_F) and the internal resistance (R_{IR}).

Secondly, the other part of this thesis aims to conduct an image analysis, specifically of PV module images. The goal is to automatically identify individual PV module areas in an image containing multiple modules. Furthermore, the identified area is to be checked for the presence of any snow to assess the amount of PV module area covered by snow. Finding the area will allow for an approximation of how much power loss is associated with how large a portion of the module area is covered by snow. Additionally, investigating if calculated partial module snow coverages can improve the accuracy of the modelled power losses. This is to be done by implementing an image analysis method in MATLAB, similarly, to what Pearce et al. [8] and Braid et al. [35] used as part of their methodology when investigating power losses associated with snow cover on PV modules. The approach is divided into different steps, these include conversion of images PV modules into different formats, such as HSV color space, greyscale, and lastly image binarization. This is necessary as the image processing toolbox available in MATLAB requires this type of image format as an input. Furthermore, by utilizing the image region analyzer (IRA) and image segmentation (IS) tools, the individual PV module areas can be identified. The detected pixel value for module areas without snow cover can then be compared against cases with variable amounts of partial snow cover. Thus, giving an estimation of what percentage of the module surface is covered by snow.

5.2 UiA PV research system

The University of Agder (UiA) has a PV system used for research purposes mounted on the top of the roof at campus Grimstad. It has been in use since 2010, although the PV modules have been frequently changed depending on different research projects that has been conducted. A variety of PV module types has been used as part of the PV system, including monocrystalline silicon (mono-Si), polycrystalline or multi-crystalline (mc-Si), and thin-film cells, such as copper indium selenium (CIS), copper indium gallium selenide (CIGS), cadmium telluride (CdTe), and amorphous silicon (a-Si). Figure 5.1 shows the PV research system as of 2016 and Table 5.1 shows the datasheet values for the different modules, and Table 5.2 presents the module type, vintage, and cell/string configuration. The modules in the PV system are mounted facing south at a 39° tilt angle with little spacing in between. Data collection is done for parameters, such as global horizontal irradiance (GHI), plane of array (POA) irradiance, back-of-module temperature, and ambient temperature. Average temperature measurements were recorded continuously in 1-minute intervals, along with I_{SC}, V_{OC}, V_{MPP}, and P_{MAX} values. In addition, IV-curves consisting of 4000 datapoints were recorded for each module if the lower irradiance limit of around 30 W/m^2 was reached [62].

Figure 5.1 – PV research system setup in 2016 located on the rooftop at UiA campus Grimstad. Source: UiA PV Research System.

*Table 5.1 – UiA PV research system PV module datasheet values and measured temperature coefficients. *Not certain these are accurate because multiple datasheet values were available, and it was uncertain whether all these were correct.*

Module data	Q-Cells A10156	Q-Cells A10160	SunTech 422	SunTech 433	SunTech 423	TITAN
P_{MPP}	224 W	223 W	235 W	236 W	235 W	250 W
V_{MPP}	30.15* V	29.74 V	29.6 V	29.6 V	29.6 V	30.72 V
I_{MPP}	7.20* A	7.47 A	7.61 A	7.61 A	7.61 A	8.14 A
V_{OC}	37.2 V	36.4 V	36.8 V	37.1 V	37.0 V	38.0 V
I_{SC}	7.89 A	8.07 A	8.49 A	8.57 A	8.47 A	8.75 A
V_{OC} and I_{SC} temperature coefficients						
β (V_{OC})	-0.339 [%/K]	-0.370 [%/K]	-0.351 [%/K]	-0.354 [%/K]	-0.321 [%/K]	-0.320 [%/K]
α (I_{SC})	0.064 [%/K]	0.082 [%/K]	0.056 [%/K]	0.059 [%/K]	0.056 [%/K]	0.019 [%/K]

In 2018 the PV systems data collection capabilities were improved by installing additional monitoring equipment. Besides the parameters that are monitored in the earlier system, the new research system includes weather data, such as wind speed, air temperature, humidity, air pressure, and precipitation. Moreover, instruments measuring other components of the solar irradiance, such as diffuse horizontal irradiance (DHI), tilted global irradiance (TGI), direct normal irradiance (DNI), global vertical irradiance (GVI), and albedo [62].

Table 5.2 – Information about PV module types, number of cells/strings, and module vintage.

PV Module	Module Type	Number of cells/strings	Vintage
Q-Cells A10156	mc-Si	60 / 3	2008
Q-Cells A10160	mc-Si	60 / 3	2008
SunTech 422	mc-Si	60 / 3	2012
SunTech 433	mc-Si	60 / 3	2012
SunTech 423	mc-Si	60 / 3	2012
TITAN	mc-Si	60 / 3	2013

The data is collected in the time-period 2011-2017, and it includes both images and IV-curve data. In this thesis the used data is from 2015 to 2017. The available image data was investigated to pinpoint snowfall events that could be of interest. These time-periods would then be used in the modelling of IV-curves and in the image analysis. Firstly, since the analysis requires multiple events with snow fall it is required that the recorded data involves such events. However, as the recorded data has a minimum irradiance limit of 30 W/m2, time-periods with too much cloud cover and heavy precipitation (snow) will not provide any data. Therefore, events with gradual snow build-up followed by clear sky days with greater irradiance levels, or higher air temperatures that allows for snow to melt and slide down the module particularly interesting to look at. Furthermore, events with uniform snow cover are also of interest as different amounts and types of module coverage could potentially be interesting to examine in further detail. For example, occurrences where snow has accumulated in smaller random areas of a PV module, covering a specific part of the module. In addition, situations with partial snow cover can also contribute to the formation of hot spots, which will damage the modules in the long run. It could potentially reduce their lifetime, thus making such events important to identify.

5.3 Recorded PV data and correction factors

The UiA PV research system is designed in such a way that for several of the modules IV data must be multiplied with a correction factor to get the correct value. This is due to voltage dividers having to accommodate for the hardware limitations of the load. The configuration of the PV research system is not uniform for all the PV modules, as some channels were connected to a 175 W load where 0-10 V corresponds to 0-10 A. Meanwhile, for other modules 0-10 V corresponds to 0-20 A, thereby requiring some current values to be multiplied by a factor of 2. Furthermore, as a variety of voltage divider ratios are used, the correction factors range from 3.7 to 9.2 for the voltage values. The correction factors for the different PV modules in the UiA PV research system are listed in Table 5.3. These factors are multiplied with the current and voltage raw data values to create the recorded IV-curves shown in this thesis.

Table 5.3 – UiA PV research system module current and voltage correction factors applied to the raw data. Source: [62].

PV Module	Current correction factor	Voltage correction factor
Q-Cells A10156	2.0	4.8755
Q-Cells A10160	2.0	4.902
SunTech 422	2.0	5.992
SunTech 433	2.0	5.996
SunTech 423	2.0	5.99
TITAN	2.0	5.99

5.4 The IV-characteristics model

The IV-characteristics model is based on a MATLAB Simulink model available from the MathWorks website [63]. It is easily editable where the amount of incoming irradiance can be specified individually for each of the three substrings, and the temperature of the corresponding cells. The irradiance and temperature connections are denoted as *Ir1, Ir2, Ir3*, and *Temp C, Temp C1, Temp C2*, on the model respectively. The three substrings are series connected with a bypass diode connection between each substring. Additionally, to illustrate snow cover a shading factor (irradiance reduction) is added to each substring, which is simply a constant value that is multiplied with the irradiance values to represent the amount of irradiance that reaches the PV module. It ranges from 1 to 0 where 1 and 0 represents no and full snow cover, respectively. An image of the MATLAB Simulink model is displayed in Figure 5.2.
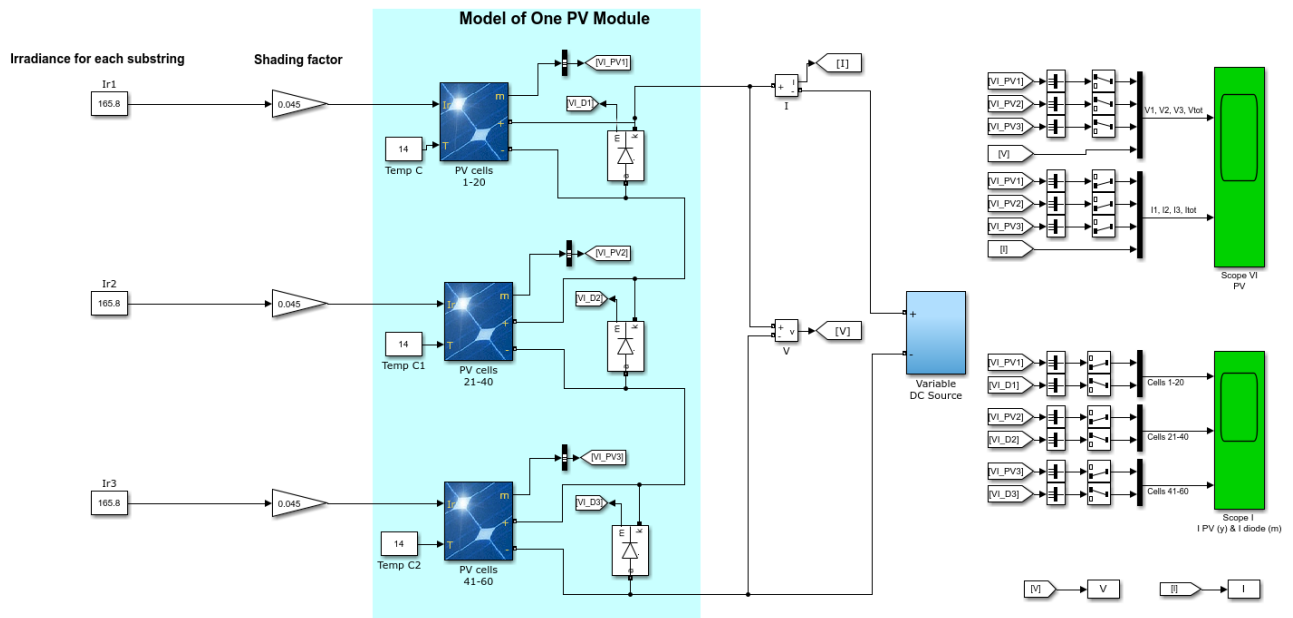
Figure 5.2 – MATLAB Simulink model of a single PV module with 60 cells. Source: MATLAB snapshot.

On the right side of the figure the voltage and current values from the three different substrings are connected to a current and voltage measurement block and summed together before being connected to the variable DC source. To allow for the illustration of both the IV

and PV-curves, the individual current and voltage measurements from each substring is passed through a scope to plot the two curves. However, first the measurement signals must be converted to a vector signal. To calculate the IV-characteristics of the PV module a variable DC voltage source is used to ramp the voltage up from 0 until a full IV-curve is created. The model utilizes the diode equation, shown in Equation (4), which is solved to calculate the current based on the different voltage values input into the equation. Furthermore, depending on which PV module is being modelled the simulation parameters must be changed accordingly.
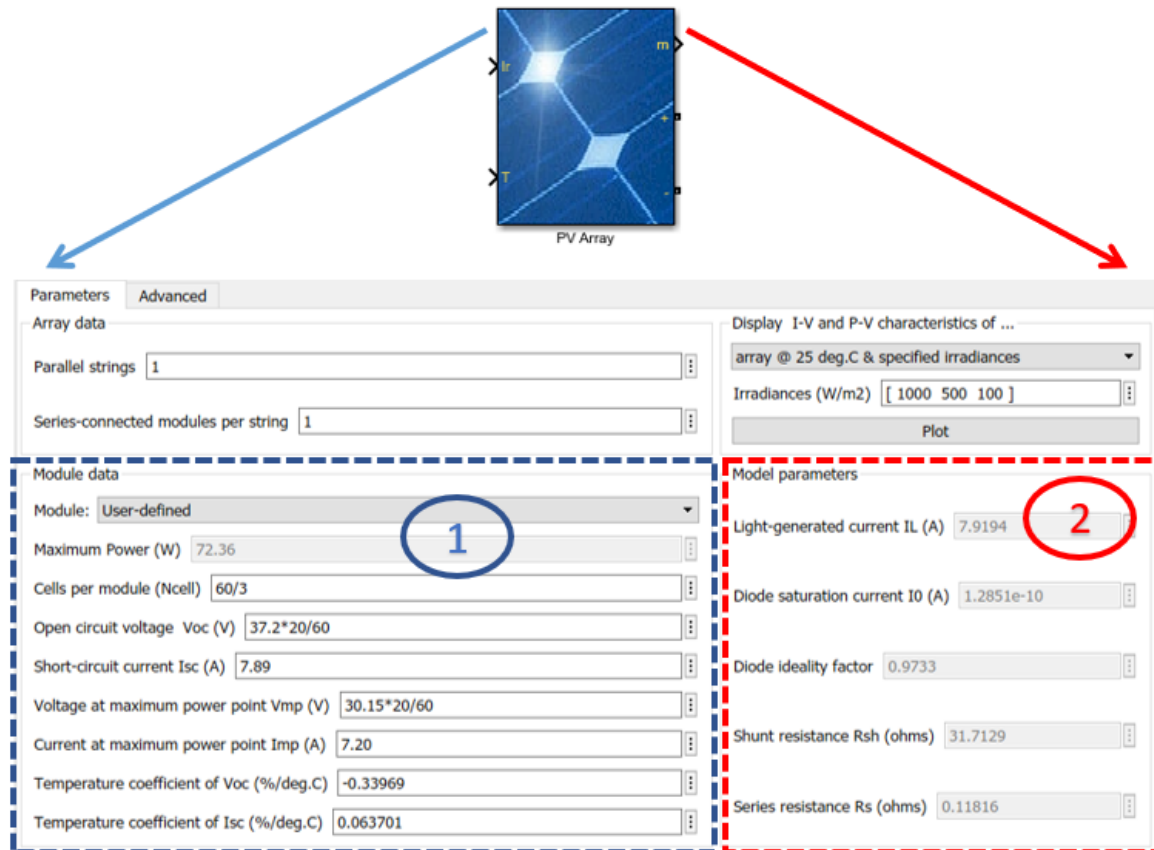
Figure 5.3 – PV module data input window (1) and model parameters (2) calculated by the MATLAB Simulink model. Source: MATLAB snapshot. Figure created by author.

Firstly, periods with snow fall are identified in the module images available from the UiA PV System. The recorded IV-curves for selected situations with PV module snow cover is compared with the simulated IV-characteristics for snow and snow free conditions. For the selected PV modules shown in Table 5.1, the datasheet values are inserted into the MATLAB model module data window (1), illustrated in Figure 5.3. These are used to estimate the required model parameters (2) necessary to run the MATLAB model. In addition, the incoming irradiance data and module temperature are extracted from the available datasets to set up the model correctly. A simple block diagram of the PV snow loss model proposed in MATLAB Simulink is displayed in Figure 5.4. The model optimization block illustrated in the block diagram is the adjustment of the irradiance reduction described in subchapter 5.1.
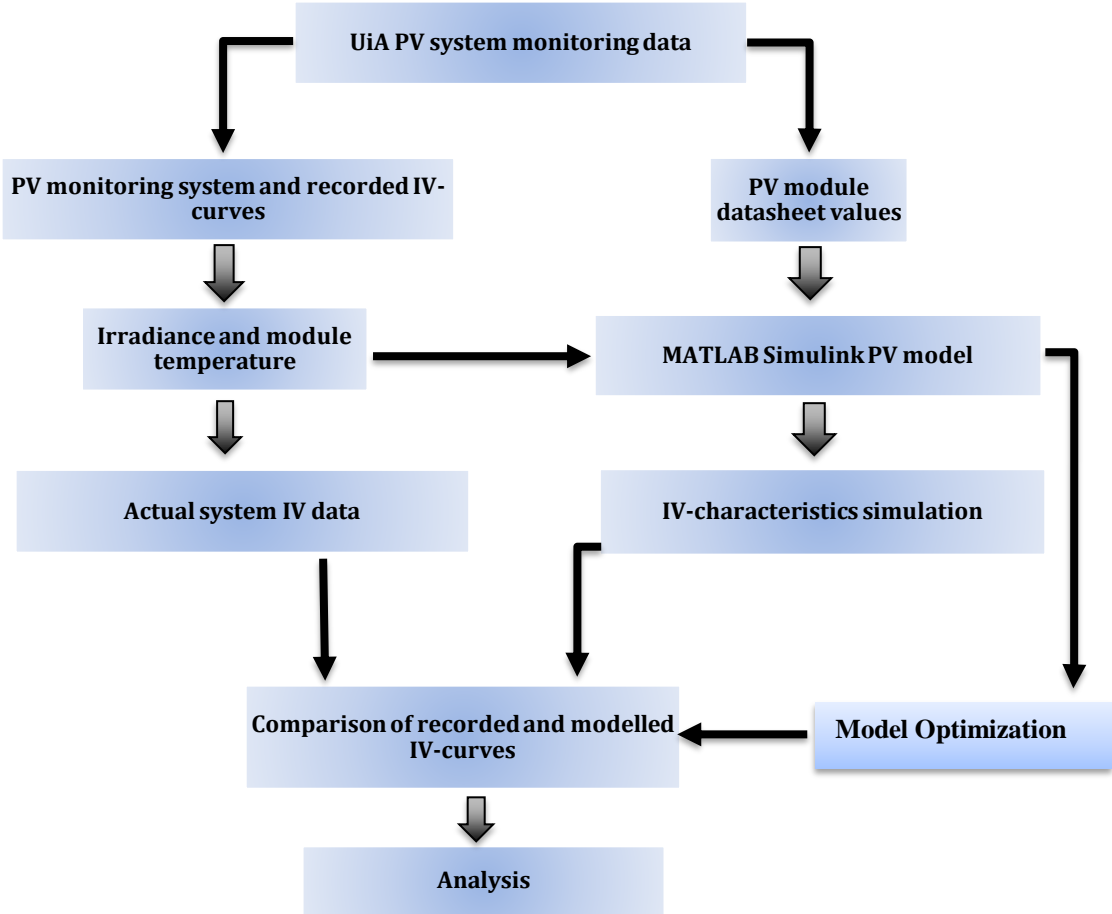
Figure 5.4 – Basic block diagram of the PV snow loss model in MATLAB Simulink. Source: Figure created by author.

5.5 Validation of the MATLAB Simulink model

Before testing the model on different variations of snow cover it is necessary to test its performance and ability to simulate the IV-curve and the P_{MPP} without any form of module shading. To get an understanding of how the model performs in situations with module snow cover it is useful to first test it under snow free and clear sky conditions. This is necessary because without knowing the model accuracy in clear sky conditions it is difficult to assess its accuracy in situations with snow cover. Therefore, the model is tested for several different situations with variable irradiance levels, and for different PV modules. The overall shape and fit of the curves are evaluated and the P_{MPP} compared to the recorded IV-curves. The calculated single diode equation parameters from the MATLAB Simulink model, and module temperature coefficients are displayed in Table 5.4.

Table 5.4 – PV Module calculated single diode equation parameters calculated based on datasheet values at STC and measured temperature coefficients.

Calculated parameters	Q-Cells A10156	Q-Cells A10160	SunTech 422	SunTech 433	SunTech 423	TITAN
I_0 [A]	1.2851e-10	3.95e-10	2.0451e-10	2.3013e-10	6.6771E-11	6.3335e-11
I_{PH} [A]	7.9194	8.085	8.5391	8.633	8.524	8.7703
R_S [Ω]	0.11816	0.094155	0.11822	0.12976	0.13308	0.11575
R_{SH} [Ω]	31.7129	50.5209	20.4386	17.6468	20.8608	53.7878
n	0.9733	0.9958	0.9790	0.9919	0.9412	0.9619
Bypass diode parameters (Identical for all modules)						
R_{IR}	0.001 **Ω**					
V_F	0.7 **V**					

To validate the MATLAB Simulink IV-curve model different test periods were considered for several PV modules. The specific date and time for each case, irradiance values, module temperature, modelled P_{MPP}, recorded P_{MPP}, and the deviation between the two P_{MPP} is listed in Table 5.5. The time slots considered are between January and April with irradiance values ranging from 100 W/m² to 1000 W/m², and module temperature values between -5.7 to +32.8°C.

Table 5.5 – Irradiance data, module temperature, and comparison of modelled and recorded P_{MPP} values for different time periods for different PV modules.

Date and time	PV Module	Irradiance [W/m²]	Module temperature [°C]	P_{MPP} modelled [W]	P_{MPP} recorded [W]	P_{MPP} deviation [%]
27/03/15 12:31	Q-Cells A10156	1005.2	25.1	218.1	221.6	1.6
13/12/15 12:30	Q-Cells A10156	526.3	11.9	121.2	120.6	0.5
05/03/16 10:46	Q-Cells A10156	171.1	3.5	39.9	38.8	2.7
02/04/15 13:09	TITAN	1010.5	27.6	249.8	229.7	8.1
13/12/15 12:30	TITAN	526.3	13.3	139.9	136.8	2.2
13/12/15 14:30	TITAN	264.3	11.1	70.4	69	2.0
18/01/16 12:45	SunTech 422	600	14.0	142.8	151.1	5.5
08/03/16 14:31	SunTech 422	200.7	9.7	48.0	49.1	2.2

| 02/04/15 13:09 | SunTech 422 | 1010.5 | 32.8 | 220.2 | 219.7 | 0.2 |
| 16/12/17 09:20 | SunTech 422 | 98.5 | -5.7 | 24.5 | 21.8 | 11 |

Results from modelling the IV-curves for the different times and conditions shows that the P_{MPP} deviation varies between around 0.2-11%. In one case the modelled P_{MPP} is almost equal to the rated power of the TITAN module, but it can also surpass the rated power of the PV module. This is due to the rated power at STC, which is based on irradiance values of 1000 W/m^2, and module temperatures of 25°C. So, an irradiance level above STC conditions and module temperatures below 25°C, can result in power values above the rated module power. The modelled and recorded IV and PV-curves for the Q-Cells A10156, TITAN, and SunTech 422 PV module is displayed in Figure 5.5, Figure 5.6 , Figure 5.7, respectively. In addition, each curve plotted individually are found in **Appendix A.2-Appendix A.4.**
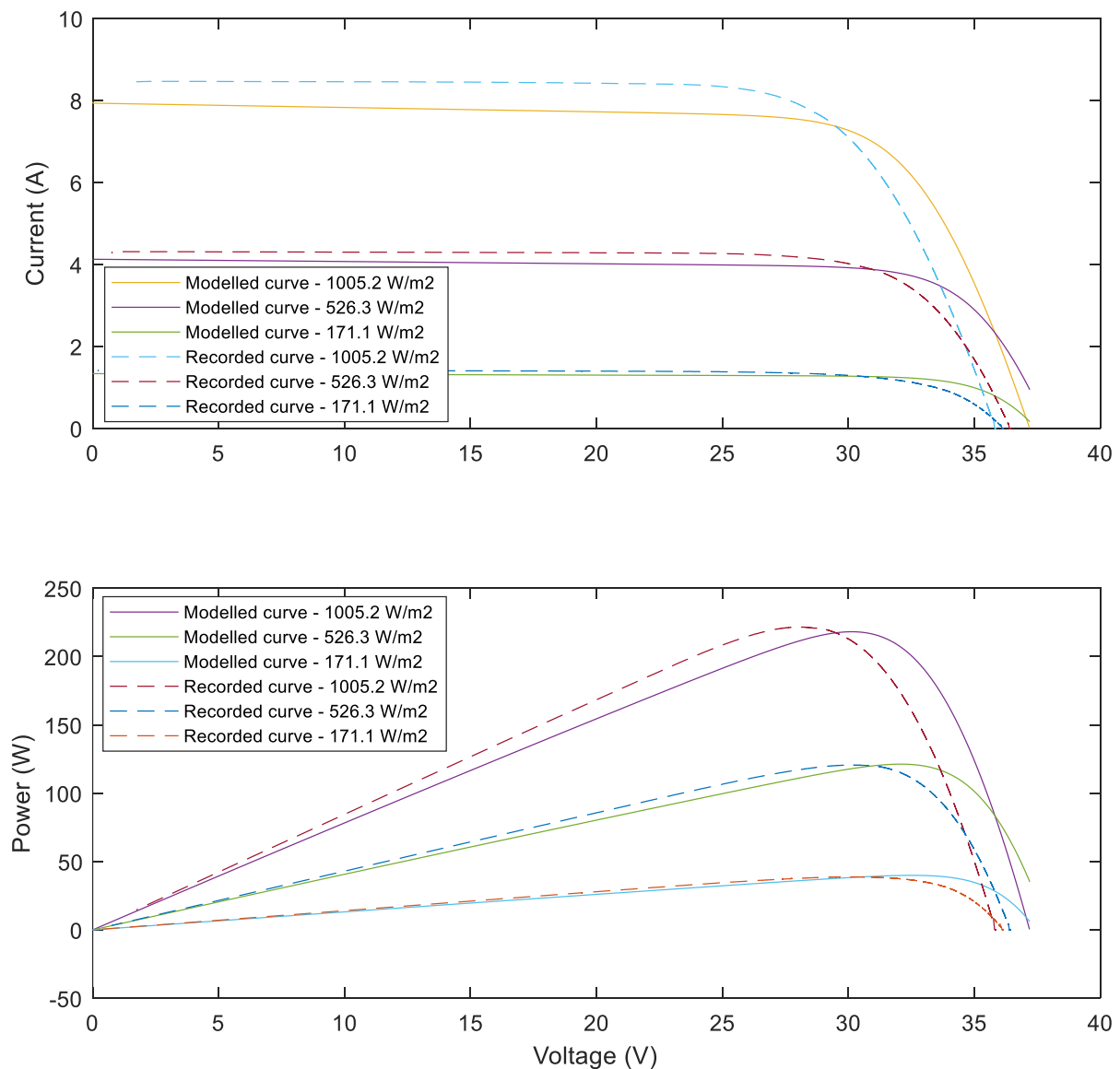
Figure 5.5 – Top graph: Modelled and recorded IV-curves for the Q-Cells A10156 module at different irradiance levels.
Bottom graph: Modelled and recorded PV-curves for the Q-Cells A10156 module at different irradiance levels.

The modelled and recorded IV and PV-curves for the Q-Cells A10156 module at three different irradiance levels, is shown in Figure 5.5. Overall, I_{sc} in the modelled curves deviates slightly from I_{sc} in the recorded ones, resulting in a P_{MPP} deviations ranging from 0.5-2.7%. However, the shape of the modelled IV-curves is similar, but as the voltage increases past 30 V the curve is shifted towards a higher voltage compared to the recorded curve. This suggests that there are some uncertainties related to the voltage datasheet values and the parameters used in the model. Thus, resulting in a greater V_{OC} for the modelled curve compared to the recorded one.
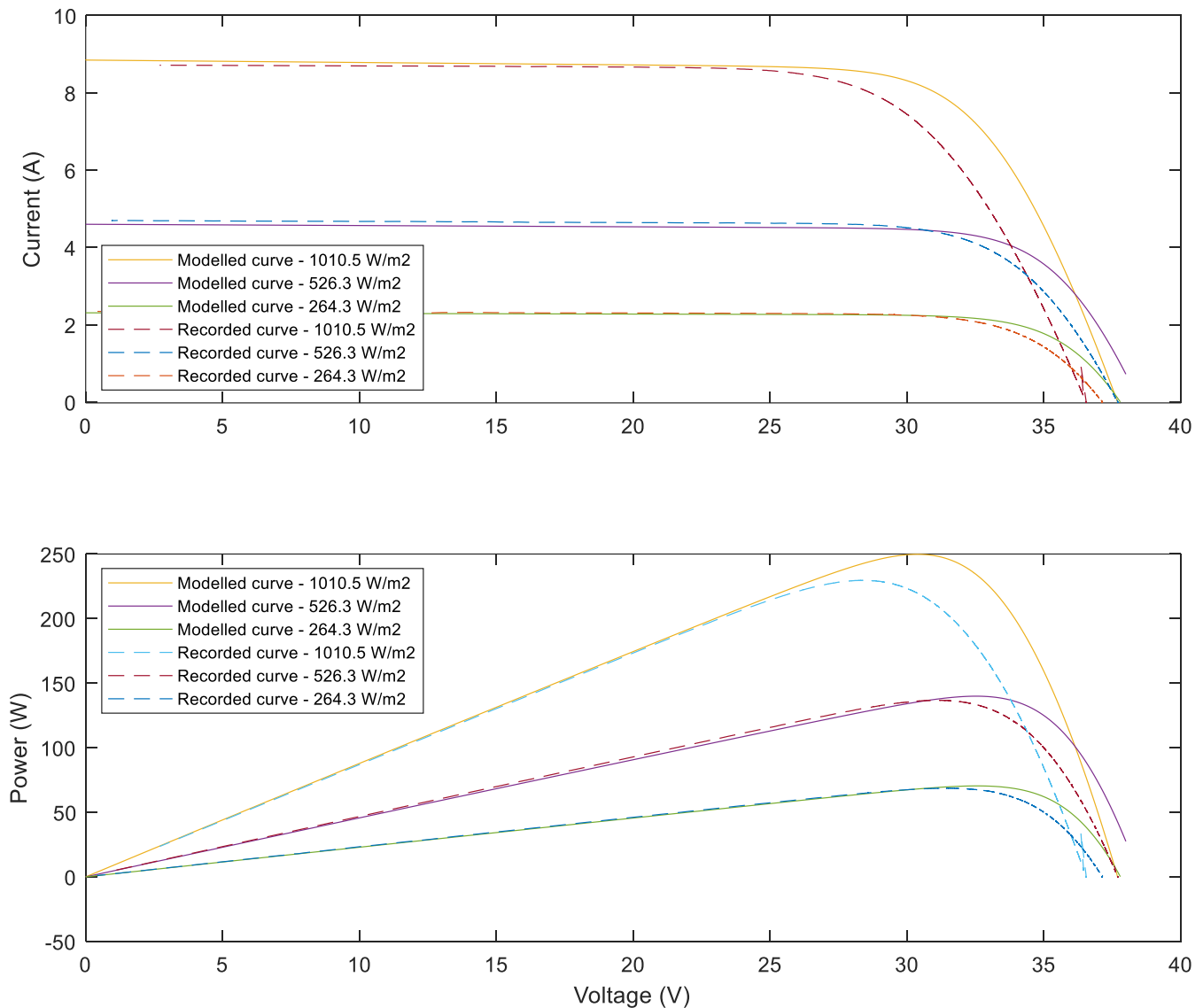
Figure 5.6 - Top graph: Modelled and recorded IV-curves for the TITAN module at different irradiance levels. Bottom graph: Modelled and recorded PV-curves for the TITAN module at different irradiance levels.

In Figure 5.6 the three irradiance levels considered for the TITAN module are similar to the previously modelled example in Figure 5.5. The worst P_{MPP} deviation in this case is 8.1% at irradiance level >1000 W/m², while the best is only different by 2% at <300 W/m². Furthermore, in the last example at irradiance levels of 526.3 W/m², the deviation is only 2.2%. Initially for the TITAN module, in this case the curves align almost perfectly, but as the

recorded curve reaches its P_{MPP} the modelled curve starts to differ more. This situation is under relatively low irradiance conditions (<300 W/m^2), so it could be somewhat affected by shunt resistance losses. Although, for the SunTech 422 module curves visible in Figure 5.7 this is more likely as the irradiance levels are <100 W/m^2. In this lowest irradiance case, the P_{MPP} deviation is at 11%, which is the highest of all the modelled situations. This is a direct result of shunt resistance losses, which is visible on the IV and PV-curves as they do not reach the modelled voltage and current levels. The low irradiance conditions for this case are potentially a direct reason for the shunt resistance losses, as the shunt resistances tends to increase with lower irradiance levels [48, 49].
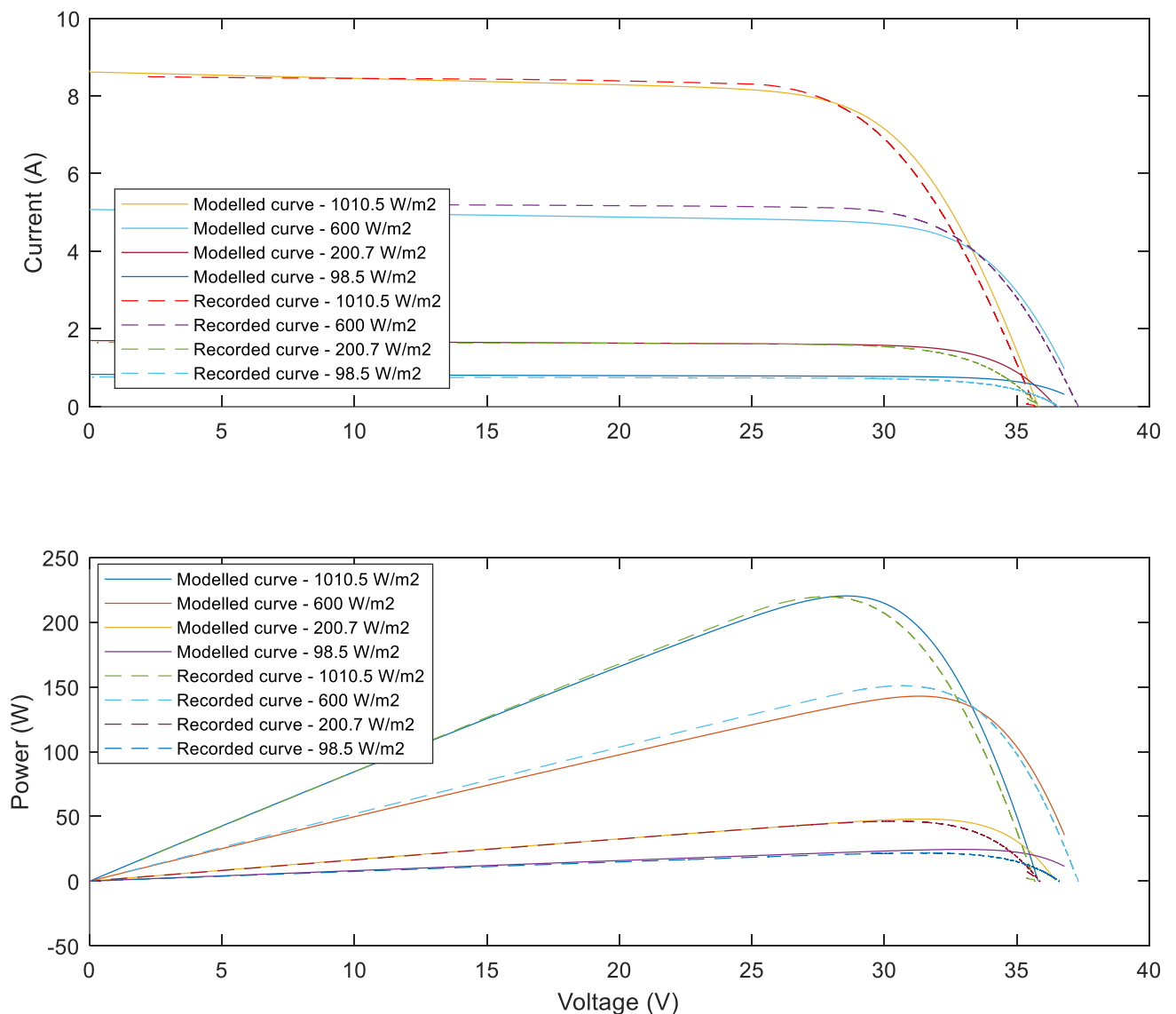
Figure 5.7 - Top graph: Modelled and recorded IV-curves for the SunTech 422 module at different irradiance levels. Bottom graph: Modelled and recorded PV-curves for the SunTech 422 module at different irradiance levels.

To sum up, the general impression is that all the modelled curves, overall does fit quite well, but in some cases the modelled P_{MPP} is larger than the recorded P_{MPP}, and vice versa. This is also the situation where the P_{MPP} deviation is the lowest with only 0.2%, but generally it varies from 0.2-11% for the different simulation cases. These differences are considered to be

low enough to model power losses as the deviations in the recorded IV-curves potentially are even larger when considering snow cover. Therefore, the proposed MATLAB Simulink model is considered satisfactory enough to perform simulations to evaluate power losses, due to different types of snow coverage on PV modules. Furthermore, at low irradiance conditions there is a tendency on the IV and PV-curves that resembles shunt resistance losses. Although only one case with irradiance levels <100 W/m^2 were tested here, it is likely to be more relevant when modelling situations including different types of snow cover. In such cases the irradiance levels may be even lower, but not below 30 W/m^2 as that is the lower irradiance limit set for the system to record IV-curves. The time slots that were modelled were in the periods from December-April, and module temperatures ranged from -5.7°C to 32.8°C.

There is no clear trend for what irradiance levels result in the largest percentagewise P_{MPP} deviations among the three different PV modules tested for validating the MATLAB Simulink model. For instance, the Q-Cells A10156 module simulations the case with highest irradiance levels resulted in the largest deviation. On the other hand, for the TITAN and SunTech 422 module, the lowest irradiance levels resulted in the largest P_{MPP} deviation.

5.6 Modelling uniform snow cover

The modelling of uniform snow cover is necessary to get an idea of how uniform snow cover impacts the IV-characteristics and to test the performance of the model. Understanding how simulation results from such a simple model compares to the recorded IV-curves will be helpful, to identify potential weaknesses, and areas of improvement that can be investigated further. Therefore, a way to do this is by using the available images of the PV modules to figure out the correlation with snow cover. First, as a starting point it is necessary to make some assumptions, such as the snow cover being equally distributed throughout the module surface. In this way it is possible to gradually adjust the irradiance reduction of the simulated snow cover, and test how this will affect the accuracy of the modelled IV-curve. In addition, weather data, such as precipitation will be useful to see how much irradiance levels are reduced due to snow cover and the snow depth. Then it is possible to compare how the recorded IV-curve fits to the simulated IV-curve and evaluate its accuracy. The recorded snow depths are not directly used as input in the MATLAB model but is useful to include to get an understanding of how the power loss correlates to the amount of snow covering the module surface.

The module that is first considered in the simulation to test the simple IV-characteristics model is the Q-Cells A10156 module. The uniform snow cover conditions that are investigated are illustrated in Figure 5.8. For this period, according to meteorological data from SeNorge, the snowfall corresponds to around 13 cm of fresh snow [61]. However, these precipitation values should only be considered an estimate and not exact values. Particularly as the snow cover in Figure 5.8 does not look like 13 cm of snow, and since the accumulation of snow on a module surface tilted 35° is likely to be less than on a flat surface, such as the ground [64].
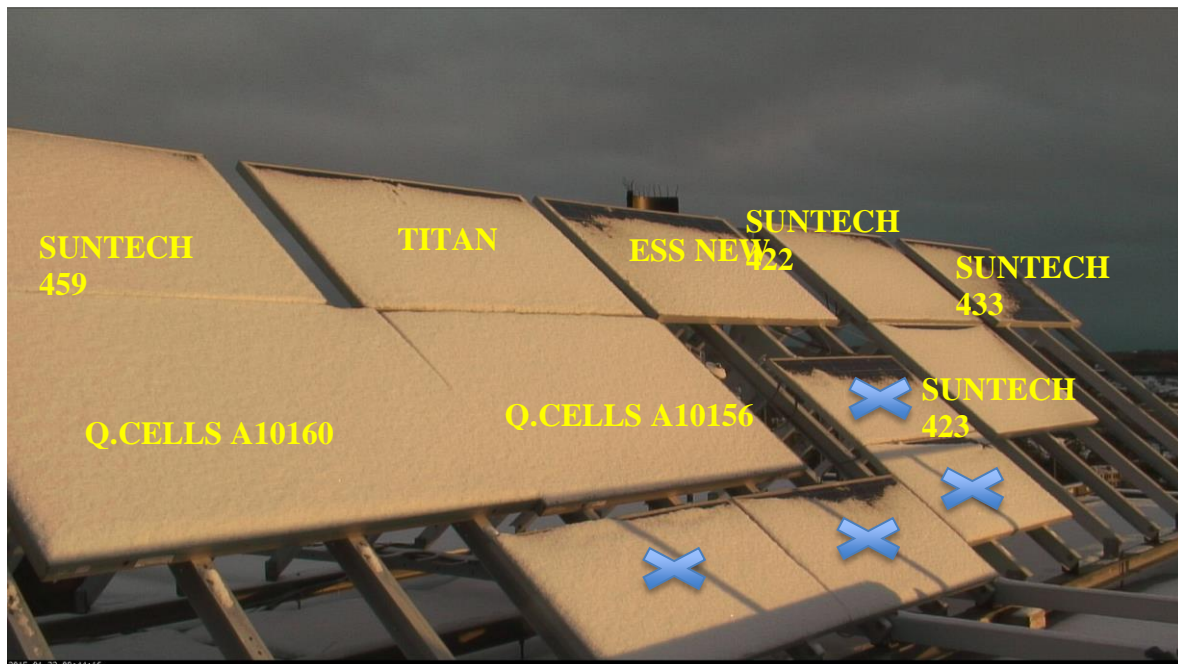
Figure 5.8 – UiA PV research system as of February 2016. Source: UiA PV research system. The modules marked with a blue cross are not in use.

Furthermore, the five simulation parameters calculated in the MATLAB Simulink model based on the Q-Cells A10156 PV module datasheet values from Table 5.1, bypass diode parameters, and the module temperature coefficients, are shown in Table 5.4. The input of these values is at STC for the selected module, and the input window into the model and diode parameters is shown in Figure 5.3 and **Appendix A.1**, respectively.

Similar five-parameter values were found by Hansen et al. [65] for a 240W c-Si PV module, although in this case the shunt resistance R_{SH} was considerably larger. In addition, a study by Song et al. [66] evaluated different methods for estimating the five-parameter values in the single diode equation. The results showed similar values for the majority of the parameters, but not all values as it largely depends on the PV module specifications, which were not specified here [66]. Also, the bypass diode parameter, such as the forward voltage V_F typically range from 0.6 to 0.7 V [53]. Therefore, using the single diode equation values calculated by the MATLAB Simulink model seem reasonable.
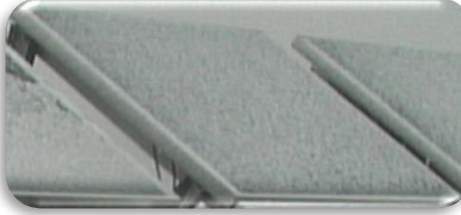
5.7 Investigating the correlation between irradiance and snow depth
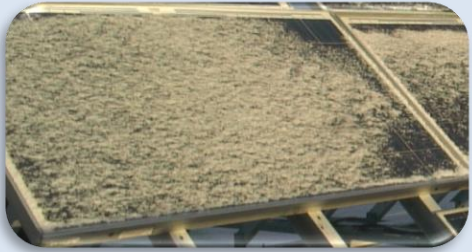
Initially, the first simulations are meant to demonstrate how the IV-characteristics is affected by the uniform snow cover of different snow depths, which blocks most of the incoming irradiance. The recorded IV-curves are compared with the simulated IV-curves that show what the IV-curve would look like without snow cover, but under the same irradiance and temperature conditions. Examining various snow depths is necessary to investigate the correlation between snow depth and power losses. According to a study by Perovich et al. [20] <5% of visible light transmittance was allowed through a snow cover of 10 cm, highlighting the impact that transmittance and snow depth has on the module power output.

Table 5.6 shows the recorded irradiance value, the recorded module temperatures, and the recorded snow depth available from SeNorge [61] for different situations. In this first case, the effects of snow cover on the IV and PV-curves are illustrated with a comparison of the modelled curves without snow and recorded curves with snow. Images of the different PV modules with snow cover is found in **Appendix A.5.** The recorded snow depths are taken from the SeNorge location of the UiA PV research system, although it should be noted that these precipitation values are considered for the ground, and not tilted surfaces like the PV modules. Therefore, the snowfall data from SeNorge should be viewed more as an estimate, and not accurate recorded data.

*Table 5.6 – Recorded module temperature, snow depths, and irradiance data for different PV modules and time periods. Source: UiA PV System, and snow depths from SeNorge [61]. *No recorded snow depths from SeNorge at this day, so 0.3 mm is assumed by looking at images with similar low recorded snow depths (case with 0.6 mm). **No recorded snow depths from SeNorge, 1.0 mm is assumed.*

Date and time	PV Module	Irradiance [W/m^2]	Module Temperature [°C]	Snow depth [mm]	Image of PV module
22/01/2015 09:44	Q-Cells A10156	165.8	-0.40	70	
19/01/2015 11:56	SunTech 423	31.5	-0.60	0.6	
26/03/2015 13:10	TITAN	72.1	3.3	27.9	
23/01/2016 12:00	SunTech 422	35.2	-2.5	1.8	

07/03/2016 10:00	SunTech 423	51.8	4.1	22.4	
17/01/2016 12:00	Q-Cells A10160	618.2	-0.59	3.0	
17/01/2016 12:00	Q-Cells A10156	618.2	5.8	3.0	
12/12/2017 10:00	SunTech 423	178.3	1.45	0.5	
03/03/2016 08:56	SunTech 433	75.0	0.39	45.6	
22/03/2015 11:44	SunTech 422	59.6	0.48	0.3*	

15/12/2015 10:19	Q-Cells A10160	213.8	0.96	2.0	
19/01/2015 10:57	SunTech 422	56.3	5.4	1.0**	

The snow covers visible on the images of the tilted PV modules for the different situations in Table 5.6 clearly illustrate that there is insufficient correlation between the recorded snow depths from SeNorge.

The modelling results showing a comparison between the modelled and recorded IV-curves based on data in Table 5.6 are displayed in Figure 5.9. The impact of the snow cover on the IV-curves is clearly visible as there is a distinct difference between the modelled and recorded curves. The measured current for the snow-covered curves is significantly lower compared to the modelled snow free curves. However, all the modelled curves without snow cover have their distinctive shape, but with some PV modules performing better and having a higher output than others. This is certainly due to different irradiance and module temperature values being used as the module input, and where a higher irradiance value results in a higher current. The three cases involving the SunTech modules are almost overlapping because they have similar irradiance values as the model input. As irradiance is one of the two input factors it has a large impact on the modelled I_{SC} in snow free conditions. On the other hand, the recorded IV-curves show a different picture as the highest irradiance situation is not the case with largest I_{SC}, due to the snow cover. The reduction in irradiance reaching the PV cells shows just how substantial the impact of snow cover is on the power output of the PV module. Furthermore, two of the IV-curves show signatures of bypass diode activation, likely since the module snow cover is not completely uniform in these two situations.
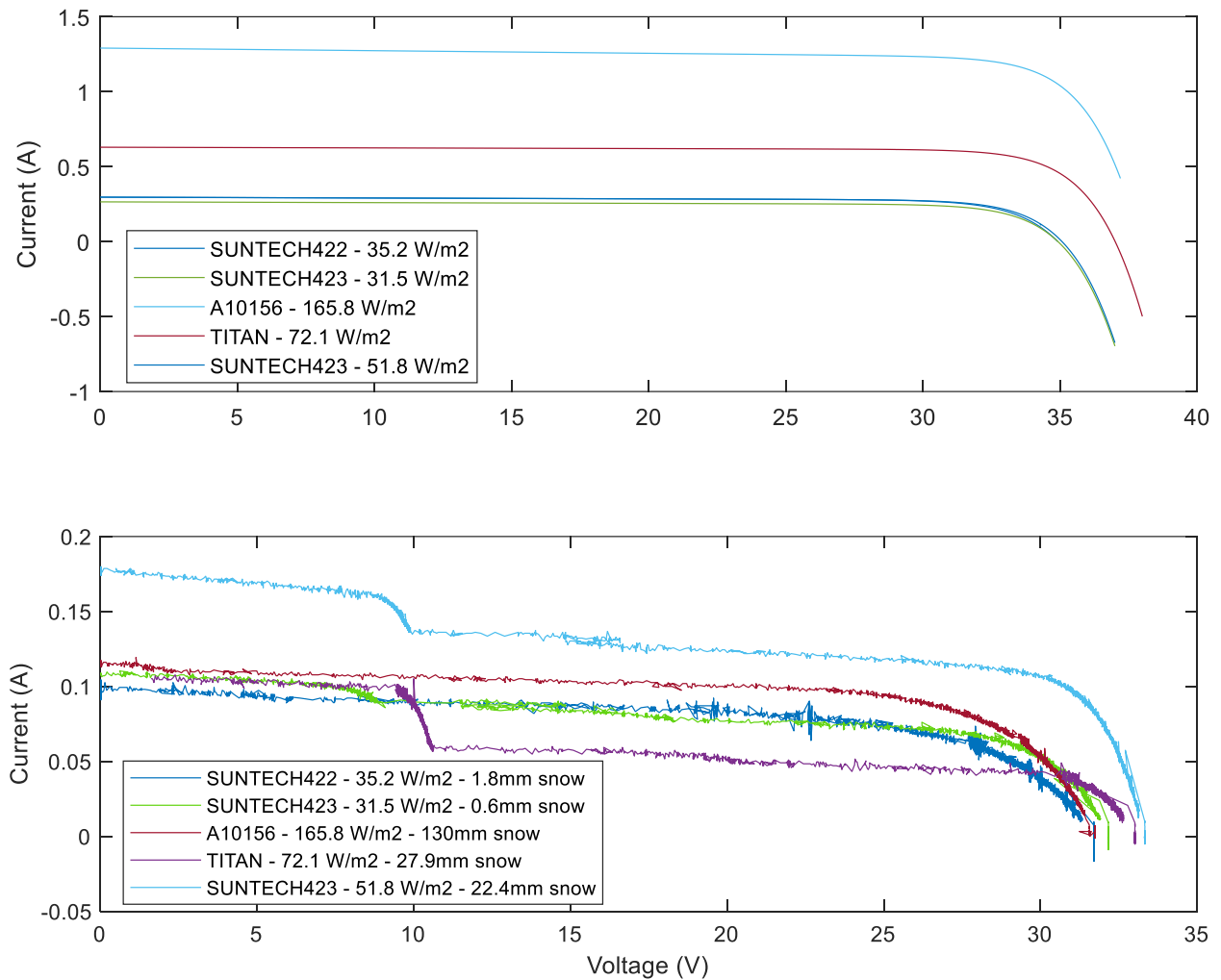
*Figure 5.9 – Top graph (no snow cover): Modelled IV-curves for different modules at various irradiance levels without any module snow cover. Bottom graph (snow cover): Recorded IV-curves at the same irradiance levels, but with actual snow cover at different snow depths. Source: UiA PV System. Figure created by author. **Note the different x-axis in the two figures.***

Figure 5.10 shows the modelled PV-curves versus the recorded ones for various irradiance levels and snow depths. This situation has very low irradiance conditions resulting in small currents, and obviously low power outputs, with the highest recorded P_{MPP} value being just 38.6 W. Overall, all the recorded curves with modules covered by snow produce similar low P_{MPP}, which ranges from 1.5-38.6 W.
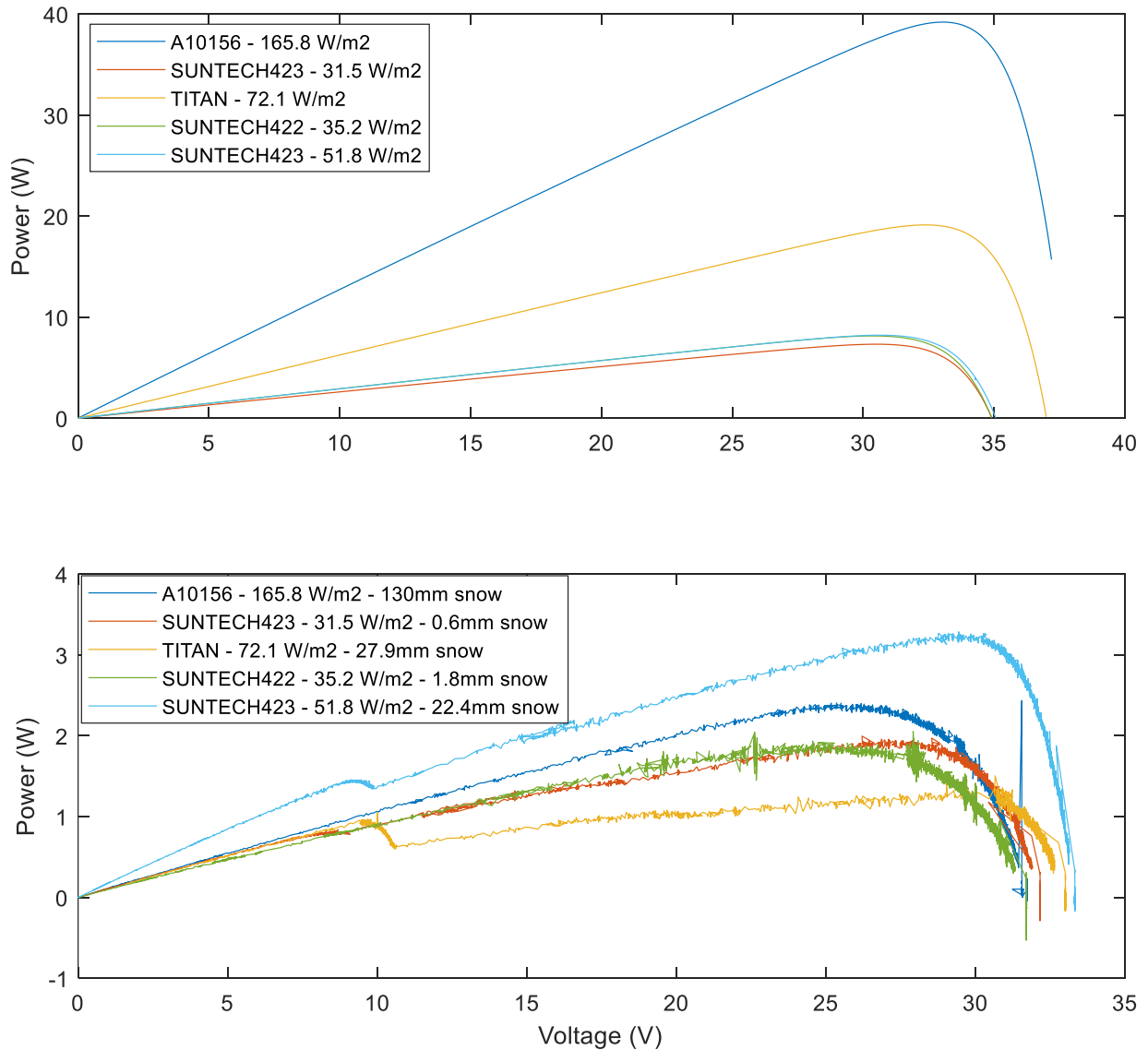
*Figure 5.10 – Top graph (no snow cover): Modelled PV-curves for different modules at various irradiance levels without any module snow cover. Bottom graph (snow cover): Recorded PV-curves at the same irradiance levels, but with actual snow cover at different snow depths. Source: UiA PV System. Figure created by author. **Note the different x-axis in the two figures.***

Calculated reductions in P_{MPP} when comparing the simulated snow-free and recorded snow-covered curves is displayed in Table 5.7. The P_{MPP} reduction ranges from 19-97% depending on the irradiance/snow depth for each case. However, it should be noted that recorded snow depths/precipitation from SeNorge [61] involve a high degree of uncertainty, as being completely sure that this amount of snow is present on the module surface is challenging. The behavior of snow is very complex to model and would ideally require additional parameters, such as snow transparency and its variability with different types of snow to model it accurately. In addition, interpreting this from images alone is difficult, but nevertheless it should give some indication as to how irradiance correlates with snow depth on the PV module surface.

Table 5.7 – P_{MPP} simulation results for various time periods with and without snow for different PV modules and snow cover depths.

Date and time	PV Module	Modelled P_{MPP} without snow [W]	Recorded P_{MPP} with snow [W]	P_{MPP} reduction [%]	Snow depth [mm]
22/01/2015 09:44	Q-Cells A10156	39.2	2.4	93.9	70
19/01/2015 11:56	SunTech 423	7.3	2.0	72.6	0.6
26/03/2015 13:10	TITAN	19.1	1.5	92.2	27.9
23/01/2016 12:00	SunTech 422	8.1	2.1	74.1	1.8
07/03/2016 10:00	SunTech 423	8.2	3.3	59.8	22.4
17/01/2016 12:00	Q-Cells A10160	152.2	13.9	90.9	3.0
17/01/2016 12:00	Q-Cells A10156	145.5	11.5	92.1	3.0
12/12/2017 10:00	SunTech 423	44.1	1.53	96.5	0.5
03/03/2016 08:56	SunTech 433	18.2	2.45	86.5	45.6
22/03/2015 11:44	SunTech 422	14.2	11.6	18.8	0.3
15/12/2015 10:19	Q-Cells A10160	51.4	38.6	24.9	2.0
19/01/2015 10:57	SunTech 422	13.1	5.5	58.0	1.0

The correlation between the estimated snow depth on the module surface and the reduction in P_{MPP} is plotted and displayed in Figure 5.11. Only five cases were chosen as it was difficult to find situations with available data and uniform snow cover as IV-curves for irradiance levels below 30 W/m^2 are not recorded. Additionally, a considerable amount of work is necessary to process the data and extract relevant information. Although, this is just based on 12 different situations, the relationship between snow depth and P_{MPP} reduction should still give an indication of how they correlate. On the other hand, when comparing two among the five cases there are two situations where the recorded snow depth is 22.4 mm and 27.9 mm, however the P_{MPP} reduction is 59.8% and 92.2%, respectively. Even though there is an irradiance difference between the two, this is not large enough to result in differences of this magnitude. For the two cases of minimal snow cover (0.6 mm and 1.8 mm) the P_{MPP} reduction is relatively equal between the two. Moreover, the two cases with the deepest snow covers produce similar reductions in P_{MPP}, although the difference in recorded snow depths are significant, but is compensated by higher irradiance levels.
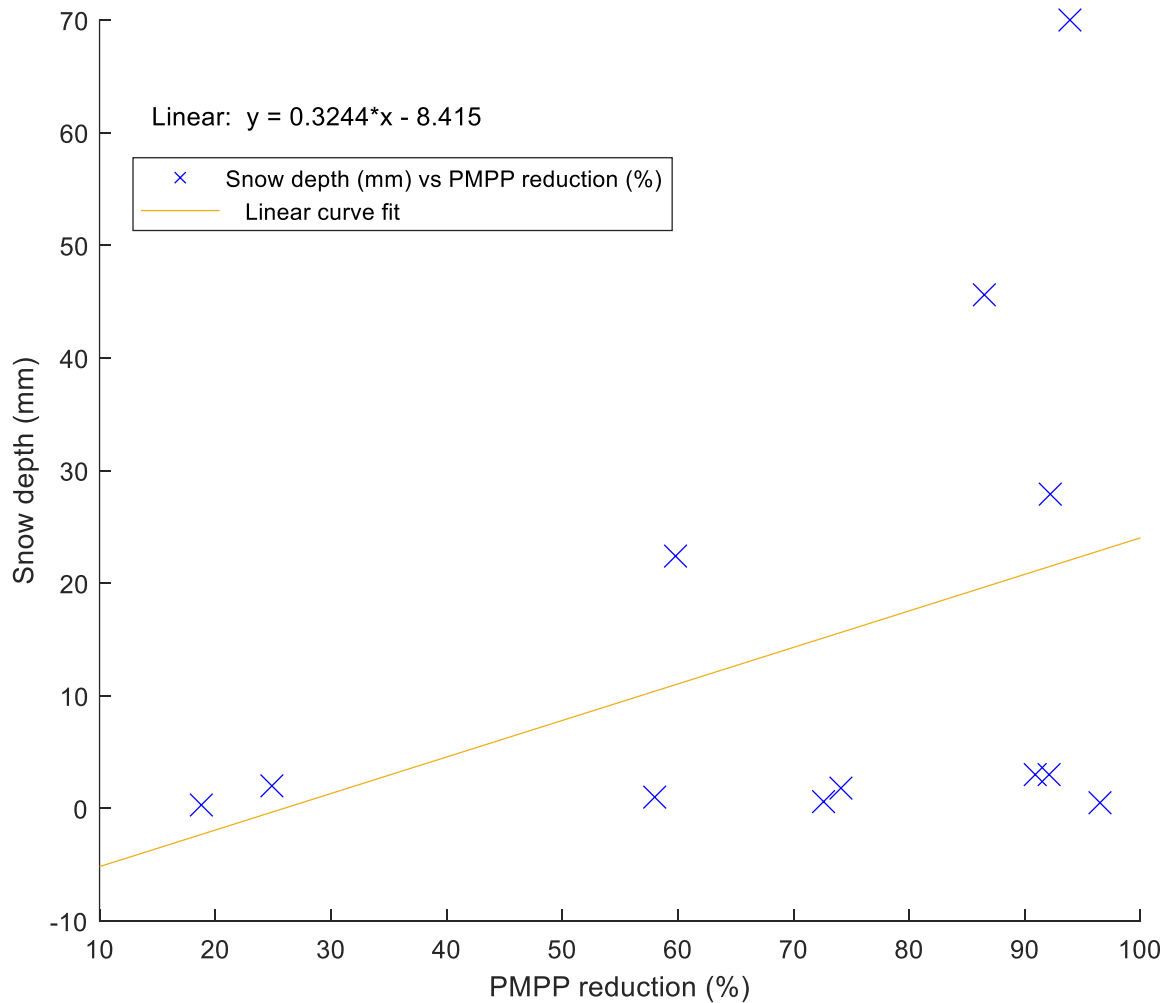
Figure 5.11 – Linear curve fit to investigate correlation between snow depth and P_{MPP} reduction based on the twelve simulated cases. Figure created by author.

5.8 Image Analysis with MATLAB IPT and IRA

The MATLAB Simulink model showed reasonable satisfactory results when modelling power loss for cases with uniform snow cover. Furthermore, an alternative approach is considered, which utilizes image analysis to estimate the snow-covered area on a PV module surface. For partial snow cover situations, the calculated percentage module snow cover is used as input to the IV-characteristics replacing the module substring irradiance reductions adjusted by a trial-and-error approach, see subchapter 5.1. This is done to determine if percentage snow coverages estimated through image analysis could improve the accuracy of the IV-curve power loss estimations. The methodology described here and in the following subchapters explains how the image analysis is completed with only module images as input. The thought is that by using the image processing toolbox available in MATLAB, PV modules areas can be detected first in clear sky conditions, and then in situations with variations of partial snow cover. The difference between the clear sky/snow covered module area makes it possible to identify what percentage of the module surface is covered by snow.

A visual inspection of the available images is considered the simplest approach to estimate how much of the PV module surface is covered by snow in different situations. However, the accuracy with such a method is time consuming and largely affected by human error. Therefore, an improved module area identification method is proposed that uses the image processing toolbox available in MATLAB.

Initially, the images are converted from RGB to hue-saturated-value (HSV) colour space because it describes colour, similar to how it is perceived by the human eye. Additionally, with RGB colour space we cannot differentiate between colour information from luminance, but this is possible with HSV and is the reason why the conversion is necessary [67]. The next step involves another conversion from HSV colour space to greyscale, which is necessary because the next step (binarization) requires this image input format. Furthermore, it is a way of compressing the image so less information is necessary for each pixel. As a result, the greyscale images reduce the computational requirements when using image analysis algorithms, allowing for faster and better performance [68]. Figure 5.12 illustrates the conversion of the image is first converted to HSV and then to greyscale.

With the image converted to greyscale a binarization can be done to identify non-module and module colours. The default method used by the MATLAB function "imbinarize" is the Otsu's method, which is an image processing thresholding algorithm that separates pixels into foreground and background classes [69]. In this way it is possible to separate out the areas containing the PV modules from other parts of the image. The MATLAB code used here is shown in **Appendix A.8**. This image binarization is also required as input to the "Image Region Analyzer" (IRA), which can then be used to detect the PV module areas from the available images without snow, to determine the total area of the PV module. A "fill-holes" function is used in IRA as it allows for some level of correction if some parts of the image were identified as a background instead of foreground class, allowing for a better estimation of the different PV module areas.

Furthermore, this can then be used as a baseline area for each module without snow cover, and now that this is established, the same procedure is repeated for images with different variations of partial snow cover. Thus, allowing for a comparison between the area of the module being covered/uncovered. The binarized, improved image, and the finalized image with identified module areas is shown in Figure 5.13. The identified module areas are given as the number of pixels in the filled area.

5.9 Image processing method

- Import selected images to MATLAB. As the images are taken from a fixed camera position the images can be used without any pre-processing of the images being necessary.
- Selection of a clear sky image of the PV system without any reflection on the module, to identify each individual module area.
- Image is converted into hue-saturation-value (HSV) before being converted again to greyscale.
- Binarization of the image to separate background and foreground classes. Processing of image to improve module area estimation accuracy using the "Image Region Analyzer".
- Utilize IRA to identify the baseline PV module area.
- Import different images with partial snow cover to estimate module area covered by snow and compare this with estimated baseline PV module area.

A similar approach is used by Pearce et al. [35], however in their study the borders of the PV modules in the binarized images were identified by using a contour algorithm. This was also considered, but the areas of the PV modules proved to be identified without the use of a contour algorithm directly. Hence, the image is binarized using the Otsu's thresholding algorithm, and not a contour algorithm, which is considered simple to implement [69].

However, in some of the cases the binarization of the image proved difficult, making it necessary to utilize the active contour function available in the Image Segmenter (IS) tool. It uses either a region-based or edge-based active contour segmentation method to refine the mask of the PV modules more thoroughly. Otherwise, many of the modules are identified as one large area instead of multiple smaller ones, making it challenging to detect the correct module area. In this case the contour algorithm runs through several iterations and identifies the borders of the PV modules more clearly, so they can be identified as separate module areas when using the IRA. Furthermore, the usability also depends on the types of images, and the background in the images being analyzed [70]. In another study by Pearce et al. [8] the detection of snow on PV modules is done based on the conversion of images to greyscale and binarization, similarly to the image processing method described above.
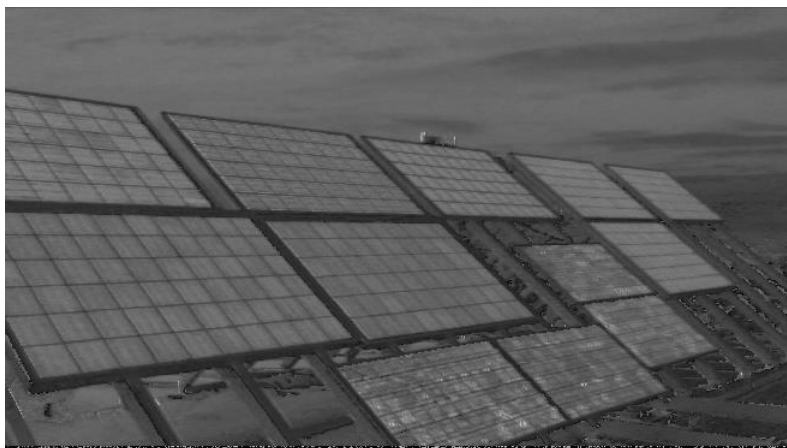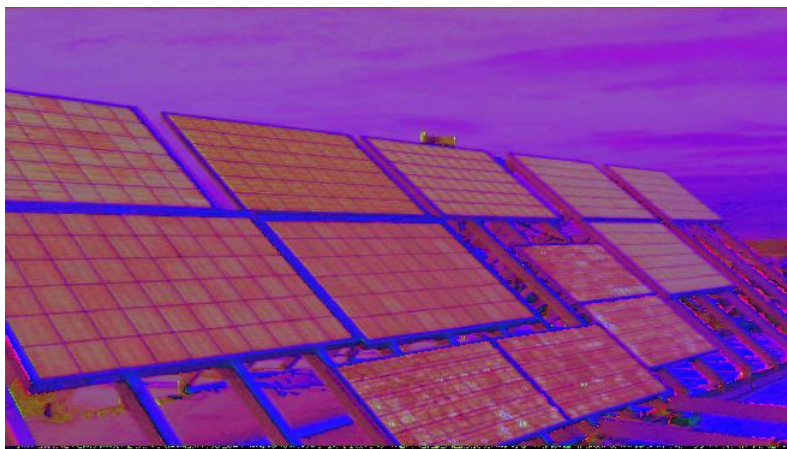
Figure 5.12 – Top image: Original image RGB color space. Middle image: image converted to HSV color space. Bottom image: HSV image converted to greyscale.

Noticeable from Figure 5.13 there are some small sections where the detected pixels are identified as black instead of white. This results in the estimated PV module area being slightly lower than it should be as but compared to the entire module area it is minimal. However, this only seems to be the case for the modules that are closest to the camera.
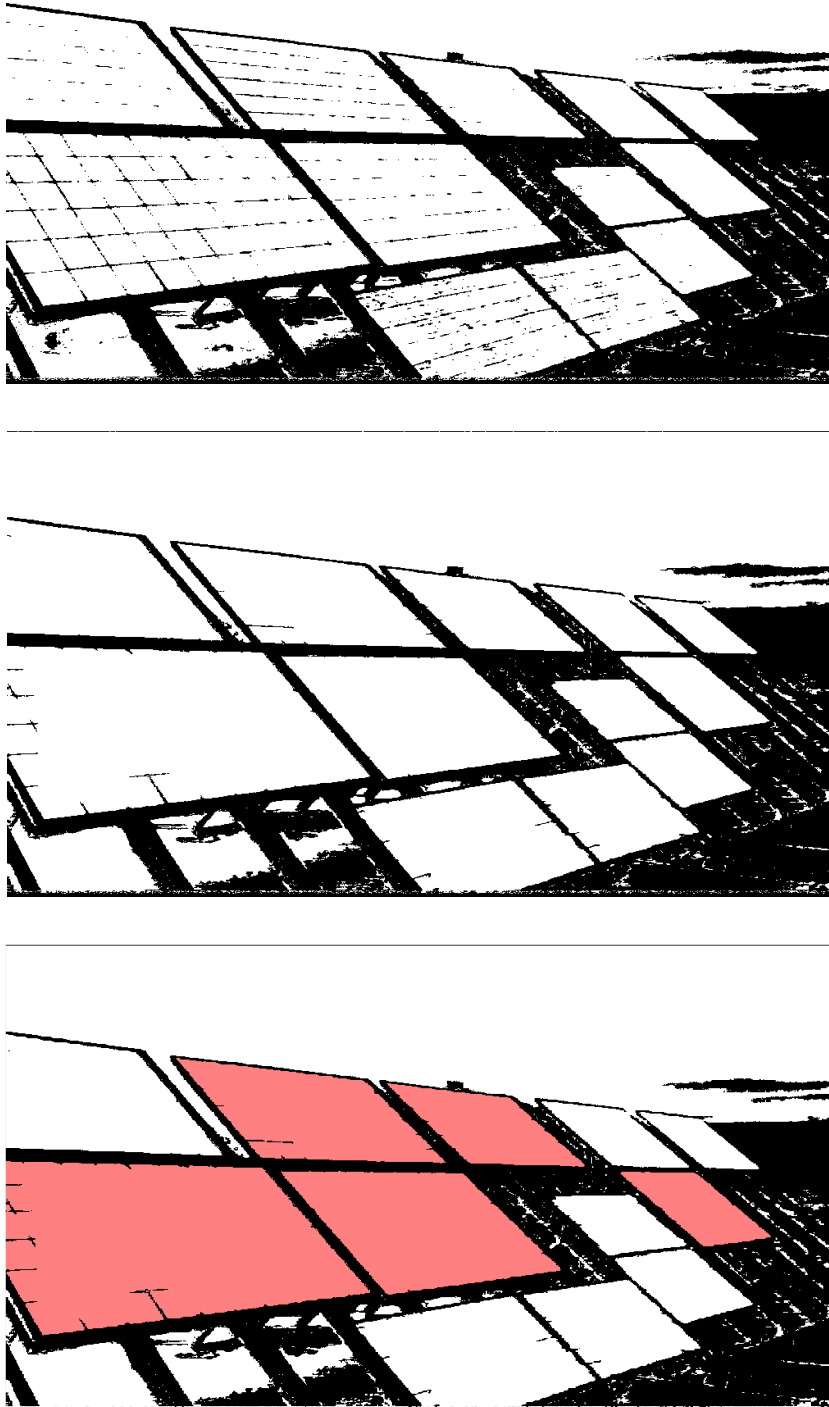
Figure 5.13 – Top image: Binarized image. Middle image: improved binarized image. Bottom image: image of several identified module areas.

The estimated PV module pixel values using IRA in MATLAB are listed in Table 5.8. It is noticeable that the pixels values do not necessarily correspond to their actual physical area, e.g., the considerable pixel value difference between the two Q-Cells modules. As one would expect similarly sized modules to have an equal number of pixels, but it is likely that the angle at which the images are taken influences this. However, because all the images that are used are taken from the same angle this will not have any negative impact.

43

Additionally, this methodology needs more work to be improved as the detection of the modules are not flawless in all weather conditions. For example, detecting modules in cloudy weather conditions proved to be challenging, making it most applicable for partial snow cover in relatively clear sky conditions. A more optimal camera angle would certainly improve the detection of PV module areas, but further development beyond that is necessary. On the other hand, this method is just considered as a demonstration that image analysis can be a useful tool for estimating power loss.

Table 5.8 – The estimated pixels in filled module areas using IRA in MATLAB.

PV Module	Estimated pixels in filled module area
Q-Cells A10156	111 326
Q-Cells A10160	249 047
SunTech 422	23 985
SunTech 433	15 211
SunTech 423	28 983
TITAN	84 305

Figure 5.14 shows an image of the PV system where the active contour segmentation method has been used to improve the detection of the PV module borders. Comparing this image with the previous ones from Figure 5.13 there is a clear improvement in the detection of module borders.
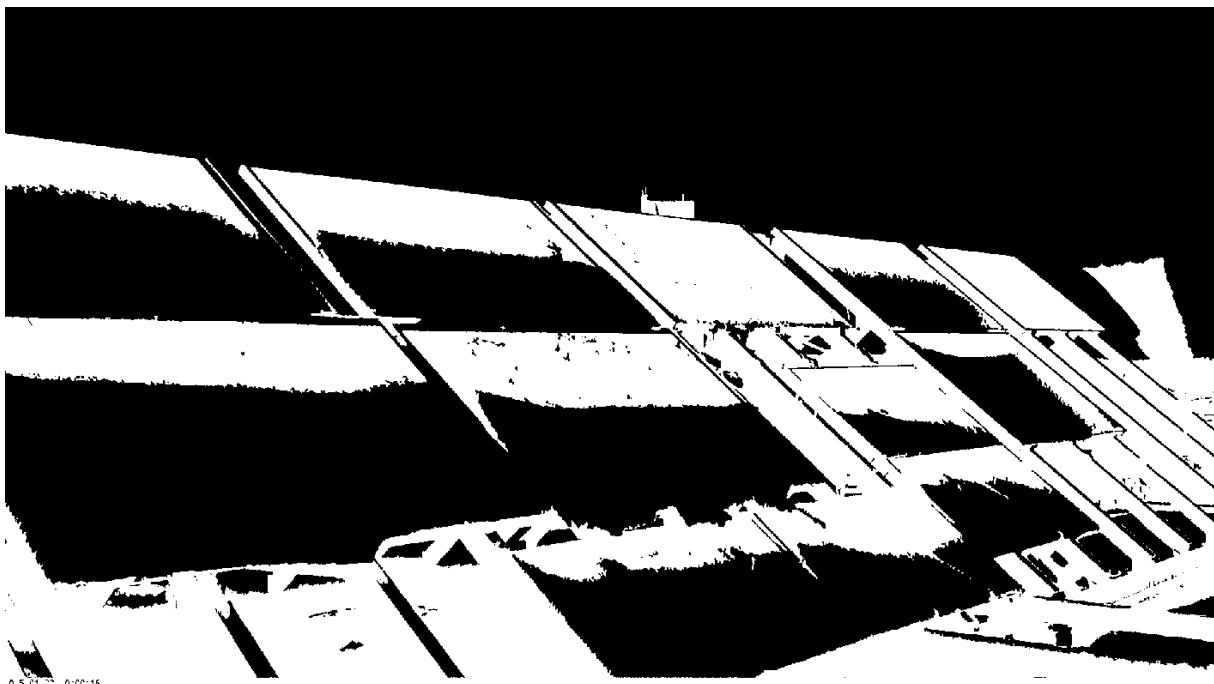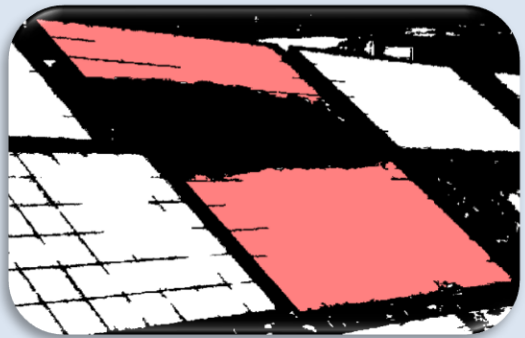
Figure 5.14 – Binarized image of the PV system with improved module borders using the active contour segmentation method in Image Segmenter (IS).

5.10   Estimating PV module areas under partial snow cover

The baseline PV module pixel area for different modules has been established in subchapter 5.9. The next step is to estimate the number of snow pixels in situations with partial module snow coverage and calculate how much of the module surface is covered by snow. The percentage of module snow cover is calculated by first taking the number of pixels estimated on the module under partial snow cover, shown in Table 5.9 and dividing it by the estimated pixels in the module area without snow cover, from Table 5.8. The result is a percentage of the area of the module that is considered free of snow. Therefore, by subtracting this value from 100% an estimated module area covered by snow is found. The original images of the PV modules for each case are displayed in **Appendix A.7**.

The estimated module snow cover for the different situations ranges from 11-80%, but there are cases where the module busbars are identified by the algorithm as snow. Leading to a slightly larger area being recognized as snow, instead of the module area. However, by looking at the images of the studied examples in Table 5.9, this is considered to have minimal impact on the estimated module snow cover. By visually studying the detected areas of snow cover, and making rough estimations, it seems that the area estimated when using MATLAB is reasonable accurate.

Table 5.9 – Estimated module pixels with snow cover and the calculated percentage of module snow cover.

Date and time	PV Module	Estimated module pixels	Estimated module snow cover [%]	Module image
27/03/2015 08:10	Q-Cells A10156	99 166	11	
27/03/2015 08:10	TITAN	36 737	56.4	TITAN (top) and A10156 (bottom)
23/01/2015 10:00	Q-Cells A10156	42 651	61.7	
23/01/2015 10:00	Q-Cells A10160	57 996	76.7	A10160 (left) and A10156 (right)
23/01/2015 10:00	SunTech 422	11 567	51.8	
25/04/2016 13:11	Q-Cells A10156	70 178	37.0	
25/04/2016 13:11	Q-Cells A10160	151 391	39.2	A10160 (left) and A10156 (right)
17/01/2016 12:42	SunTech 422	4640	80.6	
17/01/2016 12:42	SunTech 423	9286	68.0	SunTech 422 (top) and SunTech 423 (bot.)

5.11   Estimating snow coverage on individual cell/substring level

The estimation of the snow cover percentage of the PV module area using image analysis proved to be feasible. However, with this method it is not possible to estimate which cells/substrings are responsible for how much of the power reduction due to the snow cover. Therefore, the image analysis is expanded further to investigate how many cells of each substring that is covered. The previous partial snow cover model utilized an input for percentage of snow coverage for each module substring based on trial-and-error to find the best fit. However, by expanding the image analysis method the snow percentage coverage for each substring can be estimated automatically. Although, it should be noted that even as the percentage of coverage of individual cell areas is identified, there is still a large error margin as the snow transmittance will have a major impact on the power output from each cell, besides the percentage covered.

Similarly, to the previous method, described in subsection 5.9, for identifying the PV module pixel values, a clear sky image is used to estimate the baseline pixel value that will be used as a comparison. Based on this image and the selected module the mask is manually drawn as accurate as is possible. With the created module mask applied to the image the entire module area is cropped before being converted to a binarized format. Furthermore, like before the binarized image is imported to IRA where it detects the pixel values for each individual cell. The images showing this process is shown in Figure 5.15, and the calculated pixel values the Q-Cells A10156 and TITAN module are found in Table 5.10 and Table 5.11. The MATLAB code used to do this is shown in **Appendix A.9**.

Table 5.10 – Calculated Q-Cells A10156 PV module pixel values for each individual cell in each substring, from left to right, and total pixel area value.

Substring 1 (pixel area)										Total
1954	1679	1587	1495	1399	1141	1155	1177	930	776	27 125
2017	1798	1634	1545	1508	1193	1178	1249	838	872	
Substring 2 (pixel area)										
2107	1952	1739	1582	1581	1304	1262	1181	1087	869	30 067
2191	2006	1866	1666	1568	1496	1393	1104	1244	869	
Substring 3 (pixel area)										
2350	2128	1999	1784	1655	1456	1513	1178	1136	1072	33 733
2628	2174	2022	1938	1736	1695	1471	1258	1335	1205	

For some of the situations where there is snow present on parts of the PV module, it is necessary to use the contour algorithm available in IS. It improves the detection of the individual cell borders and enhances the separation of background and foreground values in the binarized image. Thus, making it easier to distinguish the cell pixel values from the snow cover pixel values. First, the 60-cell mask is applied to the image before binarizing it, and then running the contour algorithm.
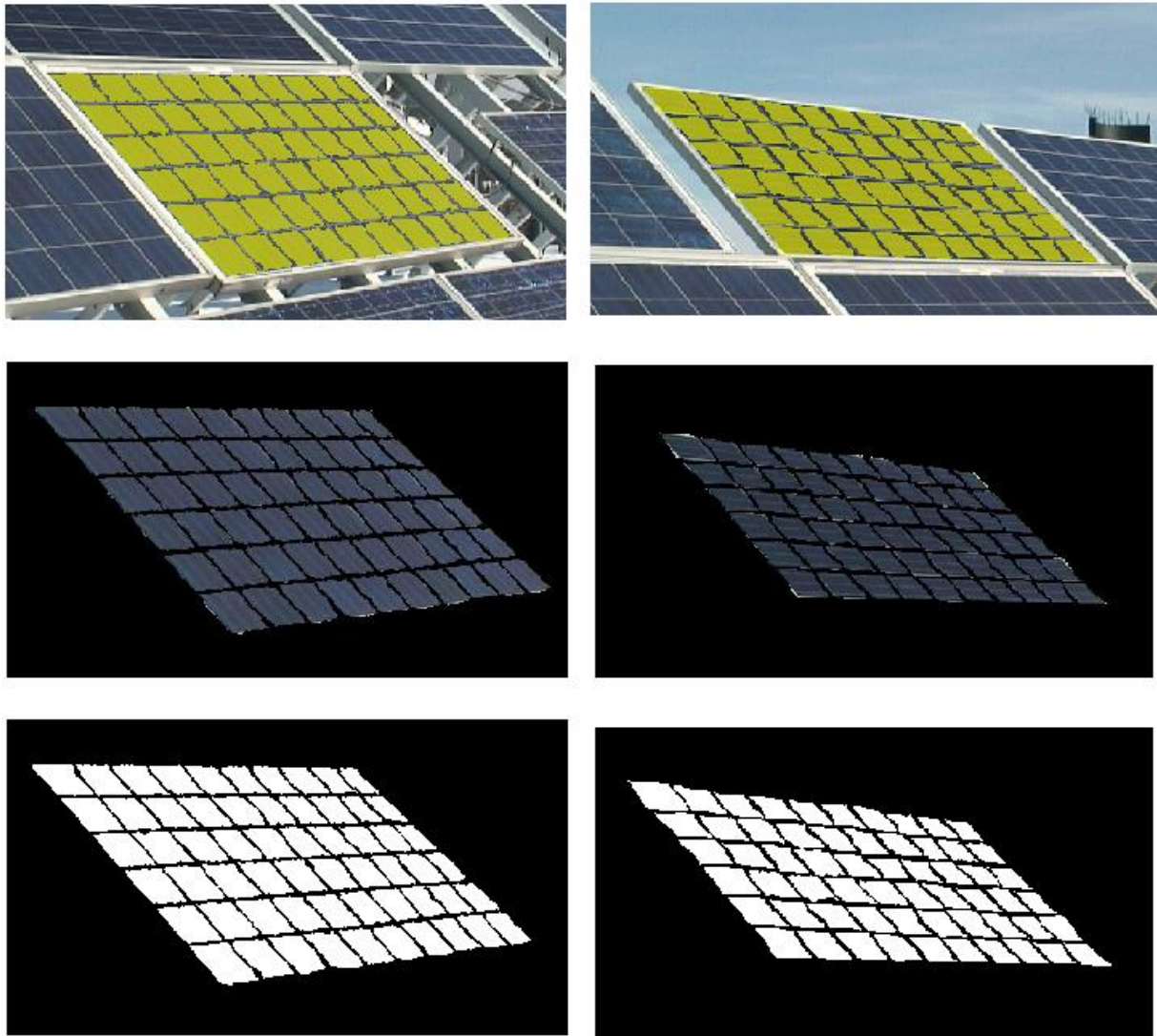
Figure 5.15 – Q-Cells A10156 PV module (left) and TITAN PV module (right), created mask to identify individual cell pixel values. Top image: Created module mask fitted to module surface. Middle image: Cropping the relevant module area. Bottom image: Binarized image of the created PV module mask.

Table 5.11 - Calculated TITAN PV module pixel values for each individual cell in each substring, from left to right, and total pixel area value.

Substring 1 (pixel area)										Total
1918	1299	1095	1107	967	920	958	745	725	630	20 425
1402	1259	1075	1188	1017	985	928	738	737	732	
Substring 2 (pixel area)										
1480	1225	1119	1325	1059	890	807	899	752	816	21 589
1720	1396	1252	1229	1220	1056	879	857	871	737	
Substring 3 (pixel area)										
1650	1392	1328	1215	1245	1149	1169	921	905	1046	23 833
1719	1573	1357	1269	1174	1007	964	951	825	974	

6. Results

The results presented in this chapter are based on the modelling of IV-characteristics for different cases of uniform and partial snow cover. Furthermore, findings from the conducted image analysis are presented, and an assessment of its feasibility for estimating power losses due to PV module snow cover. A comparison of simulated IV-curves with a modelled snow cover, and recorded IV-curves with actual snow cover, for different situations with various snow covers is presented. In addition, the feasibility of using the estimated substring snow cover percentage from the image analysis in the IV-curve model is evaluated. The estimated percentage snow coverages are utilized in situations with partial snow cover, as opposed to using a trial-and-error approach.

6.1 Modelling uniform snow cover

After validating the model and testing out the correlation between irradiance and snow depth, the next step is to test how cases with modelled snow cover compares to actual recorded cases with snow cover. As specified earlier in this case an equal reduction in irradiance must be applied to the MATLAB Simulink model for each substring. Obviously, as these cases consider snow cover on PV modules, this corresponds to very low light conditions, which has a very distinct effect on the IV- and PV-curves. A variety of situations with different irradiance values and snow depths are also considered in this case, an overview of these is presented in Table 6.1. The results presented here are based on the methodology explained in subchapter 5.7. An educated guess of the irradiance reduction is done by visually inspecting the module images with snow cover and based on the correlation between snow depth and transmittance reduction identified in literature [20]. Based on the IV-curve simulation results the irradiance reduction is then adjusted with a trial-and-error approach until a reasonable curve fit is achieved.

Table 6.1 – Simulated situations with uniform snow cover on PV module surface, including irradiance, module temperature, snow depth, and estimated irradiance reduction values.

Date and time	PV Module	Irradiance [W/m²]	Module Temperature [°C]	Snow depth [mm]	Irradiance reduction [%]
22/01/2015 09:44	Q-Cells A10156	165.8	-0.4	70	95
17/01/2016 12:00	Q-Cells A10160	618.2	-0.6	3.0	90
17/01/2016 12:00	Q-Cells A10156	618.2	5.8	3.0	90
11/12/2017 14:30	SunTech 433	35.7	0.7	0.5	87
12/12/2017 10:00	SunTech 423	178.3	1.5	0.5	96
21/01/2015 14:20	TITAN	49.7	0.3	21	90

07/03/2016 09:40	SunTech 422	100.5	0.6	22.4	80
03/03/2016 08:56	SunTech 433	75.0	0.4	45.6	85

The modelling results and comparison of the first case with the Q-Cells A10156 module IV and PV-curves are displayed in Figure 6.1. The IV-curve is modelled using the methodology described in subchapter 5.6, which uses irradiance and module temperature as input and visual inspection of module image, and IV data to generate the recorded IV-curve.
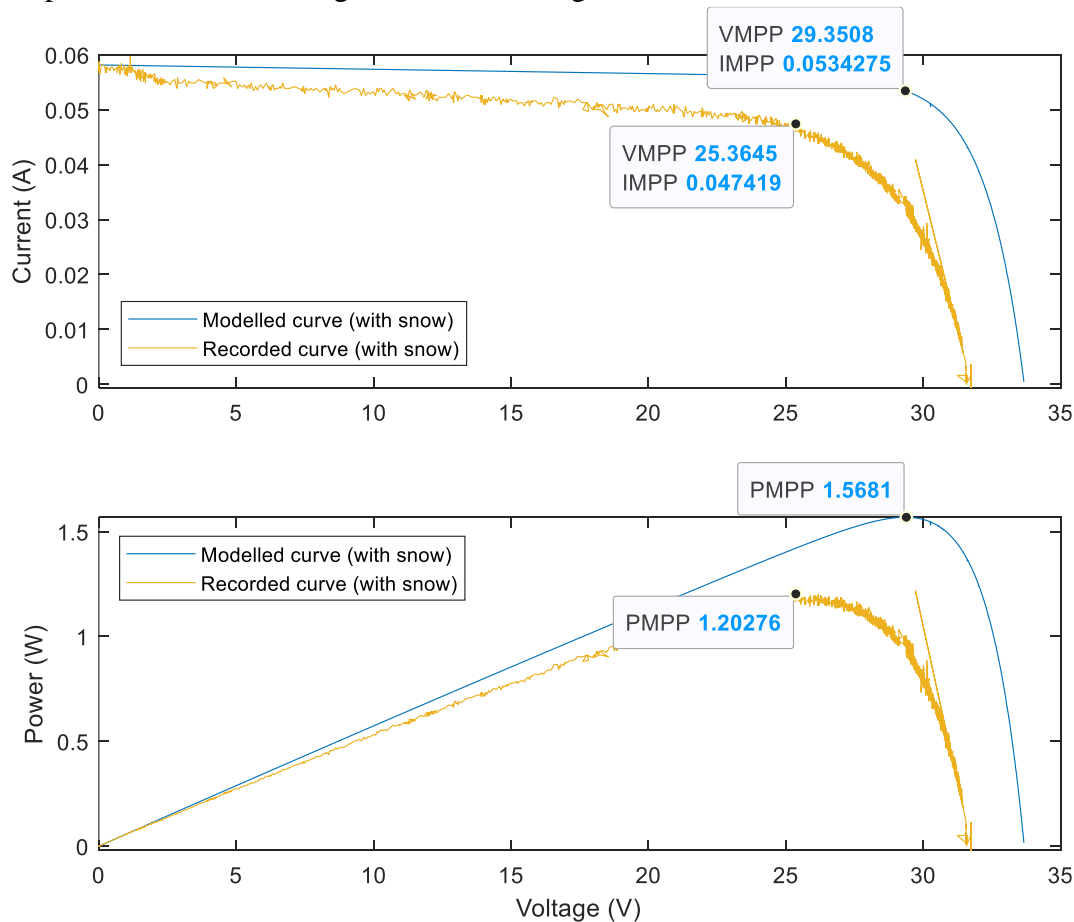
Figure 6.1 – Modelled IV and PV-curves versus recorded curves for uniform snow cover. Source: UiA PV System.

In this case the shape of the modelled IV-curve fits somewhat to the recorded curve, although the latter does not reach the same P_{MPP} level as the former. For the modelled IV-curve the P_{MPP} reaches 1.57 W compared to the recorded curve P_{MPP}, which is only 1.2 W, resulting in a difference of around 23.6%. However, the absolute P_{MPP} deviation is only 0.3 W. The difference in the modelled curve shape is somewhat affected by the V_{OC} not reaching the same levels as the recorded curve. A similar voltage deviation was observed for two of the modules (A10156 and TITAN) when validating the IV-curve model without snow cover in subchapter 5.5. The voltage deviation occurred for both low and high irradiance values.

Therefore, for this case the simple model is not very accurate, although it should be noted that the main comparison has been on the P_{MPP} and how the overall shape of the modelled curve

compares to the recorded one. Potentially, different weather conditions, such as situations
with higher irradiance and module temperatures will prove to be more advantageous when
trying to model the IV-curve.
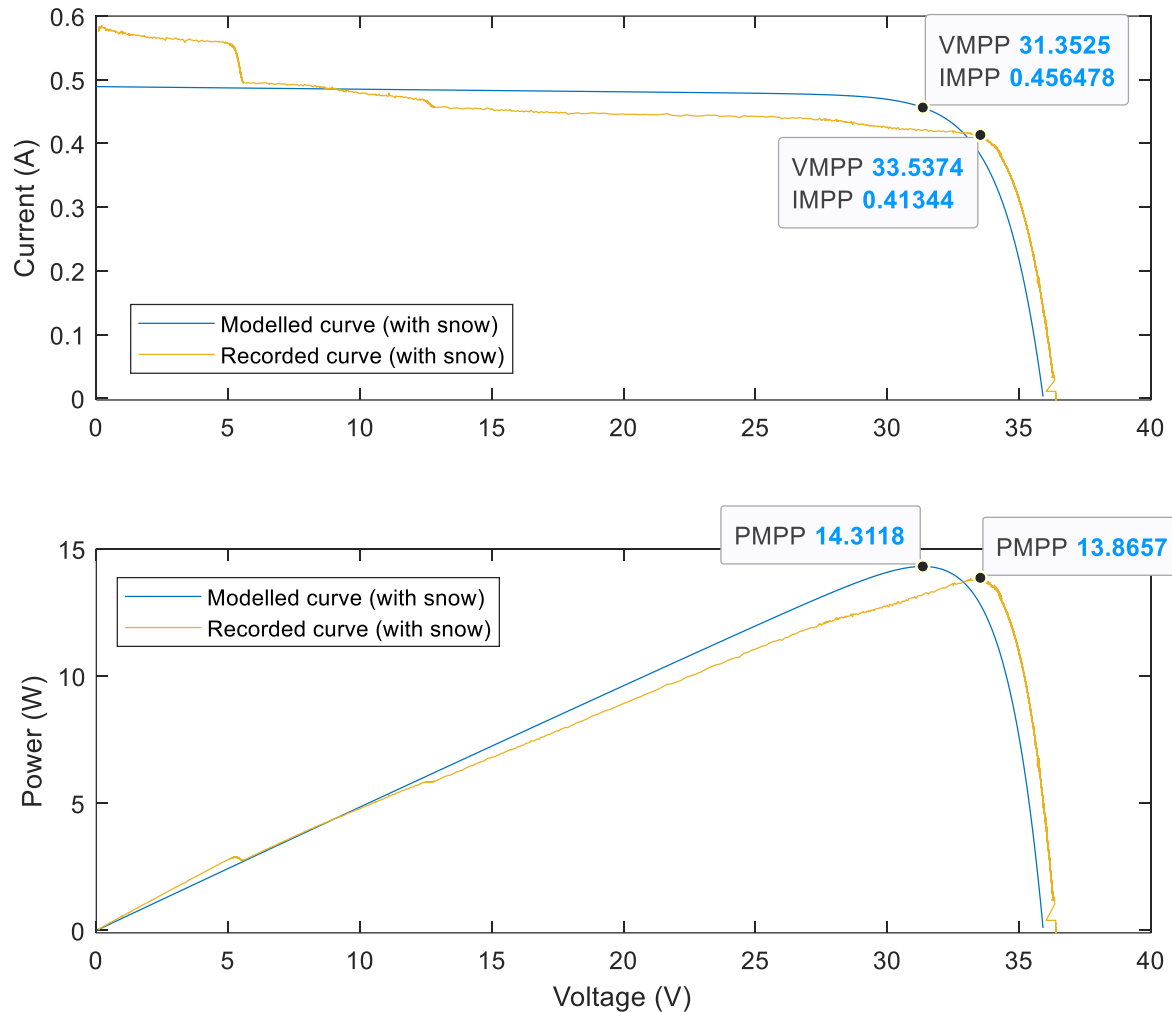
Figure 6.2 – Modelled IV and PV-curves plotted against recorded curves for Q-Cells A10160 module on 17/01/2016 at 12:00.

The two examples here simulate the same time slot for both the Q-Cells A10160 and A10156
module, with the results visible in Figure 6.2 and Figure 6.3, respectively. The recorded P_{MPP}
value for the A10160 module deviates by 2.8% from the recorded value, although the absolute
P_{MPP} deviation is only 0.4 W. However, for the A10156 module the percentage P_{MPP} deviation
is 16.7% with an absolute deviation of 2.3 W. The voltage in the modelled curve for the
A10160 module fits slightly better to the recorded curve compared to the A10156 module
curves in Figure 6.1 and Figure 6.3. The simulated IV- and PV-curves from the other
modelled situations with uniform snow cover are shown in **Appendix A.6**, while Table 6.2
displays the modelled and recorded P_{MPP} and the calculated P_{MPP} deviation.
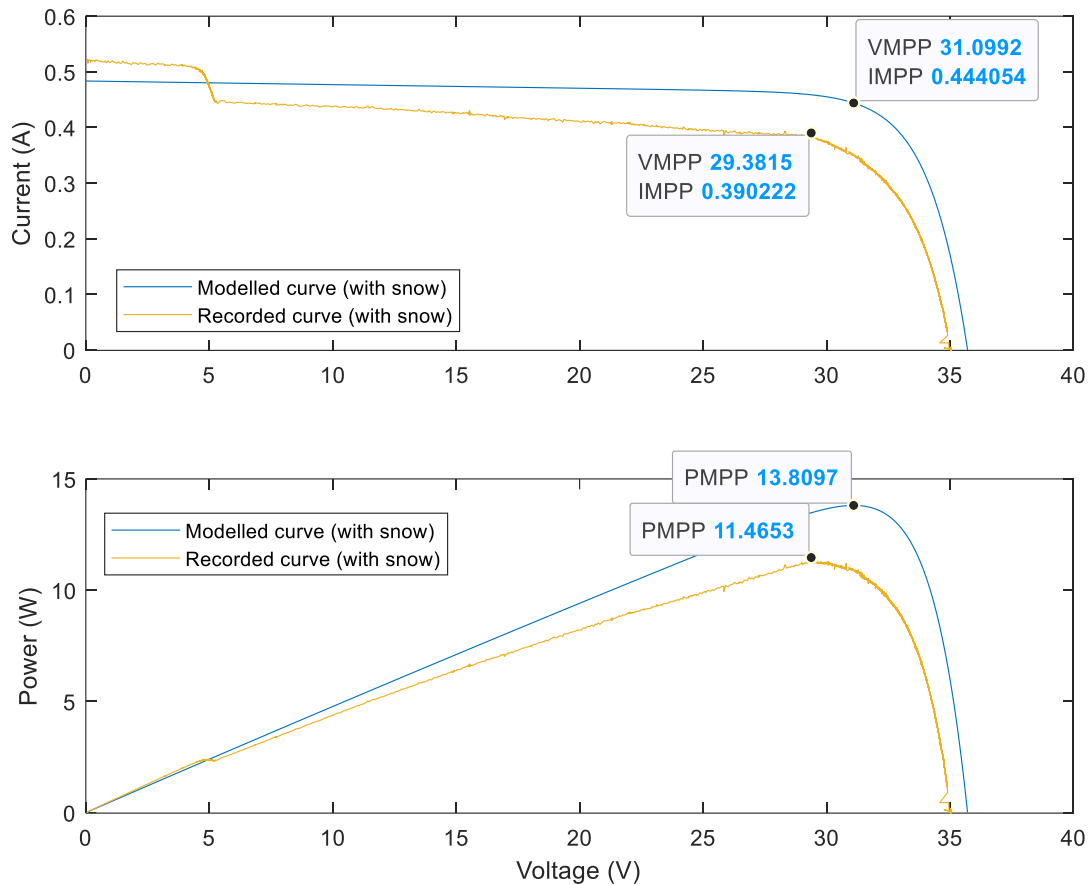
Figure 6.3 - Modelled IV and PV-curves plotted against recorded curves for Q-Cells A10156 module on 17/01/2016 at 12:00 with an irradiance reduction of 90%.

Table 6.2 – Simulation results for modelled and recorded P_{MPP} with variations of uniform snow cover.*Cases where data from SeNorge [61] seems too low when looking at images. The snow cover is modelled using the SeNorge data for the simulated curves whereas the recorded curves have the actual snow cover.

Date and time	PV Module	P_{MPP} modelled [W]	P_{MPP} recorded [W]	P_{MPP} deviation [%]	Snow depth [mm]
22/01/2015 09:44	Q-Cells A10156	1.57	1.2	23.6	70
17/01/2016 12:00	Q-Cells A10160	14.3	13.9	2.8	3*
17/01/2016 12:00	Q-Cells A10156	13.8	11.5	16.7	3*
11/12/2017 14:30	SunTech 433	1.0	0.8	20.0	0.5*
12/12/2017 10:00	SunTech 423	1.57	1.53	2.6	0.5*
21/01/2015 14:20	TITAN	1.2	1.15	4.2	21
07/03/2016 09:40	SunTech 422	4.6	4.39	4.6	22
03/03/2016 08:56	SunTech 433	2.53	2.45	3.2	46

To sum up, the modelling of uniform snow cover for different cases has shown that the calculated P_{MPP} deviation ranges from around 3% to 24%, when simulating IV-curves with snow cover and comparing it to actual recorded IV-curves from modules with snow cover. Furthermore, in some cases the activation of bypass-diodes indicates that the snow cover on the module surface is not completely uniform, which could possibly explain the larger P_{MPP} deviations. As discussed earlier the available snow depth data from SeNorge does not always seem to correspond well when inspecting the snow cover on the images of the PV modules. However, there are some cases where the IV-characteristics simulations manage to calculate P_{MPP} values that deviate <5%.

6.2 Modelling nonuniform/partial snow cover

The modelling of partial and variable snow cover is done to investigate how the MATLAB Simulink model is able replicate the effects caused by this type of snow cover visible on the IV-curves. Previous simulations done for cases of uniform snow cover typically resulted in IV-curves having a relatively normal shape, the typical shape during non-shaded conditions, although with I_{SC} being reduced. However, with some exceptions in cases where the difference in irradiance levels hitting the cells in a substring were high enough to allow the activation of one bypass diode, due to uneven snow layers on the module surface and hence not representing completely uniform conditions. Similarly, partial snow cover usually leads to the activation of bypass diodes which is easily visible on the IV-curve as kinks on the curve. For uniform snow covers situations the bypass diodes are usually not activated. By modelling variable snow cover, the objective is to get a better understanding of how the distribution of snow on the module surface and the different substrings affects the IV-curve. The accumulation of snow in certain areas of a PV module can lead to the formation of hot spots, which can damage the module and reduce its lifetime [71]. This would be mostly applicable in colder climates and areas that have long and stable winters with considerable amounts of snowfall and where it would take a long time for snow to naturally clear from the modules, allowing it to accumulate at certain areas.

The modelling of different types of partial snow cover is done using the same string-based MATLAB Simulink model as for uniform snow, but now a degree of shading must be specified for each module substring. This is necessary to simulate the reduction in irradiance caused by various types of snow cover for each individual substring. The method is explained in subchapter 5.6. The irradiance reduction for each substring is based on an educated guess by visually inspecting the module images and using the snow depths from SeNorge. Based on the simulation results the irradiance reduction is gradually adjusted until a satisfying fit between the modelled and recorded IV-curve is achieved. The uncertainty of the recorded snow depths from SeNorge and non-uniformity of snow distribution is the reason for combining these two methods.

Table 6.3 lists different situations with partial shading that is simulated, all with variable degrees of snow depth and irradiance levels. Some of the situations that are investigated relies on snow depths from SeNorge recorded the day before, and as evaporation of snow is affected by the air temperature, solar and wind conditions, the snow depth may be reduced due to sublimation [72]. According to a study by Stigter et al. [73] the average daily sublimation rate is around 1.0 mm, although this was measured at a considerable altitude, and under favourable conditions. Therefore, in cases where the recorded snow depth value is considered a day later, the sublimation loss is unlikely to be very high, and can in most cases be neglected. In addition, as discussed earlier in Chapter 3 there is less accumulation of snow on a tilted surface [64].

*Table 6.3 – Recorded module temperature, irradiance data, snow depth, and module image for different time slots with various degrees of partial snow cover. *Note that the recorded snow depth is from SeNorge for the given date, but actual snow depth visible on the images is after melting has occurred. Source: UiA PV System.*

Date and time	PV Module	Irradiance [W/m²]	Module Temperature [°C]	Snow depth [mm]	Module image
23/01/2015 10:00	Q-Cells A10160	357.6	2.5	70*	
27/03/2015 08:16	TITAN	460	7.2	27.9*	
27/03/2015 08:39	TITAN	536	9.9	27.9*	
27/03/2015 09:21	TITAN	651.2	19.7	27.9*	
12/12/2017 10:20	SunTech 433	332.6	1.5	0.5*	

The first situation specified in Table 6.3 is shown in Figure 6.4 where the Q-Cells A10160 module is under partial snow cover. The recorded snow depth from the previous day according to SeNorge is 7 cm, but as there is no additional precipitation occurring during the night, it is reasonable to conclude that the sublimation is negligible, meaning the snow depth should still be around 7 cm.

Figure 6.4 – Q-Cells A10160 PV module from the UiA PV System as of 23. January 2015 at 10:00. Source: UiA PV System.
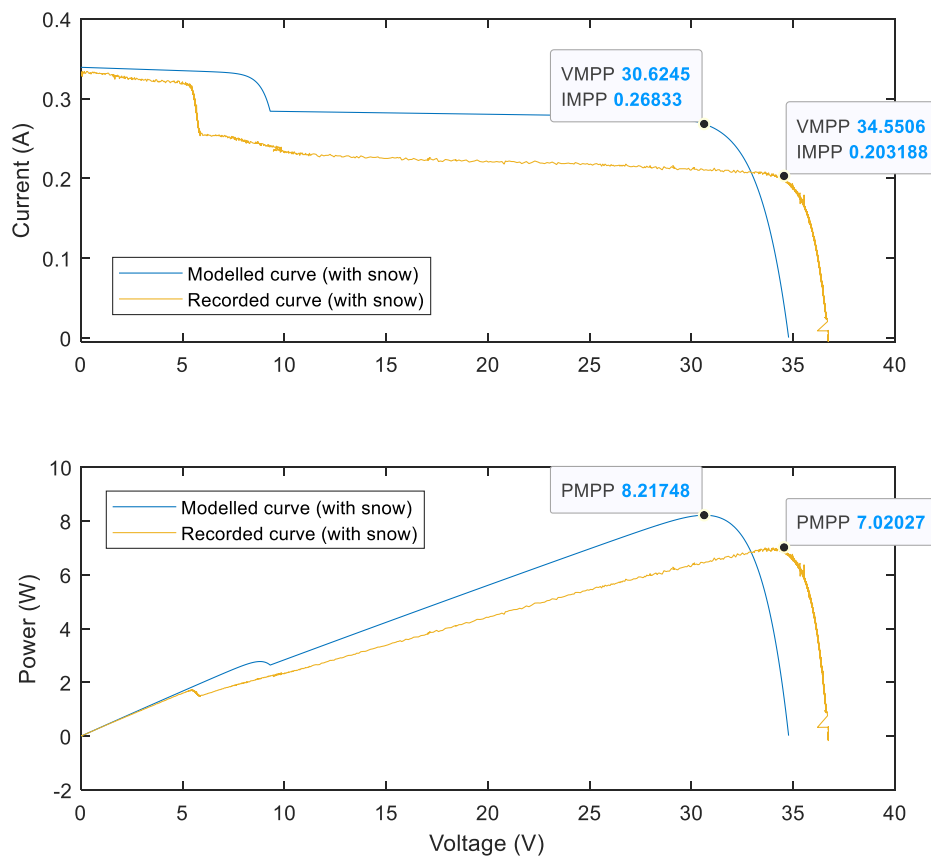
Figure 6.5 – Modelled IV and PV-curves versus recorded curves for the partial snow cover situation on module Q-Cells A10160 shown in Figure 6.4. Source: UiA PV System.

The IV and PV-curve result from modelling the Q-Cells A10160 module on 23/01/2015 at 10:00 is presented in Figure 6.5. In this case the P_{MPP} for the recorded curve (with snow) is 7.02 W, while for the modelled curve (with snow) it is 8.22 W, resulting in a 14.6% difference. As the model is string-based (20 cells) it is visible from Figure 6.5 that the bypass diode activation on the recorded curve (with snow) does not fit well. In substring 1 there are only a few cells completely and partially covered by snow, while the remaining two substrings are totally covered. The irradiance reduction applied for substring 1-3, are 88, 90, and 90%, respectively. Otherwise, the general shape of the curve has some similar traits, but V_{OC} for the recorded curve exceeds the value of the modelled one by 2-3 V.

Figure 6.6 – TITAN PV module and the three substrings, each consisting of 20 solar cells. Image from the 27. March at 08:16, 08:39, and 09:21 with partial snow cover. Source: UiA PV System.

Figure 6.6 displays the TITAN module with its three substrings of solar cells. The image is from the 27. March at 08:16, 08:39, and 09:21 showing a situation with partial snow cover that gradually decreases. This is a scenario at different times with different module temperatures and irradiance values, which are compared. At the first image in Figure 6.6 each of the three substrings are illustrated. Here it is clearly visible that substring 1 is completely free of any snow. Meanwhile in substring 2 less than 10 cells are without any snow cover, and in substring 3 all the cells are almost entirely covered by snow. Furthermore, looking at the second image at 08:39, substring 2 has less snow cover, and is completely free of snow at 09:21. However, most of substring 3 remains partly covered at all timeslots.
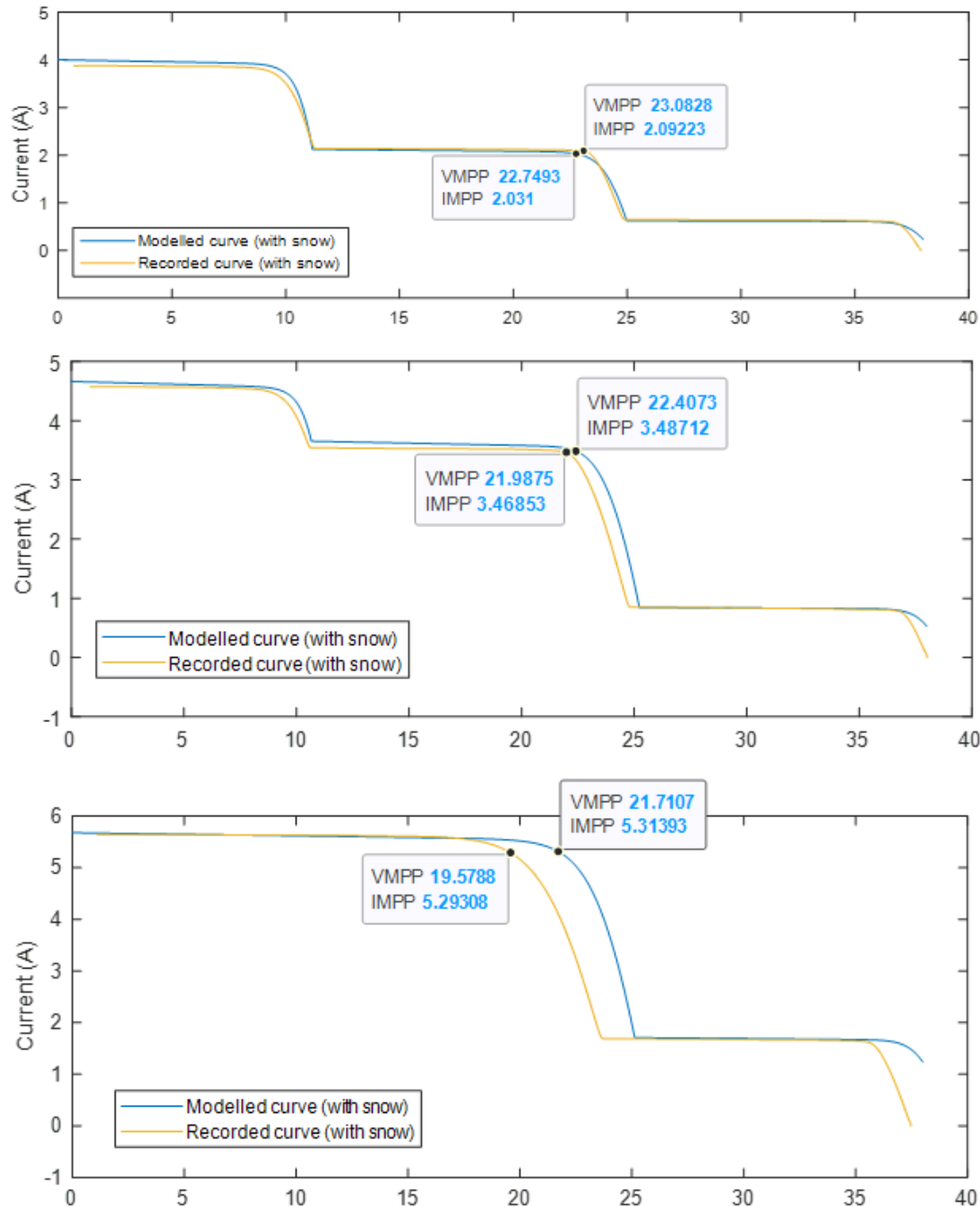
Figure 6.7 – IV-curve modelling results for the three different times with various types of partial snow cover for the TITAN module. Top figure represents the timeslot at 08:16, middle figure the one at 08:39, and the bottom figure timeslot at 09:21. The activation of the three bypass diodes is clearly visible on the IV-curve.

The results from the different simulations are shown in Figure 6.7, and the PV-curves are found in **Appendix A.6**. Figure 6.8 illustrates the modelled and recorded curves for the SunTech 433 module under the partial snow cover visible in Table 6.3. In this case, the first parts of the curve up to the first local P_{MPP} does not fit completely well, however the remaining sections do, and the P_{MPP} deviation is <1%.
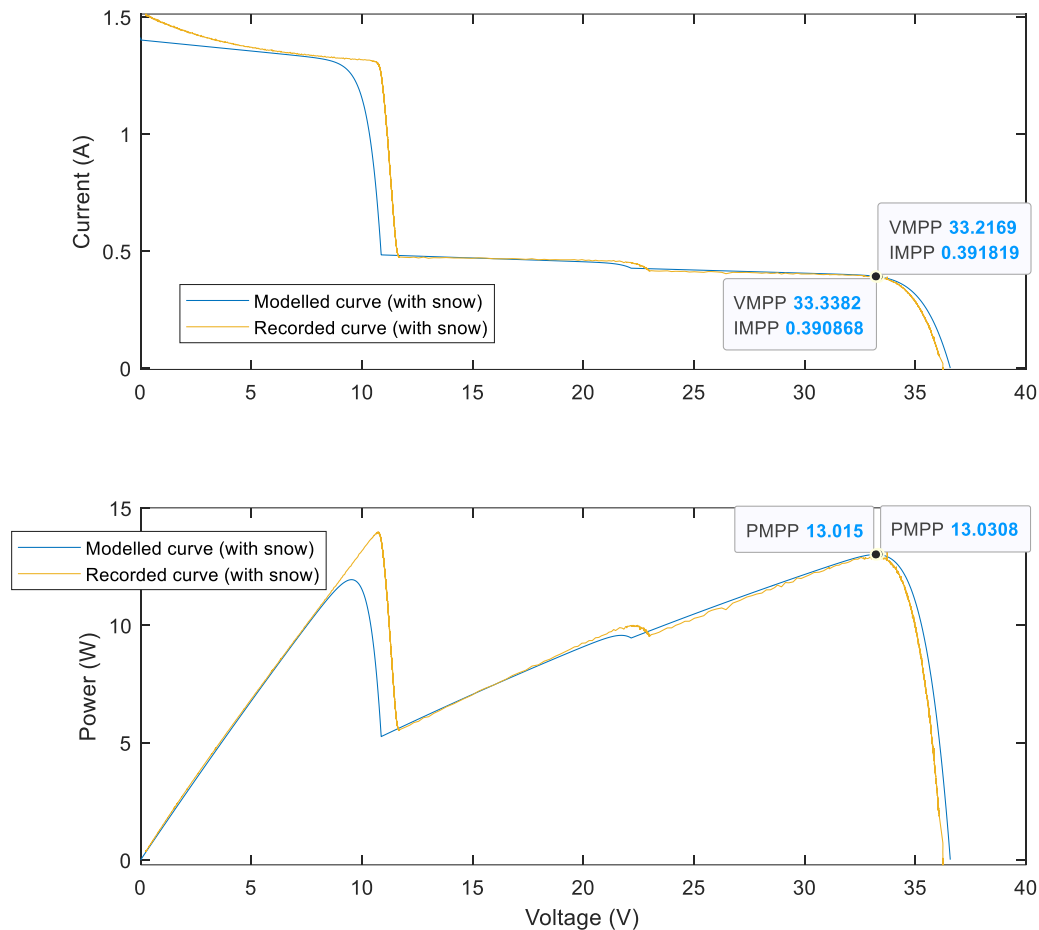
Figure 6.8 – IV and PV-curve modelling results for the SunTech 433 module with partial snow cover compared against the actual recorded IV and PV-curves from the UiA PV system.

Table 6.4 – Simulation results for different PV modules and situations with variations of partial snow cover. Including the irradiance reduction per substring, modelled, recorded, and P_{MPP} deviation.

Date and time	PV Module	Irradiance reduction Substring 1 [%]	Irradiance reduction Substring 2 [%]	Irradiance reduction Substring 3 [%]	P_{MPP} modelled [W]	P_{MPP} recorded [W]	P_{MPP} deviation [%]
23/01/2015 10:00	Q-Cells A10160	88	90	90	8.2	7.0	14.6
27/03/2015 08:16	TITAN	0	47.2	84.5	46.2	48.3	4.3
27/03/2015 08:39	TITAN	0	22.0	82.0	78.1	76.3	2.3
27/03/2015 09:21	TITAN	0	0	70.0	115.4	103.6	10.2
12/12/2017 10:20	SunTech 433	50	83	85	13.03	13.01	0.12

The values listed in Table 6.4 show the three different timeslots for the TITAN module case in Figure 6.6, the corresponding module temperature and, irradiance data for each case, and the respective substring irradiance reductions. As expected, the trend is that for each scenario the irradiance levels increase along with the module temperatures. Simultaneously, the partial snow cover is slowly reduced over time. The simulated cases show that the calculated P_{MPP} deviation ranges from 0.1-14.6% for the cases investigated. However, when considering curves with activated bypass diodes, resulting in additional local P_{MPP}, these do not frequently fit as well. It should be noted that the case with the highest P_{MPP} deviation involves very low power values, which implies higher uncertainty.

6.3 Comparing recorded IV-curves and modelled curves using calculated substring snow coverages from image analysis

At first, looking at the images of the PV modules with estimated snow cover it is possible to draw some conclusions. Because of the relationship between irradiance and I_{SC} it is expected that, at best, half of the module power output is available under a 50% area-based module thick snow cover, unless bypass diodes are activation which will result in a voltage drop. Furthermore, if a larger area-based snow cover is present the reduction in power is decreased equally to the percentage of the estimated snow cover. However, this is a simplification as the snow layer is unlikely to have uniform depth, especially in partial snow cover situations. Additionally, if bypass diodes were activated the power reduction would not correlate directly with the magnitude of the snow cover. In this subchapter the recorded IV-curves and their P_{MPP} is compared to modelled IV-curves using the estimated percentage snow coverages from the image analysis, see subchapter 5.8-5.10 for methodology.

The two Q-Cells A10156 modelled situation from Table 6.5 with partial snow coverage is shown in Figure 6.9. The top images show the created 60-cell mask for the Q-Cells A10156 module applied to the two module images. The middle images show the binarized, but distorted images trying to separate the PV cells pixels from the snow cover pixels. Therefore, by using the contour algorithm in IS the improved image is generated, shown as the bottom images in Figure 6.9. Note that the PV cells covered partially or entirely, by snow are displayed in white color, whereas the uncovered cells are shown in black. This process is then repeated for each of the simulated cases shown in Table 6.5, and the results are visible in Figure 6.9 and Figure 6.10.

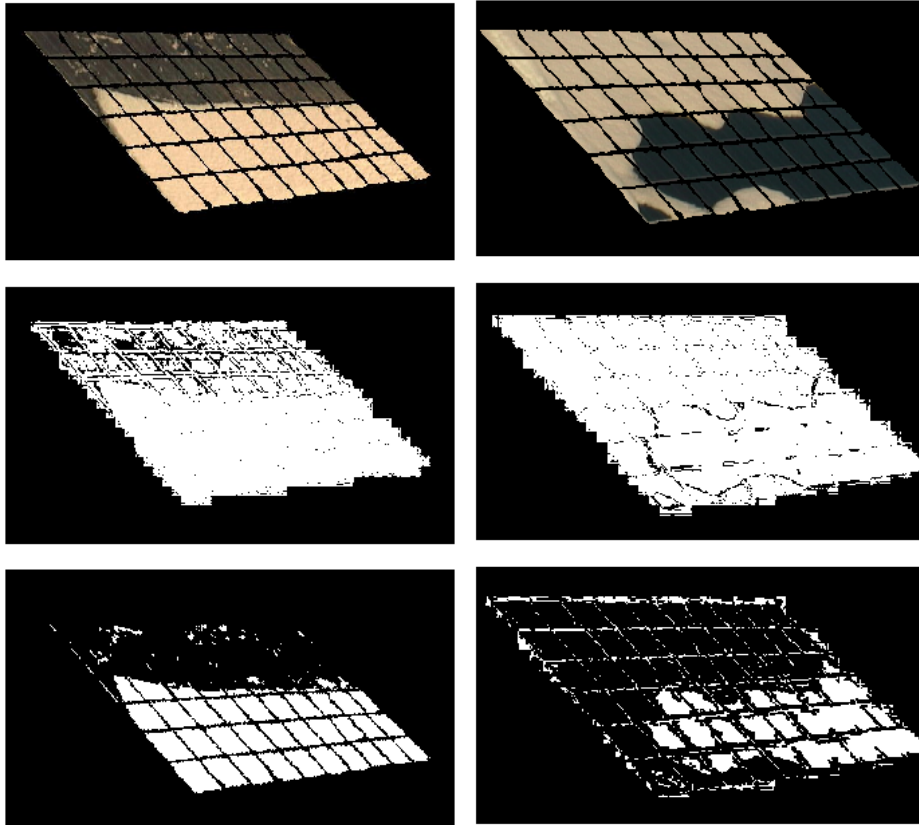*Figure 6.9 – Top images: Created Q-Cells A10156 mask applied to the two images. Middle images: binarization of masked images. Bottom images: improved version of masked binarized images using active contour algorithm in IS.*
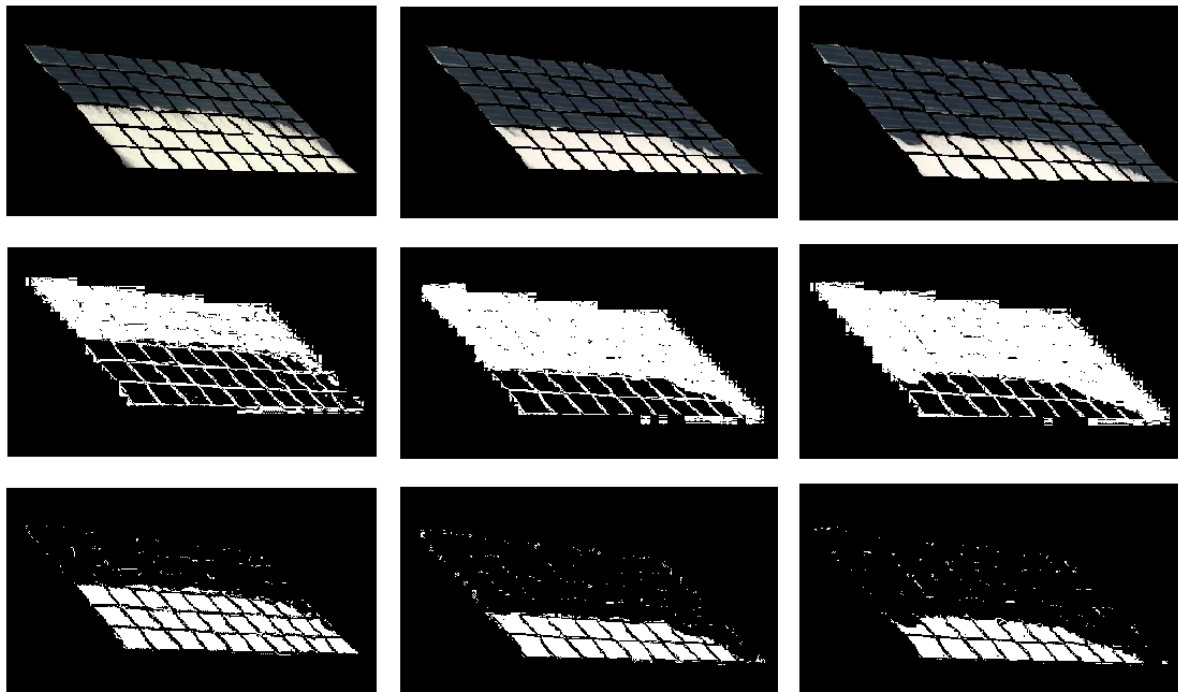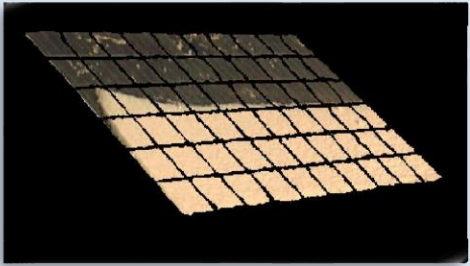
Figure 6.10 – Top images: Created TITAN module mask applied to the three images. Middle image: binarization of masked images. Bottom images: improved version of masked binarized images.

Table 6.5 displays cases with different PV modules under different types of partial snow cover together, with the calculated module snow pixel value for each substring, and the masked module image. Similarly, to before the module pixel area covered by snow is found by taking the calculated snow pixel values from Table 6.5 divided by the baseline pixel values for each substring from Table 5.10. Figure 6.11-Figure 6.15 shows the simulated IV and PV-curves for the modelled curves using the estimated percentage substring snow coverages from Table 6.6.

Table 6.5 – Calculated total module substring pixel values for different situations with partial snow cover.

Date and time	PV Module	Calculated pixels substring 1	Calculated pixels substring 2	Calculated pixels substring 3	Module image with mask
23/01/2015 10:00	Q-Cells A10156	1 368	20 548	33 712	
27/03/2015 08:16	TITAN	No snow	10 625	22 225	
27/03/2015 09:07 Irr.: 589.4 W/m^2 Temp: 18.6°C	TITAN	No snow	No snow	21 057	
27/03/2015 09:21	TITAN	No snow	No snow	18 419	
17/01/2016 15:00 Irr.: 335.6 W/m^2 Temp: 3.3°C	Q-Cells A10156	Covered	6 540	18 254	
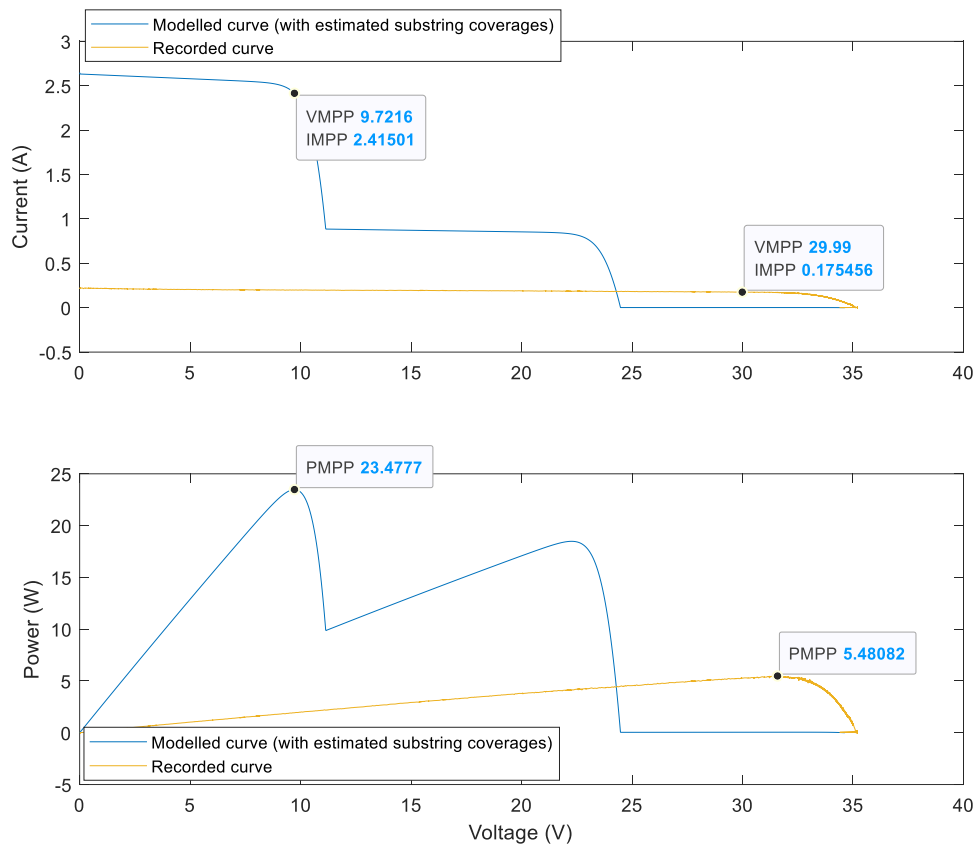
Figure 6.11 – Modelled IV and PV-curves, using the estimated substring snow coverages, and the recorded IV and PV-curves for the Q-Cells A10156 module on 23/01/2015 at 10:00.
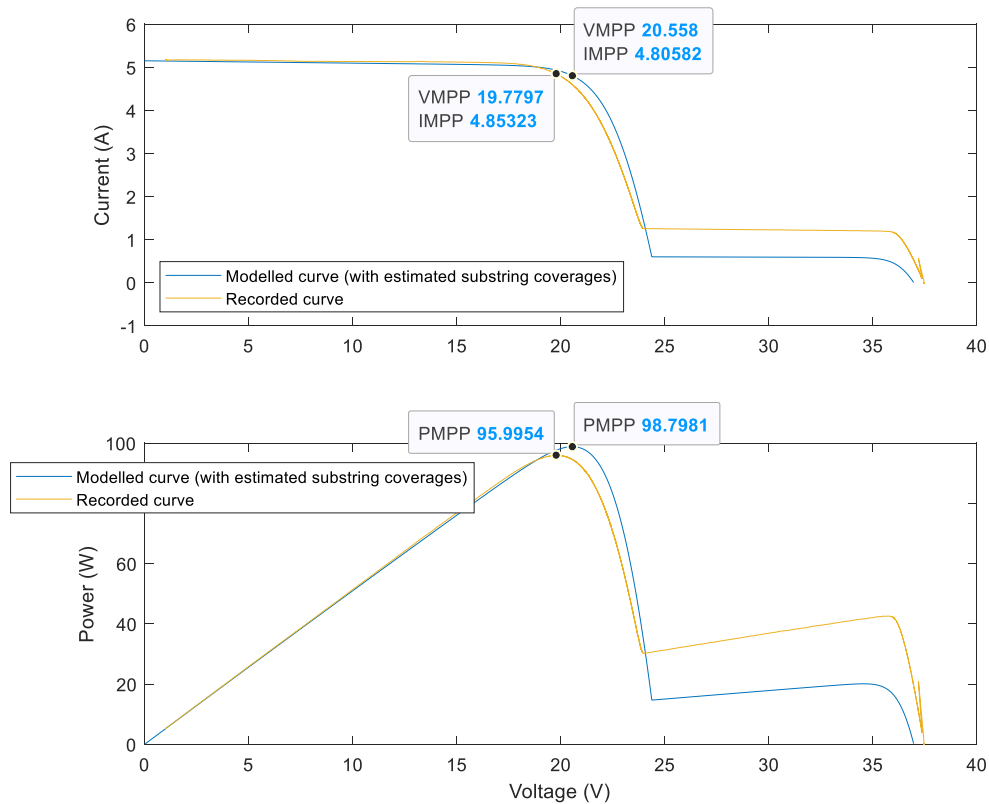
Figure 6.12 – Modelled IV and PV-curves, using the substring snow coverage estimated using image analysis, and the recorded IV and PV-curves for the TITAN module on 27/03/2015 at 09:07.
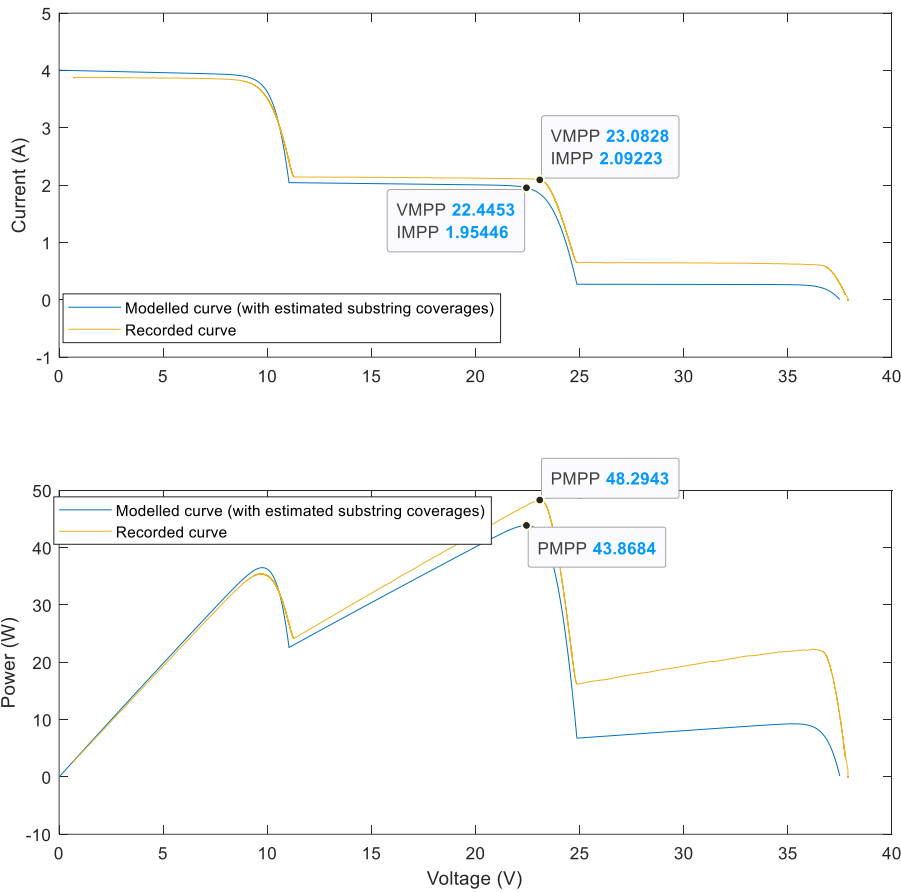
Figure 6.13 – Modelled IV and PV-curves, using the estimated substring snow coverages from the image analysis, and the recorded IV and PV-curves for the TITAN module on 27/03/2015 at 08:16.
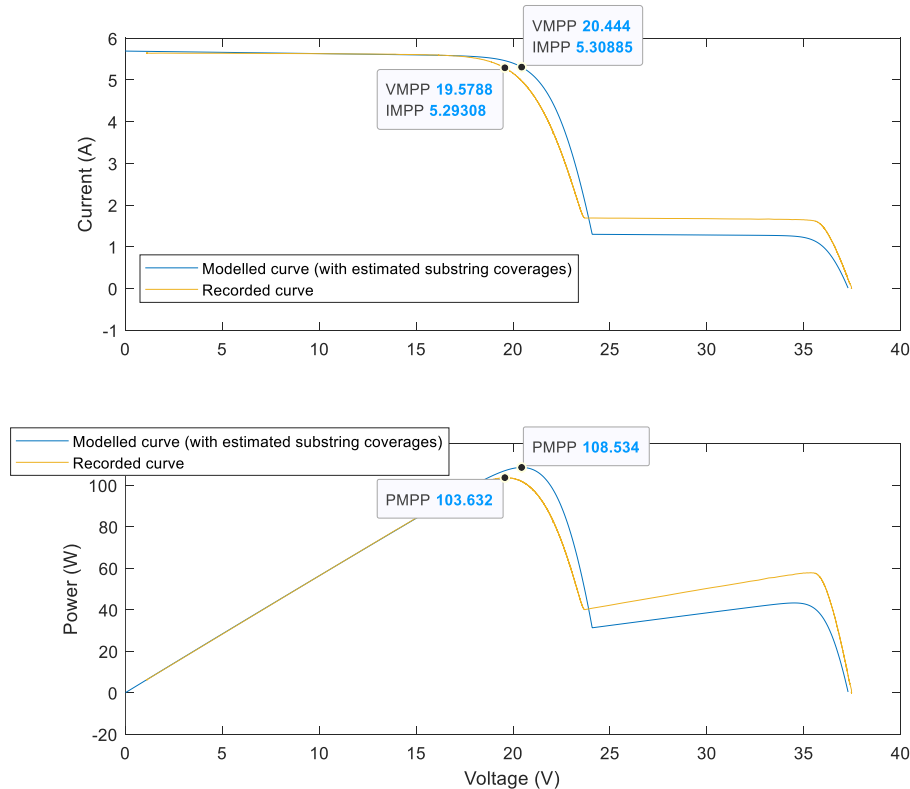
Figure 6.14 – Modelled IV and PV-curves, using substring coverages estimated through image analysis, and the recorded IV and PV-curves for the TITAN module on 27/03/2015 at 09:21.
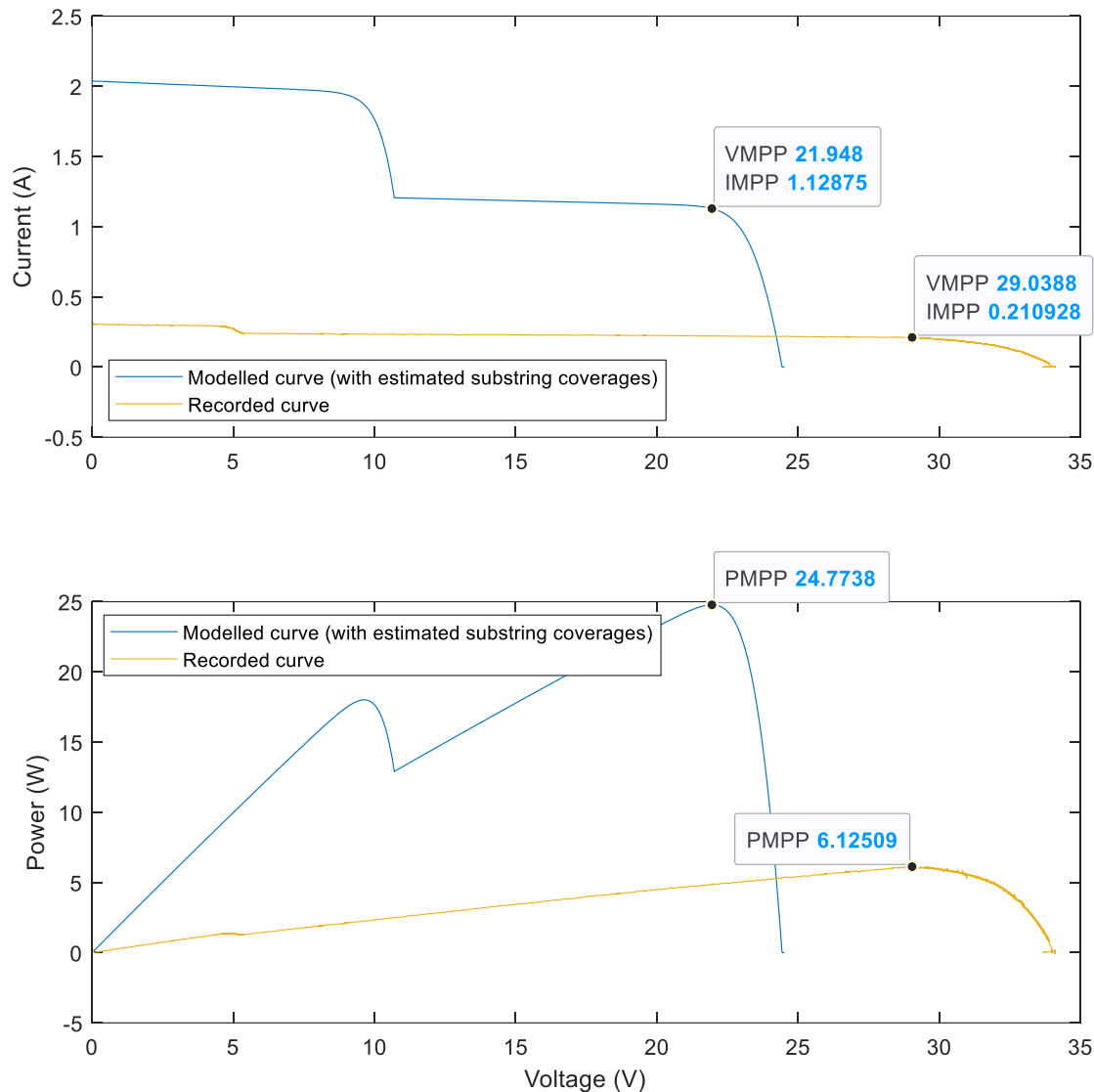
Figure 6.15 – Modelled IV and PV-curves, using estimated substring coverages from image analysis, and the recorded IV and PV-curves for the Q-Cells A10156 module on 17/01/2016 at 15:00.

The simulation results after using the calculated irradiance reductions for each substring from the image analysis as input into the MATLAB Simulink IV-characteristics model is displayed in Table 6.6. Comparing the curves for the Q-Cells A10156 module with the recorded curves, it is apparent that the model fails to resemble them in the two cases tested. Additionally, in both cases there is no bypass diode activation visible on the recorded curves, as opposed to the modelled ones where it is a direct consequence of the input substring irradiance reductions. The calculated snow coverage seems reasonable; however, the MATLAB model assumes that the irradiance hitting the PV module is reduced similarly to the module area covered by snow. That is an oversimplification, since considering the transparency of the snow layer requires additional data that could be difficult to gather and would require a more complex IV-characteristics model. As a result, the calculated P_{MPP} deviation equals 75.4% and 76.6% in these two cases for the Q-Cells A10156 module, although it should be noted that these cases involve the lowest recorded power values, which makes the uncertainty of the data higher [74]. For instance, the recorded P_{MPP} is 6.1 W and 5.5 W, respectively, which are

extremely low power values. On the other hand, for the three TITAN module cases at different time slots, the calculated P_{MPP} deviation is in the range 2.8-9.1%. The activation of the bypass diodes on the modelled and recorded curves also matches to some degree. That is a significant improvement compared to the previous situations with the A10156 module.

The mismatch between the recorded and modelled IV-curves for the TITAN module was much greater compared to the Q-Cells A10156 module IV-curves. Simulations done earlier with the Q-Cells A10156 module (see Figure 6.1 and Figure 6.3) seem to work fine and gave reasonable matching IV-curves and P_{MPP} deviations. However, the activation of the bypass diodes has not been demonstrated clearly on any of the previously recorded curves for the Q-Cells A10156 module. Therefore, it is possible that one or more of the bypass diodes are not working properly, which would result in a drop in power output visible on the IV-curve if this was the case. On the other hand, it could potentially be a coincidence and that additional simulations would have given better results for both modules, but that is just speculation.

Table 6.6 – Simulation results for different cases of module partial snow coverage showing the calculated substring irradiance reductions, and a comparison between the modelled and recorded P_{MPP}.

Date and time	PV Module	Calculated available irradiance Substring 1 [%]	Calculated available irradiance Substring 2 [%]	Calculated available irradiance Substring 3 [%]	P_{MPP} modelled [W]	P_{MPP} recorded [W]	P_{MPP} deviation [%]
23/01/2015 10:00	Q-Cells A10156	94.95	31.65	0.062	23.5	5.5	76.6
27/03/2015 08:16	TITAN	100	50.79	6.75	43.9	48.3	9.1
27/03/2015 09:07	TITAN	100	100	11.64	98.8	96.0	2.8
27/03/2015 09:21	TITAN	100	100	22.72	108.5	103.6	4.5
17/01/2016 15:00	Q-Cells A10156	0	45.9	78.25	24.8	6.1	75.4

6.4 Investigating the impact of current limiting by individual solar cells
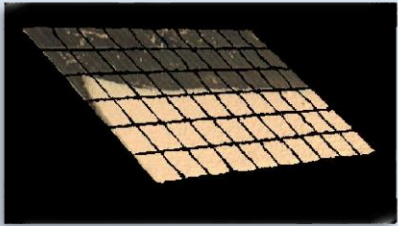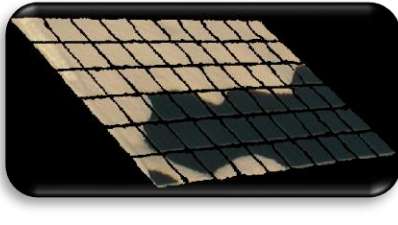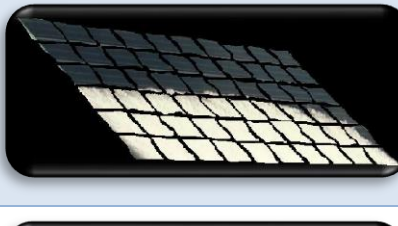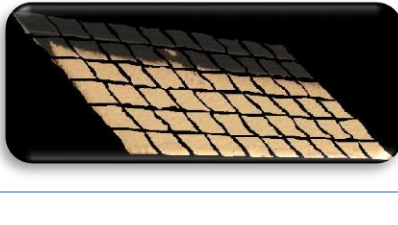
The power output of a module substring is limited by the output of the least producing cell. Therefore, a larger snow cover on an individual cell will be responsible for restricting the power output from the entire substring in the module. The two modelled cases with the largest P_{MPP} deviation for the previous chapter is considered again, but this time the most covered cell in each substring is identified, along with its pixel value. This is done to try and represent the least producing cell in the substring, to assess if it improves the results. The methodology used here is described in subchapter 5.11.

Similarly, to before the pixel value of each snow-covered cell is compared to baseline pixel value (free of snow) of the cell. The cell with the largest pixel difference compared to the

baseline value is considered the most limiting cell. Then based on this, the available irradiance for the limiting cell in each substring is calculated and used as input in the MATLAB IV-characteristics model. The binarized images displaying the identified snow-covered solar cell areas for the cases with the A10156 and TITAN modules are presented in Figure 6.16.

Figure 6.17-Figure 6.20 shows the simulated IV and PV-curves for the partial snow cover situations for the Q-Cells A10156 and TITAN modules displayed in Figure 6.16. Whereas the results from modelling the IV-characteristics based on the most limiting solar cell in each substring identified using the image analysis method is shown in Table 6.8.

Table 6.7 – Recorded irradiance and PV module temperature data, and module image for the selected situations.

Date and time	PV Module	Irradiance [W/m^2]	Module Temperature [°C]	Module image
23/01/2015 10:00	Q-Cells A10156	357.6	2.5	
17/01/2016 15:00	Q-Cells A10156	335.6	3.3	
27/03/2015 08:16	TITAN	460	7.2	
22/01/2015 10:00	TITAN	296.3	4.6	
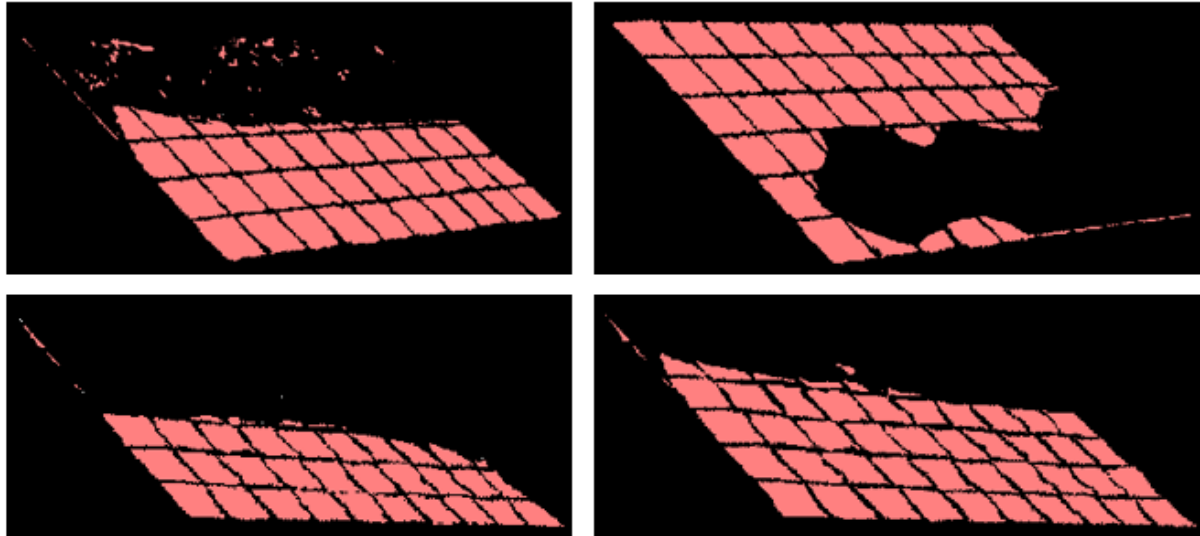
Figure 6.16 – Top images: Binarized images of the Q-Cells A10156 modules, identifying all the snow-covered cell areas (red) for the two modelled cases from the previous chapter. The left and right images showing the cases on 17/01/2016 and 23/01/2015, respectively. Bottom images: Binarized images of the TITAN module, showing the identified snow-covered cell areas (red) for the two situations. The left image shows the partial snow cover case on 27/03/2015 and the right image shows the situation on 22/01/2015.
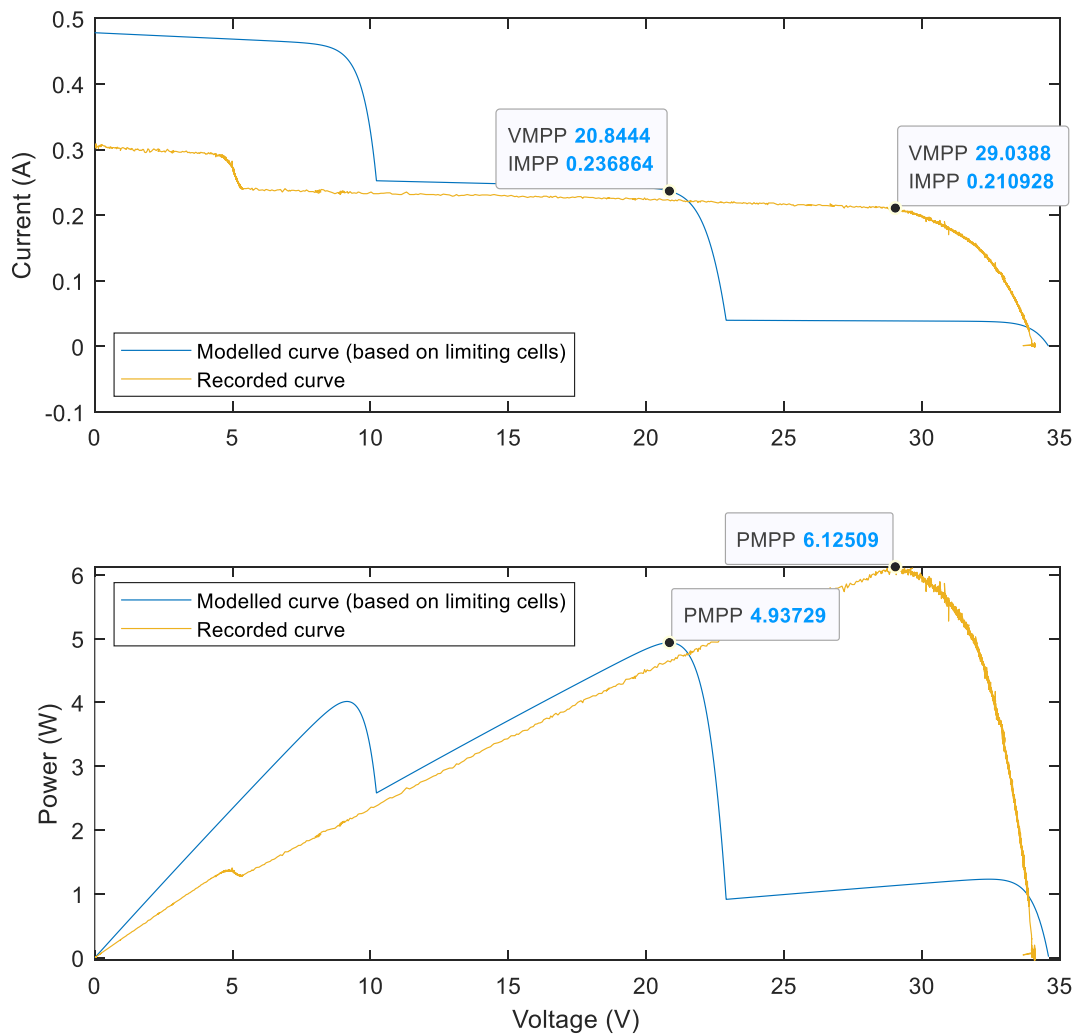
Figure 6.17 – Modelled IV and PV-curves, using the estimated available irradiance based on the limiting cell in each substring, compared to the recorded curves for the A10156 module on 17/01/2016.
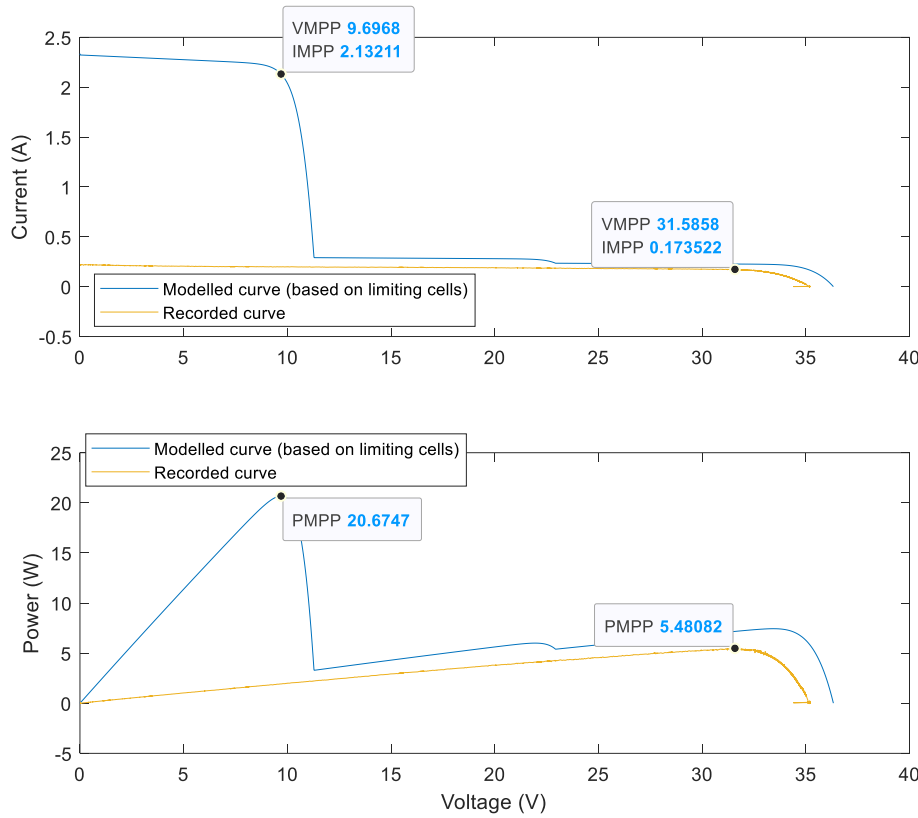
Figure 6.18 – Simulated IV and PV-curves, using the estimated available irradiance based on the limiting cell in each substring, compared to the recorded curves for the A10156 module on 23/01/2015.
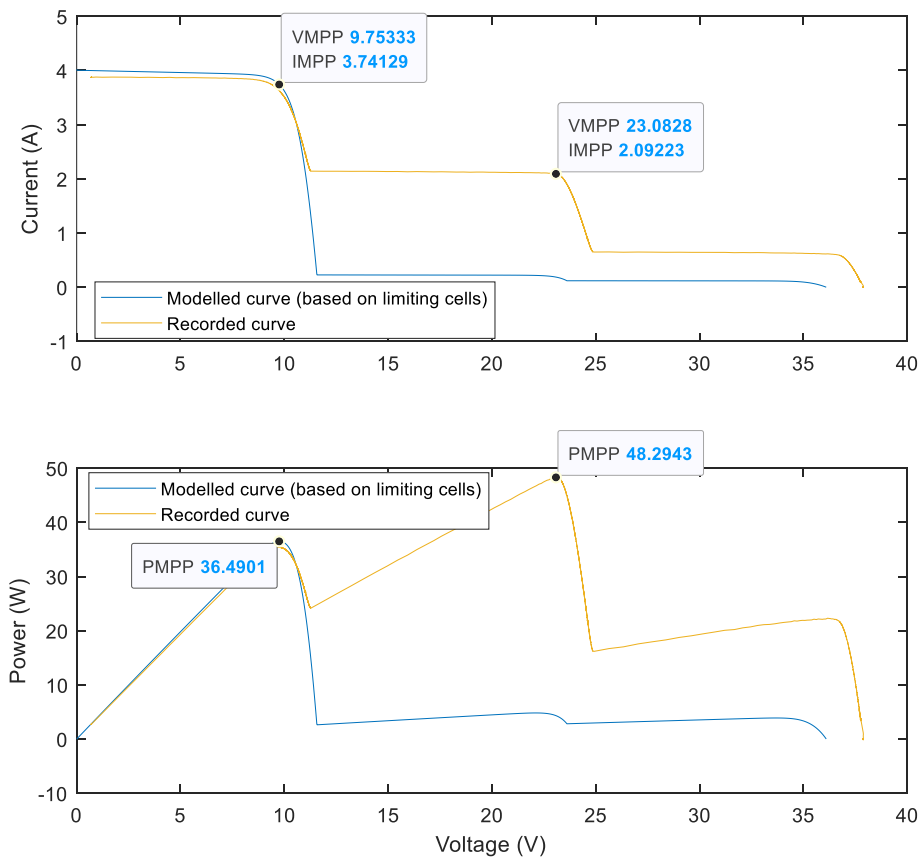
Figure 6.19 – Modelled IV and PV-curves, using the available irradiance estimated based the most limiting cell in each substring, compared to the recorded curves for the TITAN module on 27/03/2015.
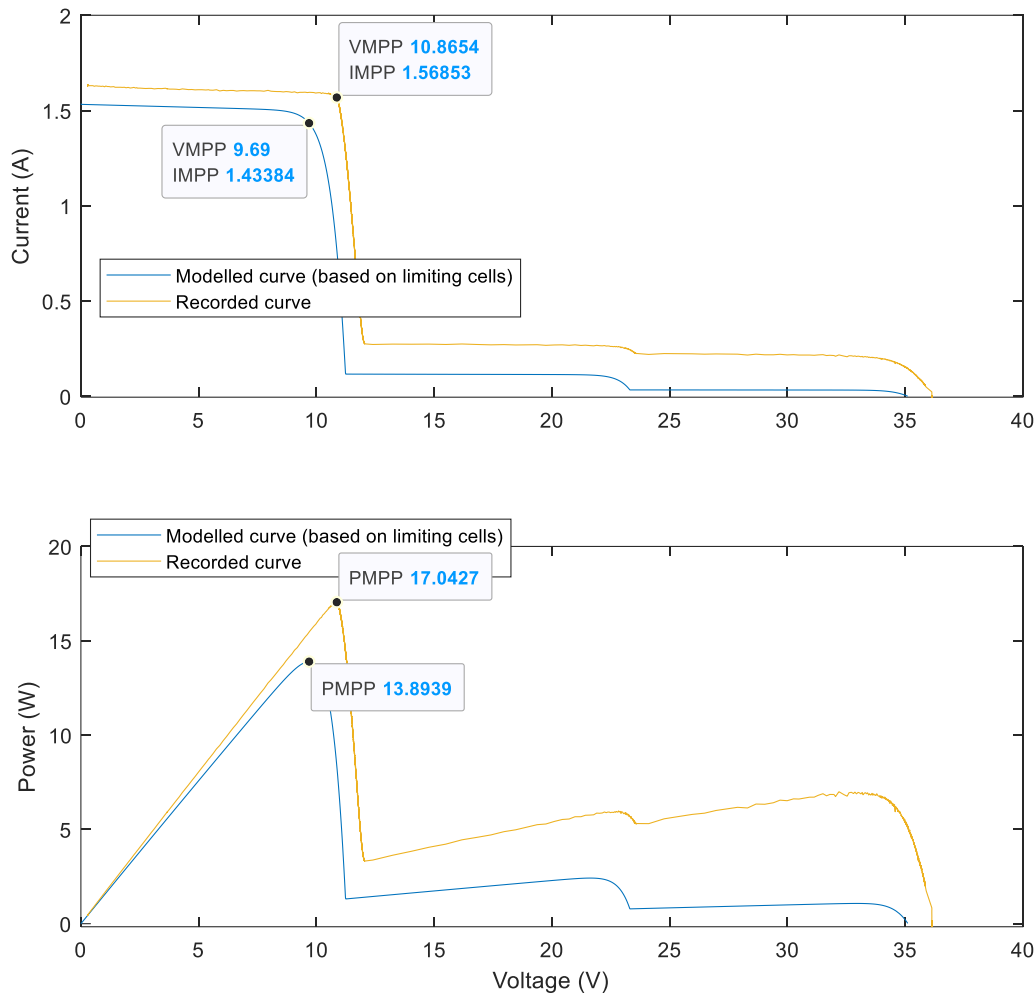
Figure 6.20 – Simulated IV and PV-curves, using the available irradiance values estimated based on the limiting cell for each substring, compared to the recorded curves for the TITAN module on 22/01/2015.

The idea was to investigate if the results could be improved by using an alternative approach and taking advantage of the image analysis where individual cell pixel values were already identified. With the calculated limiting cell irradiances available from each substring shown in Table 6.8, the P_{MPP} deviation is 73.4% for the case for the A10156 module shown in Figure 6.18. Consequently, the modelled curve differs considerably from the recorded one. In contrast, the other case visible in Figure 6.17 showed a larger improvement with a P_{MPP} difference of 19.7%. However, this is still a substantial deviation, but the overall curve does fit better for simulations done with the cell-based model.

Furthermore, the two simulated cases for the TITAN module, illustrated in Figure 6.19 and Figure 6.20, showed P_{MPP} deviations of 24.4% and 18.2%, respectively. The first case was modelled earlier, shown in Figure 6.7, not using the image analysis approach. In that case the P_{MPP} deviation was only 4.3%, however using the limiting cell-based method resulted in a 20% greater P_{MPP} deviation, and thus a worse result. The last case produced the lowest P_{MPP} deviation of the four modelled situations with 18.2%. Studying the IV-curves for these cases the overall curve shape fits, although not the magnitude of the current/voltage. The comparison between the string-based model and cell-based model is discussed further in subchapter 7.5.

Table 6.8 – Modelling results for the two Q-Cells A10156 module and two TITAN module cases displaying the calculated limiting cell available irradiance for each substring, and the modelled and recorded P_{MPP}.

Date and time	PV Module	Limiting cell available irradiance Substring 1 [%]	Limiting cell available irradiance Substring 2 [%]	Limiting cell available irradiance Substring 3 [%]	P_{MPP} modelled [W]	P_{MPP} recorded [W]	P_{MPP} deviation [%]
23/01/2015 10:00	Q-Cells A10156	83.8	8.4	10.4	20.7	5.5	73.4
17/01/2016 15:00	Q-Cells A10156	18.35	9.61	1.52	4.9	6.1	19.7
27/03/2015 08:16	TITAN	100	2.97	5.65	36.5	48.3	24.4
22/01/2015 10:00	TITAN	59.4	4.5	1.3	17.0	13.9	18.2

7. Discussion

In this chapter, the results from the modelling of IV-characteristics for different situations with variable amounts of both uniform and partial snow cover are discussed. The significance and uncertainty of input parameters that impact the modelling results, namely recorded irradiance, and module temperature data is debated. Moreover, the importance of transmittance and snow depth when modelling IV-curves is explained, and the findings from the image analysis is presented and evaluated.

7.1 The impact of uncertainty in measurements

There are numerous things that can lead to the incorrect measurements when irradiance and temperature data is collected, which can have negative effects if used to model IV-curves. Incorrect irradiance and temperature measurements can lead to larger differences between simulated and actual IV-curves [75]. Since the MATLAB Simulink model that was used to perform the simulations relies on two input parameters, namely irradiance and temperature, the importance of accurate measurements is evident.

During this work several temperature measurements that had been used to simulate IV-curves had to be changed, and the simulations repeated because of misread values being used as input. These changes made some of the P_{MPP} deviations, for certain modelled situations, more accurate, whereas in other cases the opposite happened. The exposure to sunlight and higher irradiance values results in an increasing module temperature. Therefore, as there are multiple PV modules in the system the IV-curves for each individual module can be plotted together and compared. A module with temperature data that is not following the irradiance as expected is then easily detected. Furthermore, for some of the PV modules the temperature

sensors were damaged and did not provide any useful data. In these cases, average module temperature values of similar neighboring PV modules were utilized.

In addition to abnormal cases of increased uncertainties there are several uncertainties related to normal operation. The electrical equipment used to do measurements always involves some degree of uncertainty. The IV-curve measurements that are done in the UiA PV system uses electrical loads that involve measurement uncertainties, which according to the datasheet specifications has, for instance, a wattmeter accuracy of ± 0.5% [76]. In addition, the Kipp&Zonen pyranometer that does the irradiance measurements is listed with a measurement uncertainty <2% [77]. Additionally, the temperature sensors have a measurement uncertainty of ±0.2°C for the temperature range -40°C to +70°C [78].

The module temperature measurements that are registered also depend on where the temperature sensor is located on the backside of the module. A uniform snow cover on the module surface is likely to give more accurate temperature measurements compared to a partial snow cover situation. The temperature measurement for a single location with a module under partial snow cover will not be representative for the entire module surface. For example, if a large snow cover accumulated around the module frame and the module center remained snow free, a temperature sensor mounted in the center would result in a higher measurement uncertainty. This is likely to occur in situations that involve snow melting which results in different irradiance values due to snow cover and therefore also different temperatures.

7.2 The effects of snow cover

The IV-curves modelled using the MATLAB Simulink model showed variable degrees of fit when compared to the recorded IV-curves from the UiA PV system. Additionally, it is expected that the modelled and recorded IV-curves will be very different from each other, as IV-curves with and without snow cover is being compared. Figure 7.1 displays the correlation between irradiance and snow depth, and P_{MPP} reduction for the different modelled cases. Firstly, most of the cases consider irradiance values <200 W/m^2, although two situations have irradiance levels at around 600 W/m^2. The simulation results for irradiance <200 W/m^2 shows that the P_{MPP} reduction varies greatly, with values ranging from as low as 20% up to over 90% for some cases. The difference in irradiance may impact the overall P_{MPP} deviation results as higher uncertainty involving low irradiance values has been confirmed in different publications [74, 79]. Simultaneously, the snow depth for these cases varies from 0.30-70 mm, although there are situations with high irradiance, low snow depths, and high P_{MPP} reductions, relative to other examples. A higher irradiance values means that there is more radiant energy striking the module surface area compared to a situation with lower irradiance. The higher radiant energy could result in more sunlight penetrating the snow layer when the irradiance is higher and speed up the melting process of snow. However, it is evident that the power reduction on the recorded IV-curves with snow compared to the modelled IV-curves without snow is substantial. For instance, the two highest irradiance cases (>600W/m^2) have a

P_{MPP} reduction of 91% and 92%, respectively, despite both cases having a recorded snow depth of only 3.0 mm. In contrast to situations with irradiance levels of 166 W/m^2 and 72 W/m^2, resulting in P_{MPP} reductions of 94% and 92%, respectively. Regardless of these situations having considerably higher recorded snow depths of 70 mm and 28 mm.
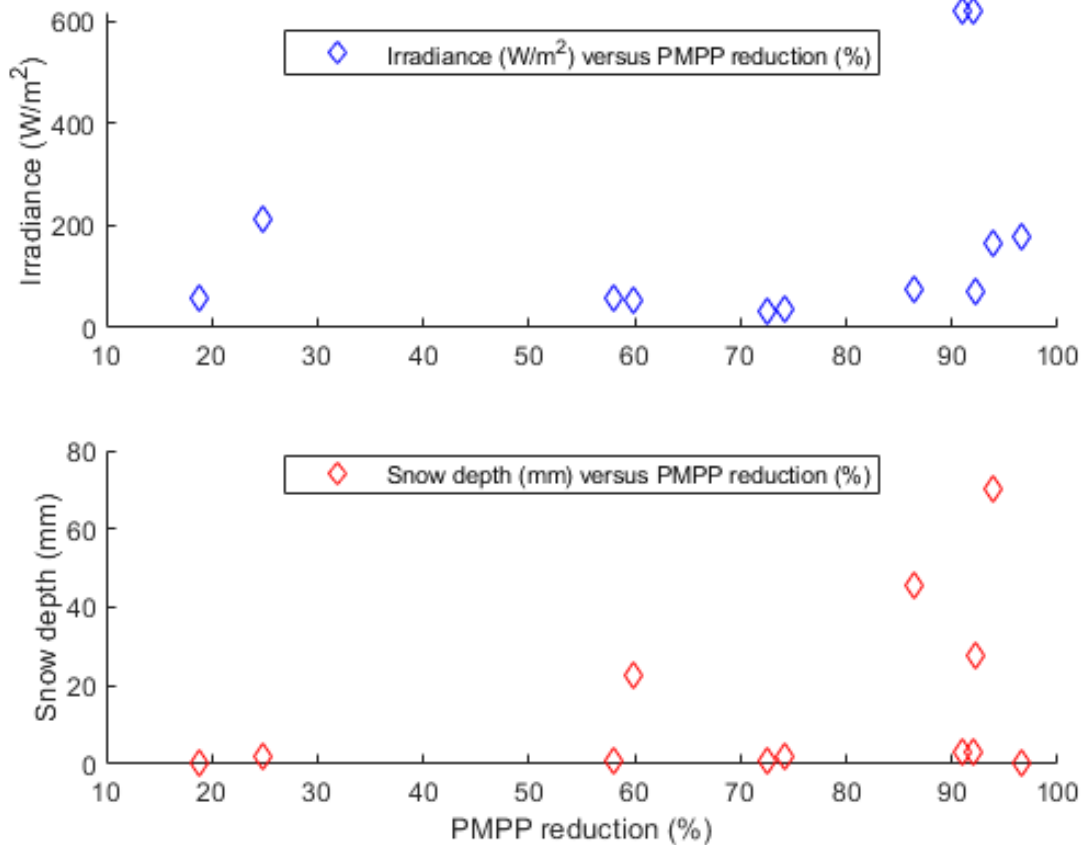
Figure 7.1 – Results from modelled IV-curves for different situations showing irradiance values and snow depth plotted against the calculated P_{MPP} reduction for each case.

Moreover, of the five different cases with irradiance levels <60 W/m^2 four of them have snow depths <2.0 mm, but with P_{MPP} reductions varying between 18.8-74.1%. However, in the fifth case the P_{MPP} reduction is 59.8%, even though the recorded snow depth is 22.4 mm. Overall, it is possible to spot something resembling a trend, which with increasing snow cover results in larger P_{MPP} reductions, but ideally, they should be more consistent to draw any conclusions.

Considering some of the findings from Perovich et al. [20], referring to the transmittance reduction related to snow cover, and the research from Andenæs et al. [7], the results from some of the cases are acceptable. Particularly cases with P_{MPP} reductions around 90% for relatively low snow depths, however, there are situations where this clearly is not the case. However, there is a significant uncertainty in the recorded snow depths that is used, which is available from SeNorge. For many of the examples the accuracy of the recorded snow depth is questionable because a simple glance at the module images is sufficient to disprove it. It should also be pointed out that the recorded snow depths are based on the available meteorological data, and not a snow gauge specifically designed to measure snow depths at an exact location.

To get a better understanding of snow accumulation on a tilted surface a possible snow depth measurement could be to mount a snow gauge at an inclination similar to the tilt angle of a PV module or system. Similar to what Powers et al. [10] did with PV modules mounted at different inclination angles, although the snow measurements used here were for a horizontal and not a tilted surface. To achieve this a possibility would be to apply some form of adhesive layer to prevent snow sliding and see how snow would accumulate on the module surface.

Moreover, snow depth is a complex thing to measure because snow tends to accumulate randomly around on the module surface [6, 8]. The inclination of the PV module and the module shape heavily impacts how snow will accumulate. So, for a module mounted at a certain inclination it is likely that snow accumulating results in different snow depths throughout the module surface. Furthermore, unevenness on the module surface could potentially increase the chances of snow accumulation at certain areas, but wind is another factor that affects snow accumulation [64]. Therefore, even if relatively accurate snow depth measurement were available it would still involve some form of uncertainty.

The power loss caused by snow cover on a PV module surface is not expected to have a linear relationship to the depth of the snow layer. The transmittance is impacted by snow crystals existing in numerous shapes and forms with different characteristics [22]. For example, a wet snow layer with a higher water content and a dryer snow layer of the same depth will certainly result in varied power losses [7]. Moreover, a snow layer will also change over time, and an old, deformed snow layer is likely to be more compacted together, which can impact the transmittance in different ways.

7.3 Simulated versus recorded IV-curves

The IV-curves modelled (with snow) using the MATLAB Simulink model were compared with the recorded IV-curves (with snow) from the UiA PV system. The comparison was done for different types of snow cover. Simulation results for uniform and partial snow cover are illustrated in Figure 7.2 and Figure 7.3 showing the percentage P_{MPP} deviations and absolute P_{MPP} deviations, respectively. Analyzing both percentage and absolute values is necessary because it is easy to misinterpret the results when only looking at percentage values. The P_{MPP} deviation is used to evaluate how the MPP from the modelled and recorded IV-curve matches.

The optimal reduction in irradiance used in the MATLAB model was first assumed based on viewing the module images and the relationship between irradiance reduction and snow depth from published literature [7, 12, 20]. Based on the fit between the modelled and recorded IV-curve the reduction in irradiance was adjusted accordingly by using a trial-and-error approach. However, the P_{MPP} deviation was not calculated for every reduction in irradiance that was tested as this would be very time consuming. Visual inspection was used to determine the overall fit based on the shape of the IV-curve and the P_{MPP}. Therefore, it is likely that in some situations the P_{MPP} deviation could have been decreased, although it is unlikely that the results would have been extremely different.

Most uniform snow cover situations that have irradiance levels <200 W/m² has P_{MPP} deviations at <5%, however two of the cases had differences of >20%. Simultaneously, for the two cases with high irradiance levels (>600 W/m²) the results were more variable, with P_{MPP} deviations of <5% and >15%. Studying the snow depth for the cases with the least P_{MPP} deviation no clear trend is visible. For instance, of the five uniform snow cover cases with P_{MPP} deviations <5%, two situations have snow depths <3 mm, while the two other have snow depths >20 mm, and the remaining one has snow depths >40 mm. Nevertheless, the three cases with the highest P_{MPP} deviations (all >15%) has recorded snow depths as low and high as 0.5 mm and 70 mm, respectively, all with very different irradiance levels. Therefore, the cases with lowest irradiance values are not consistent enough to indicate that low irradiance results in low P_{MPP} deviations.

Figure 7.2 – P_{MPP} deviation results for modelled IV-curves (with modelled snow) with uniform and partial snow cover compared to recorded curves (with snow) for different irradiance and snow depth values.

For various cases of partial snow cover the simulation results are visible in Figure 7.2 where all the modelled situations have irradiance levels >300 W/m². In the same way as the IV-curves modelled with uniform snow cover, the P_{MPP} deviation for the partial snow cover cases are equally variable. The P_{MPP} deviation fluctuates between values from 0.1% to 14.6%, where both cases have similar irradiance values, although the recorded snow depths are 0.5 mm and 70 mm, respectively. In contrast, the remaining three cases consider different time

slots with the same snow depth, even though some snow melting occurs. Still, the P_{MPP} deviation in the first (least snow melted) of these three times starts at 4.3% before decreasing to 2.3% and increasing again to 10.2% for the last situation (most snow melted).

The absolute P_{MPP} deviation for the uniform and partial snow cover situations is illustrated in Figure 7.3. The P_{MPP} deviation for most uniform snow cover cases is <0.5 W with irradiance levels <200 W/m^2, which is a minor difference when comparing the modelled and recorded power values. For the partial snow cover cases the irradiance is more variable (300-500 W/m^2) along with the P_{MPP} deviation that ranges from <0.1 W to 2 W.

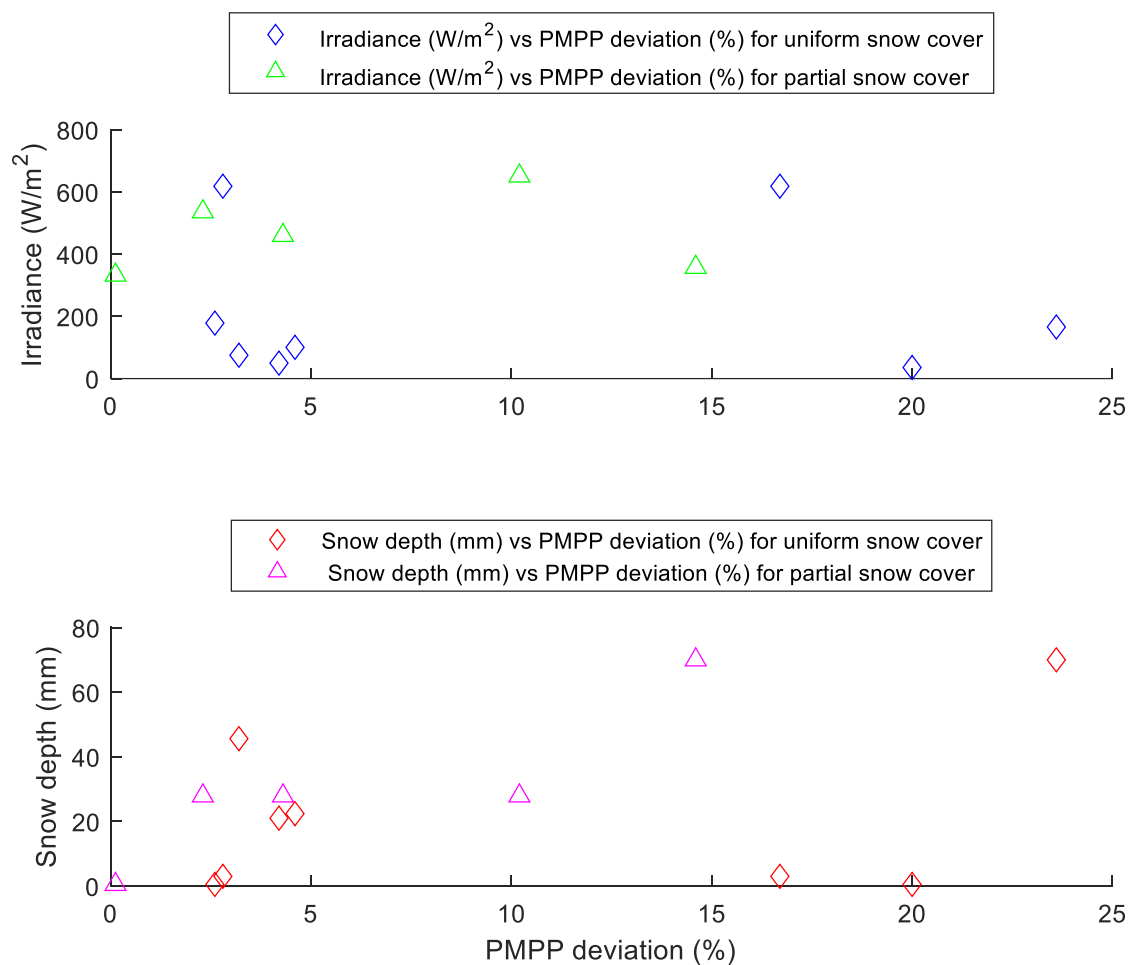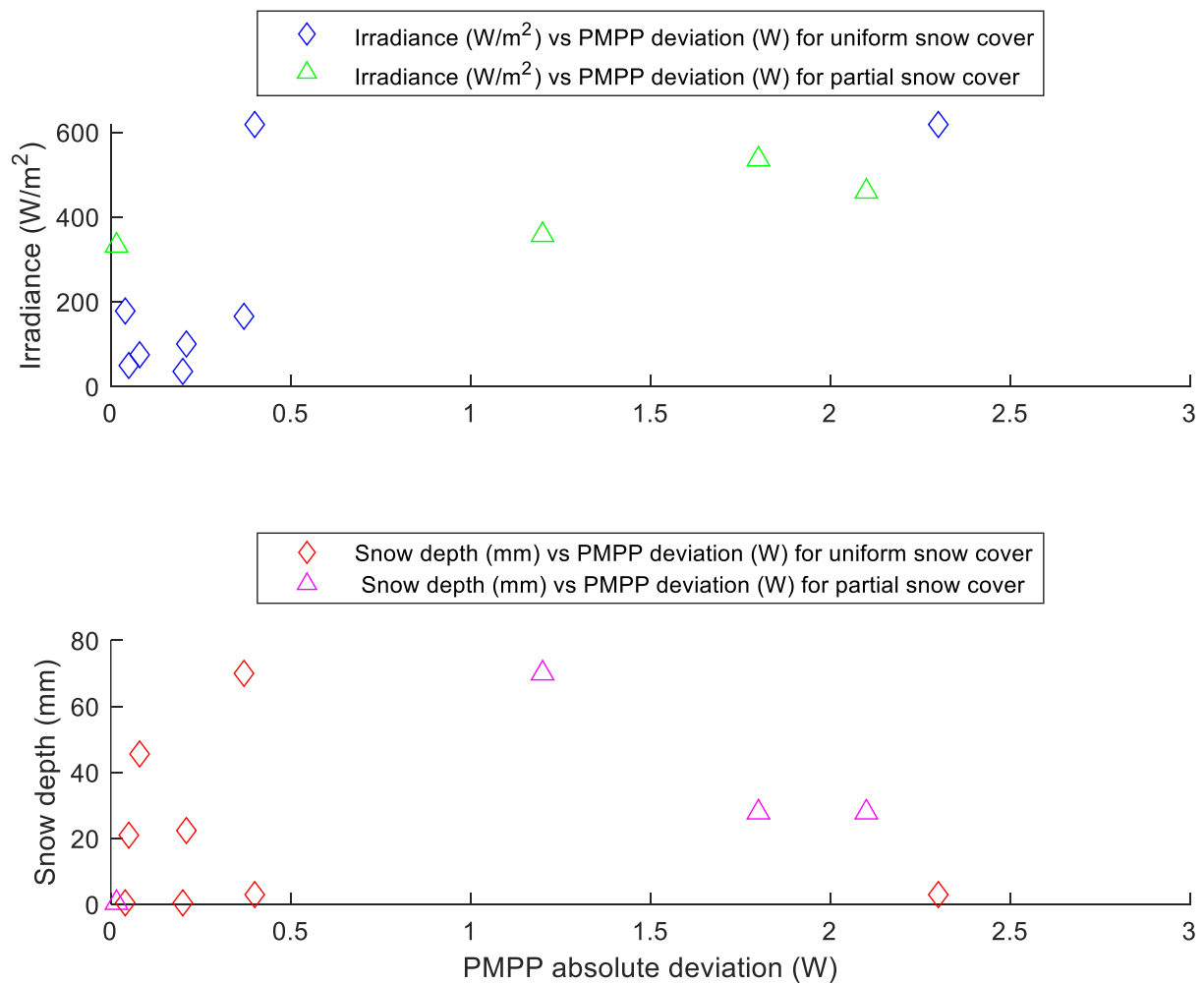*Figure 7.3 – Absolute P_{MPP} deviation results for modelled IV-curves (with modelled snow) with uniform and partial snow cover compared to recorded curves (with snow) for different irradiance and snow depth values. Note that in this plot one outlier (one case with 27.9 mm snow depth) have been removed as it had an absolute deviation value of 12 W and expanded the x-axis too far making it difficult to see the remaining values.*

The uniform snow situations involve snow depths ranging from 0.5 mm to 70 mm, although the absolute P_{MPP} deviation is <0.5 W for most cases. This minimal differences in P_{MPP} for many different snow depths are largely a consequence of the high uncertainty regarding the recorded snow depth values. On the other hand, the partial snow cover situations result in higher absolute P_{MPP} deviation overall for many of the same snow depths when compared to

uniform snow cover. Furthermore, the largest absolute P_{MPP} deviation for both uniform and partial snow cover is slightly above 2 W, which is all in all an insignificant difference.

Comparing the percentage and actual P_{MPP} deviations it is evident that percentage values can give a false impression of the model performance. For instance, a percentage deviation of 20% is considered large, but when the actual P_{MPP} deviation value is <1 W it is not that significant after all. The majority of the absolute P_{MPP} deviation are <2 W both for uniform and partial snow cover situations, however for the same cases the percentage P_{MPP} deviations are >14% for multiple cases, but with the majority being <5%.

The two cases with a recorded snow depth of 70 mm can be identified as clear outliers as the snow depth value is extremely uncertain, and result in a percentage P_{MPP} deviation close to 25%, visible in Figure 7.2. However, at the same time these two cases have an actual P_{MPP} deviation of only 0.4 and 1.2 W, which illustrates that only considering percentage values is not necessarily always a reliable solution.

7.4 Image analysis

In this thesis an image analysis methodology was used to identify uniform and partial snow covers which achieved great results. However, trying to detect module snow coverage for module images taken on days with overcast weather proved to be challenging. Part of the problem was identified as the camera likely not having an optimal angle as some modules ended up being far away and harder to detect. Images taken directly in front and not at an angle would make identifying the module areas and snow covers easier and more precise. Additionally, having a stationary camera setup is also beneficial when relying on and comparing pixel values, because they will vary depending on the camera angle. Furthermore, like the detected areas of uniform snow cover the detected areas for partial snow cover situations also seemed very reasonable. The use of automatically detected irradiance reductions for each module substring as input in the IV-curve model gave moderately more accurate modelled IV-curves, and P_{MPP} deviations that were smaller. Nevertheless, the lack of transmittance data increases the uncertainty of the detected snow layers substantially as the model assumes that for a module area with snow cover there is zero transmittance through the snow layer. To improve the image analysis method including transmittance data is required because it is too essential not be included.

However, a possibility could be to attempt power loss estimations by only using and analysing images, although, this is difficult to do with the image analysis methodology proposed here. The module snow coverages in the form of pixel values were identified, but without having additional data that includes information about the snow cover, beyond how large the covered area is, the use of only images seems questionable. Perhaps a PV module setup designed especially for this purpose with a specialized camera setup in combination with different sensors, and by using snow pixel intensities on a snow cover if they are detectable. In the literature researched during this thesis there is no approach like the one described above using

only images to do power loss estimations that has been discovered. The studies that consider image analysis uses it as part of a more comprehensive methodology, for instance in Braid et al. [35] to identify snow shedding rates. Similarly, in Andrews et al. [8] image analysis was used to determine module clearance and areas on the PV module where snow frequently accumulated. Therefore, the possibilities for relying entirely on image analysis may be a questionable solution, but not completely unthinkable.

7.5 String based model versus cell-based model

To test if the cell-based model performed any better compared to the string-based model, three of the same situations modelled earlier with the string-based model were simulated with the cell-based model. The irradiance and snow depth values for the three previously modelled cases are shown in Table 7.1. The remaining percentage and absolute P_{MPP} deviation results from modelling the IV-curves with the string-based and cell-based model is displayed in Figure 7.4.

Table 7.1 – Irradiance, snow depths, and the percentage and absolute P_{MPP} results from modelling the IV-curves with both the string-based model and the cell-based model.

Irradiance [W/m²]	Snow depth [mm]	P_{MPP} string-based model		P_{MPP} cell-based model	
		Percentage (%)	Absolute (W)	Percentage (%)	Absolute (W)
336	0.5	75.4	18.7	19.7	1.2
460	27.9	4.4	4.4	24.4	11.8
358	70	76.6	18	73.4	15.2

Modelling results show that with the string-based model the percentage P_{MPP} deviation is >75% for two of the cases, while with the cell-based model one case improves greatly (from 75% to 20%), but the other remains almost unchanged. Simultaneously, the absolute P_{MPP} deviation improves by dropping from 18 W to 15 W, and from 19 W to 1 W. However, in the third case the cell-based model performs worse, which increases the P_{MPP} deviation. In the last simulation case using the cell-based model the percentage P_{MPP} deviation is 18% compared to an absolute deviation of only 3 W.
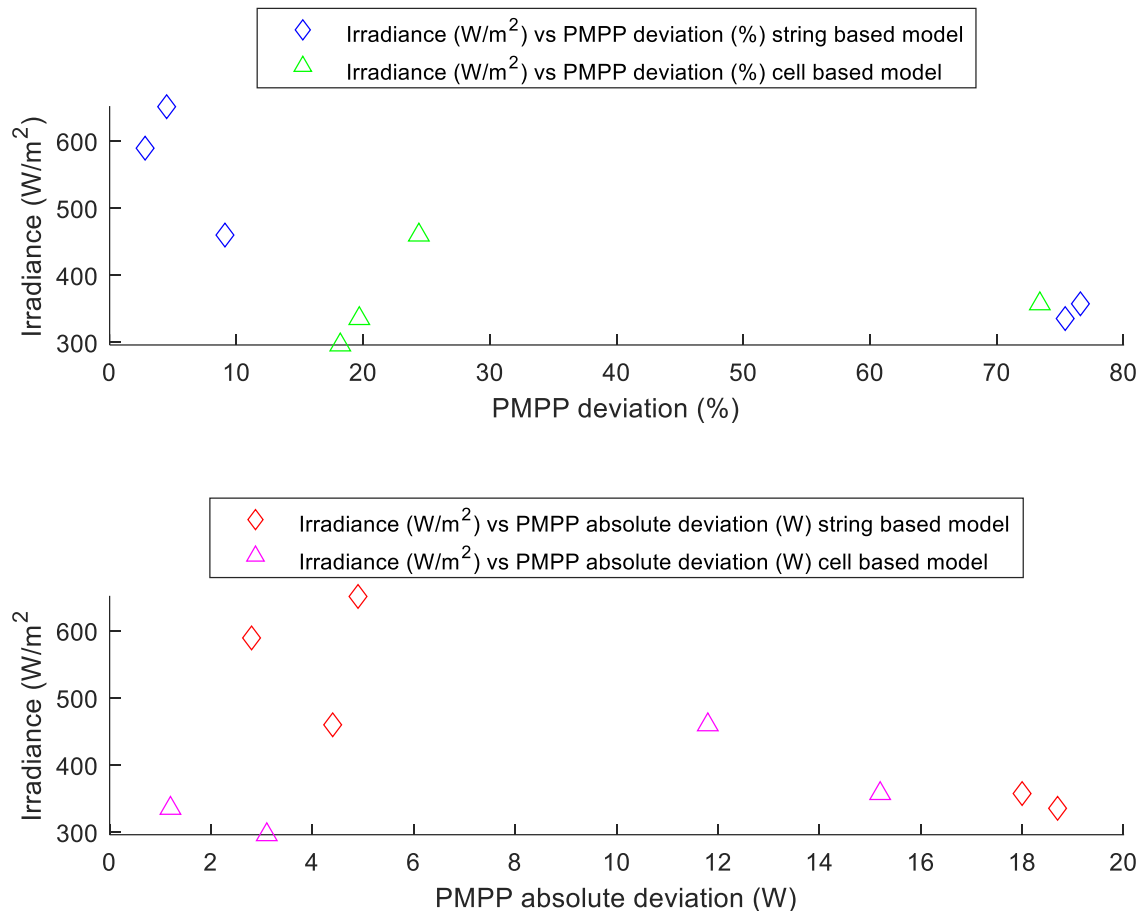
Figure 7.4 – Percentage and absolute P$_{MPP}$ deviations for modelled IV-curves (with modelled snow) with partial snow cover compared to recorded curves (with snow) for different irradiance levels.

To sum up, for some cases there were improvements when using the cell-based model over the string-based model, although in a few cases the string-based model performed better. It could be argued that the advantage of using a cell-based model disappears where there is no transmittance data available.

7.6 Transmittance of snow cover

To simulate snow cover using the MATLAB Simulink model a reduction in the available irradiance reaching each substring of the PV module was implemented. The modelled irradiance reductions were achieved by multiplying the incoming irradiance by a figure between 0 and 1. A limited amount of data was available from the UiA PV system, which did not include any transmittance data. It should be emphasized that transmittance is complicated to measure and is not typically, unless for specific research projects, data that would be recorded for a regular PV system [7]. Not including transmittance is a substantial model simplification as there will be some transmittance through the snow layer dependent on the snow type and depth. However, the current MATLAB Simulink model (with estimated module coverages) assumes that if an area is covered by snow there is no transmittance through the snow layer.

The transmittance on a snow surface is another aspect that is challenging to assess and has a considerable impact in combination with snow depth. Naturally, it will vary based on the snow depth, but also depending on the characteristics of snow. For instance, as snow melts and the water content increase a larger portion of the electromagnetic radiation hitting the snow layer is absorbed. Thus, resulting in less radiation reaching the PV module surface [20]. In contrast, snow can be fluffy or hard packed giving it different optical properties, but the transmittance of snow is also influenced by other factors [7].

As a result, for some of the simulations that are done based on the estimated module coverages by using the proposed image analysis method, the P_{MPP} deviations varies considerably. An improvement could be to consider a 60-cell model where the irradiance for each cell could be specified, instead of assuming it to be equally distributed throughout each individual substring. Nevertheless, this would require transmittance data for the snow layer covering the entire PV module surface, and a more complicated IV-characteristics model to utilize it. The lack of transmittance data being incorporated into the IV-curve modelling, described in the previous chapters, can be considered a likely explanation for the variability and uncertainty in situations with large P_{MPP} deviations and poor IV-curve fit.

7.7 Uncertainty in low irradiance values and angle of incidence

Another aspect closely related to transmittance is the available solar irradiance. Since the situations modelled requires snow, the simulations are based on different timeslots between December and April. During these months the suns position on the sky is relatively low, especially in December and January, which results in the irradiance having a higher incidence angle, and sunrays travelling further, i.e., lowering their intensity [7]. Irradiance is one of the two inputs into the MATLAB Simulink model based on the recorded irradiance data from the pyranometers at the UiA PV System. Thus, resulting in larger reflection losses for the PV modules due to the higher angle of incidence [79, 80]. Meaning that there could potentially be a greater variance between the measured irradiance levels at the pyranometer, and the irradiance reaching the module surface.

This could be one factor that contributes to larger differences between the recorded and the modelled IV-characteristics, and thus higher P_{MPP} deviations. At the same time, several of the situations that were modelled involves low irradiance values, typically <100 W/m^2. This resulted in a decrease in power output not directly proportional to the reduction in irradiance, i.e., a drop in cell efficiency. Additionally, in low light conditions, cells with a higher R_{SH} achieved greater efficiencies contrary to cells with lower R_{SH} values. However, a reduction in cell efficiency was observed even at irradiance levels between 400-600 W/m^2 [50].

Furthermore, the deviations between the recorded and the modelled IV-curves is something that impacts the final P_{MPP} reduction and deviation results. It is already established that there is a mismatch between the recorded and modelled IV-curves, which was confirmed when validating the IV-characteristics model. In a study by Huld et al. [74] the modelled power

values for situations with irradiance levels <100 W/m^2, were lower than the measured power values and deviated by 5-10%. In comparison, the simulation results in this thesis largely had modelled power values that were larger than the recorded power values.

To summarize, of the impacting factors discussed it is undoubtedly the snow layer depth that has the most significant impact in combination with the snow cover transmittance. This is especially noticeable when the snow coverages calculated from the image analysis method is used as input in the IV-curve model. For the modelled IV-curves compared with the recorded IV-curves the largest deviations are likely due to the lack of transmittance data. However, the combination of model uncertainties, such as the low irradiance, angle of incidence, and the IV-characteristics model not being able to completely replicate IV-curves does also impact the results.

8. Conclusion

To conclude, the performance of PV modules is significantly reduced when covered by even small layers of snow. Considerable uniform snow covers result in a reduction in I$_{SC}$ visible on the IV-curves, however for less uniform and partial snow cover situations the activation of bypass diodes is recognizable.

The results from modelling different types of snow cover using the MATLAB model show an acceptable fit between the modelled and recorded IV-curves. The different types of uniform and partial snow cover show small percentage P$_{MPP}$ deviations, but with some exceptions. However, many of the modelled situations involve low irradiance conditions that results in low absolute P$_{MPP}$ values and deviations. This minor absolute deviation is not reflected adequately when percentage P$_{MPP}$ deviation is considered. Furthermore, some cases of better IV-curve fit between modelled and recorded IV-curves indicates that the IV-characteristics model improved under higher irradiance conditions, however no clear trend could be established. The explanation could be that with decreasing irradiance values the uncertainty associated with them increases, and that the IV-characteristics model is incapable of perfectly duplicating the recorded IV-curves. In addition, some uncertainty is linked to irradiance measurements in the winter months, because of a higher angle of incidence and increased reflection losses in the PV modules.

The modelling of IV-curves to determine power loss due to snow cover is challenging, especially for situations with partial snow cover. However, the intention is that after demonstrating that power loss can be estimated with the IV-curve model, and with acceptable performance, it could be developed further to only use external input data like irradiance, temperature, and snow depth. Additionally, the IV-curve model could be used to evaluate what irradiance reductions to expect for different snow cover scenarios, which could be used to establish a more precise correlation between irradiance and snow depth.

The image analysis method proved to be efficient in identifying snow on a PV module surface. Image analysis has a lot of potential, but to utilize it fully transmittance data must be taken into consideration as snow accumulates differently on the module surface. Additionally, transmittance will vary based on the snow depth and snow characteristics. Modelled IV-curves using the estimated PV module substring snow coverages from the image analysis, as input to the IV-curve model, performed variably when used for different partial snow cover situations. In some cases, the simulated IV-curves improved by using the cell-based model compared to the string-based model, however in one case it performed worse.

Summing up, this thesis has demonstrated that the negative impacts of snow cover on PV modules is considerable, and that it is somewhat feasible to model IV-curves to predict the power loss caused by snow cover. The image analysis method is a promising tool that is suitable to detect snow cover, but it should be developed further to utilize its full potential.

9. Recommendations

For future research, a more diverse and greater collection of data would be beneficial and should be collected over time, since the availability of data with situations where PV modules had snow cover was limited. This would allow for better optimization of the model for a variation of different snow cover conditions, and because of a larger data quantity, a more statistically significant assessment of the results.

It is recommended that the image analysis methodology is developed further to include the detection of pixel intensity values, and not just a greyscale/binarized conversion. The idea is to utilize pixel intensity values to estimate the snow reflectance and use the reflectance to approximate the transmittance. Achieving this could help identify how layers of snow are spread out on a PV module surface, to determine which solar cells are covered and preferably by what magnitude. Furthermore, to perform simulations based on image analysis it is necessary to incorporate transmittance values into the model as this must be accounted for to improve the accuracy. Alternatively, having a way to estimate the transmittance, or making assumptions based on the snow type that is present, such as fresh snow likely having a higher transmittance, in contrast to older and more compressed snow.

The IV-characteristics model manages to estimate power losses due to snow cover when compared with recorded IV-curves with acceptable deviations. The next step for the IV-curve model is to develop and improve it further so that only external input is used, that includes irradiance and module temperature, which was done in this thesis, but also incorporating snow depth could be a significant improvement. No recorded IV-curves would be used with this improved version of the model, which was only necessary to use as a basis for comparison in this thesis to test the model performance.

10. References

[1]   Ø. Bjørgum, "The Effects of Snow on IV-curves and PV Module Performance," University of Agder, Final Report ENE503 Energy Research Project (Internal report, not published), December 2021.

[2]   U. Mandadapu, V. Vedanayakam, and K. Thyagarajan, "EFFECT OF TEMPERATURE AND IRRADIANCE ON THE ELECTRICAL PERFORMANCE OF A PV MODULE," *International Journal of Advanced Research,* vol. 5, pp. 2018-2027, 03/31 2017, doi: 10.21474/IJAR01/3720.

[3]   C. Honsberg and S. Bowden. "Effect of Temperature." PVEducation. https://www.pveducation.org/pvcdrom/solar-cell-operation/effect-of-temperature (accessed 01.11, 2021).

[4]   IEA, "Renewables 2021: Analysis and forecast to 2026," The International Energy Agency, IEA, Paris, 2021. Accessed: 08.05. [Online]. Available: https://www.iea.org/reports/renewables-2021

[5]   D. H. Wirth, "Recent Facts about Photovoltaics in Germany," Fraunhofer ISE, 2021. Accessed: 08.05. [Online]. Available: https://www.ise.fraunhofer.de/en/publications/studies/recent-facts-about-pv-in-germany.html

[6]   R. E. Pawluk, Y. Chen, and Y. She, "Photovoltaic electricity generation loss due to snow – A literature review on influence factors, estimation, and mitigation," *Renewable and Sustainable Energy Reviews,* vol. 107, pp. 171-182, 2019, doi: https://doi.org/10.1016/j.rser.2018.12.031.

[7]   E. Andenæs, J. Bjørn, R. Kristin, K. Tore, S. Josefine, and F. Sean, "The Influence of Snow and Ice Coverage on the Energy Generation from Photovoltaic Solar Cells," *Solar Energy,* vol. 159, pp. 318-328, 01 2018, doi: 10.1016/j.solener.2017.10.078.

[8]   R. Andrews, A. Pollard, and J. Pearce, "The Effects of Snowfall on Solar Photovoltaic Performance," *Solar Energy,* vol. 92, pp. 84-97, 04 2013, doi: 10.1016/j.solener.2013.02.014.

[9]   B. Marion, R. Schaefe, H. Caine, and G. Sanchez, "Measured and modeled photovoltaic system energy losses from snow for Colorado and Wisconsin locations," *Solar Energy,* vol. 97, pp. 112-121, 2013, doi: https://doi.org/10.1016/j.solener.2013.07.029.

[10]   L. Powers, J. Newmiller, and T. Townsend, "Measuring and modeling the effect of snow on photovoltaic system performance," *2010 35th IEEE Photovoltaic Specialists Conference,* pp. 000973-000978, 2010.

[11]   R. Andrews and J. Pearce, "Prediction of energy effects on photovoltaic systems due to snowfall events," *Photovoltaic Specialists Conference (PVSC), 2012 38th IEEE,* pp. 003386-003391, 2012, doi: 10.1109/PVSC.2012.6318297.

[12]   M. B. Øgaard, B. L. Aarseth, Å. F. Skomedal, H. N. Riise, S. Sartori, and J. H. Selj, "Identifying snow in photovoltaic monitoring data for improved snow loss modeling and snow detection," *Solar Energy,* vol. 223, pp. 238-247, 2021/07/15/ 2021, doi: https://doi.org/10.1016/j.solener.2021.05.023.

[13]   I. Hanssen-Bauer *et al.*, "Climate in Norway 2100 - a knowledge base for climate adaptation," The Norwegian Centre for Climate Services (NCCS), 2017. Accessed: 04.11. [Online]. Available: https://www.miljodirektoratet.no/globalassets/publikasjoner/M741/M741.pdf

[14]   P. Bulanyi and R. Zhang Si, "Shading Analysis & Improvement for Distributed Residential Grid-Connected Photovoltaics Systems," presented at the Solar2014: The 52nd Annual Conference of the Australian Solar Council, Si Clean Energy Pty Ltd, Coffs Harbour, NSW 2450 Australia, 2014.

[15]   C. Honsberg and S. Bowden. "Mismatch Effects." PVEducation. https://www.pveducation.org/pvcdrom/modules-and-arrays/mismatch-effects (accessed 15.11, 2021).

[16]   K. Mertens, *Photovoltaics: Fundamentals, Technology, and Practice, 2nd Edition*. John Wiley & Sons Ltd, 2018, p. 368.

[17]   Y. Jiang, J. A. A. Qahouq, and M. Orabi, "Matlab/Pspice hybrid simulation modeling of solar PV cell/module," in *2011 Twenty-Sixth Annual IEEE Applied Power Electronics Conference and Exposition (APEC)*, 6-11 March 2011 2011, pp. 1244-1250, doi: 10.1109/APEC.2011.5744752.

[18]   M. Aljumaili, A. Abdalkafor, and M. Taha, "Analysis of the Hard and Soft Shading Impact on Photovoltaic Module Performance Using Solar Module Tester," *International Journal of Power Electronics and Drive Systems,* vol. 10, 06/13 2019, doi: 10.11591/ijpeds.v10.i2.pp1014-1021.

[19]   G. Becker, B. Schiebelsberger, W. Weber, C. Vodermayer, M. Zehner, and G. Kummerle, "AN APPROACH TO THE IMPACT OF SNOW ON THE YIELD OF GRID CONNECTED PV SYSTEMS," Bavarian Association for the Promotion of Solar Energy, Munich, Bavaria, Germany, 2006. Accessed: 30.09.2021. [Online]. Available: http://citeseerx.ist.psu.edu/viewdoc/download?doi=10.1.1.464.8842&rep=rep1&type=pdf

[20]   D. Perovich, "Light reflection and transmission by a temperate snow cover," *Journal of Glaciology - J GLACIOLOGY,* vol. 53, 03 2007, doi: 10.3189/172756507782202919.

[21]   G. Mathiak, J. Sommer, W. Herrmann, N. Bogdanski, J. Althaus, and F. Reil, "PV Module Damages Caused by Hail Impact and Non-Uniform Snow Load," presented at the 32nd European Photovoltaic Solar Energy Conference and Exhibition, 2016, 3-936338-41-8.

[22]   M. Ross, "Snow and Ice Accumulation on Photovoltaic Arrays: An Assessment of the TN Conseil Passive Melting Technology," Energy Diversification Research Laboratory, CANMET, Natural Resources Canada, Varennes, CANMET, 1995. Accessed: 04.11. [Online]. Available: http://rerinfo.ca/documents/trPVSnowandRime.pdf

[23]   Innos. "WEIGHT WATCHER." https://www.innos.no/weight-watcher/ (accessed 08.10, 2021).

[24]   J. Selj, M. Øgaard, and B. B. Aarseth. "Kan bruke strøm til å smelte snøen på solcellene." Dagens Næringsliv. https://www.dn.no/teknologi/solceller/solenergi/fornybar-energi/kan-bruke-strom-til-a-smelte-snoen-pa-solcellene/2-1-535954 (accessed 08.10, 2021).

[25]   B. P. Jelle, "The challenge of removing snow downfall on photovoltaic solar cell roofs in order to maximize solar energy efficiency—Research opportunities for the future," *Energy and*

Buildings, vol. 67, pp. 334-351, 2013/12/01/ 2013, doi: https://doi.org/10.1016/j.enbuild.2013.08.010.

[26]   L. Burnham, D. Riley, and J. Braid, "Design Considerations for Photovoltaic Systems Deployed in Snowy Climates," presented at the 37th European Photovoltaic Solar Energy Conference and Exhibition, 2020, 3-936338-73-6. [Online]. Available: https://www.eupvsec-proceedings.com/proceedings?paper=49817.

[27]   M. B. Øgaard, H. N. Riise, H. Haug, S. Sartori, and J. H. Selj, "Photovoltaic system monitoring for high latitude locations," *Solar Energy,* vol. 207, pp. 1045-1054, 2020/09/01/ 2020, doi: https://doi.org/10.1016/j.solener.2020.07.043.

[28]   C. Schill, S. Brachmann, and M. Koehl, "Impact of soiling on IV-curves and efficiency of PV-modules," *Solar Energy,* vol. 112, pp. 259-262, 2015/02/01/ 2015, doi: https://doi.org/10.1016/j.solener.2014.12.003.

[29]   W. Marion and K. Urban, "User's Manual for TMY2s: Typical Meteorological Years," NREL, National Renewable Energy Laboratory, 1995. [Online]. Available: https://www.nrel.gov/docs/legosti/old/7668.pdf

[30]   T. Townsend and L. Powers, "Photovoltaics and snow: An update from two winters of measurements in the SIERRA," in *2011 37th IEEE Photovoltaic Specialists Conference*, 19-24 June 2011 2011, pp. 003231-003236, doi: 10.1109/PVSC.2011.6186627.

[31]   S. Yunlin, C. Siming, X. Liying, H. Ruijiang, and S. Hui, "Investigating the Impact of Shading Effect on the Characteristics of a Large-Scale Grid-Connected PV Power Plant in Northwest China," *International Journal of Photoenergy,* vol. 2014, 03 2014, doi: 10.1155/2014/763106.

[32]   A. Xenophontos and A. Bazzi, "Model-Based Maximum Power Curves of Solar Photovoltaic Panels Under Partial Shading Conditions," *IEEE Journal of Photovoltaics,* vol. PP, pp. 1-6, 11/16 2017, doi:10.1109/JPHOTOV.2017.2764488.

[33]   V. Tamrakar, S. C. Gupta, and Y. Sawle, "Single-Diode Pv Cell Modeling And Study Of Characteristics Of Single And Two-Diode Equivalent Circuit," *Electrical and Electronics Engineering: An International Journal,* vol. 4, pp. 13-24, 08/31 2015, doi: 10.14810/elelij.2015.4302.

[34]   B. L. Aarseth and E. S. Marstein, "Defect Recognition and Power Loss Estimation of PV Systems Using Infrared Thermography," presented at the 36th European Photovoltaic Solar Energy Conference and Exhibition, 2019, 3-936338-60-4.

[35]   J. Braid, D. Riley, J. Pearce, and L. Burnham, "Image Analysis Method for Quantifying Snow Losses on PV Systems," presented at the 2020 IEEE 47th Photovoltaic Specialists Conference (PVSC), 2020.

[36]   T. Saga, "Advances in crystalline silicon solar cell technology for industrial mass production," *NPG Asia Materials,* vol. 2, no. 3, pp. 96-102, 2010/07/01 2010, doi: 10.1038/asiamat.2010.82.

[37]   S. Bowden and C. Honsberg. "Types of Silicon." PVEducation. https://www.pveducation.org/pvcdrom/manufacturing-si-cells/types-of-silicon (accessed 14.12, 2021).

[38]   D. Kang, T. White, and A. Thomson, "PV Module Recycling: Mining Australian Rooftops,"
        presented at the 2015 ASIA-PACIFIC SOLAR RESEARCH CONFERENCE, The Australian National
        University (ANU), Canberra 0200, Australia, 2015.

[39]   C. Honsberg and S. Bowden. "Module Materials." PVEducation.
        https://www.pveducation.org/pvcdrom/modules-and-arrays/module-materials (accessed
        06.11, 2021).

[40]   J. Svarc. "Solar Panel Construction." Clean Energy Reviews.
        https://www.cleanenergyreviews.info/blog/solar-panel-components-construction (accessed
        11.10, 2021).

[41]   V. Eremeyev and K. Naumenko, "A layer-wise theory for laminated glass and photovoltaic
        panels," *Composite Structures,* vol. 112, pp. 283–291, 06 2014, doi:
        10.1016/j.compstruct.2014.02.009.

[42]   C. Honsberg and S. Bowden. "Measurement of Solar Cell Efficiency." PVEducation.
        https://www.pveducation.org/pvcdrom/characterisation/measurement-of-solar-cell-
        efficiency (accessed 15.11, 2021).

[43]   C. Honsberg and S. Bowden. "Diode Equation." PVEducation.
        https://www.pveducation.org/pvcdrom/pn-junctions/diode-equation (accessed 14.01,
        2022).

[44]   S. Bowden and C. Honsberg. "IV Curve." PVEducation.
        https://www.pveducation.org/pvcdrom/solar-cell-operation/iv-curve (accessed 15.12, 2021).

[45]   A. E.-B. Wafaa, A. M. A. E. Maksood, and F. A. S. Soliman, "Mathematical Model for
        Photovoltaic Cells," *Leonardo Journal of Sciences,* no. 23, July-December 2013, pp. 13-28,
        2013.

[46]   K. Mertens, "Photovoltaics: Fundamentals, Technology, and Practice, 2nd Edition," John
        Wiley & Sons Ltd, 2018, ch. 4: Structure and Method of Operation of Solar Cells, pp. 85-90.

[47]   S. Bowden and C. Honsberg. "Series Resistance." PVEducation.
        https://www.pveducation.org/pvcdrom/solar-cell-operation/series-resistance (accessed
        26.01, 2022).

[48]   F. Mavromatakis, F. Vignola, and B. Marion, "Low irradiance losses of photovoltaic modules,"
        Solar Energy, vol. 157, pp. 496-506, 2017/11/15/ 2017, doi:
        https://doi.org/10.1016/j.solener.2017.08.062.

[49]   C. S. Ruschel, F. P. Gasparin, E. R. Costa, and A. Krenzinger, "Assessment of PV modules shunt
        resistance dependence on solar irradiance," *Solar Energy,* vol. 133, pp. 35-43, 2016/08/01/
        2016, doi: https://doi.org/10.1016/j.solener.2016.03.047.

[50]   P. Grunow *et al.*, "Weak light performance and annual yields of PV modules and systems as a
        result of the basic parameter set of industrial solar cells," *Proc. 19th European Photovoltaic
        Solar Energy Conf.,* 01/01 2004.

[51]   B. Litzenburger, S. Pingel, S. Janke, S. Held, and R. Alam, "LOW LIGHT PERFORMANCE OF
SOLAR CELLS AND MODULES," presented at the 29. European Photovoltaic Solar Energy
Conference, Amsterdam, Netherlands, 2014.

[52]   C. Honsberg and S. Bowden. "Shading." PVEducation.
https://www.pveducation.org/pvcdrom/modules-and-arrays/shading (accessed 01.11, 2021).

[53]   S. Bowden and C. Honsberg. "Bypass Diodes." PVEducation.
https://www.pveducation.org/pvcdrom/modules-and-arrays/bypass-diodes (accessed 21.10,
2021).

[54]   B. B. Pannebakker, A. C. de Waal, and W. G. J. H. M. van Sark, "Photovoltaics in the shade:
one bypass diode per solar cell revisited," *Progress in Photovoltaics: Research and
Applications,* https://doi.org/10.1002/pip.2898 vol. 25, no. 10, pp. 836-849, 2017/10/01
2017, doi: https://doi.org/10.1002/pip.2898.

[55]   M. Köntges *et al.*, "Review of Failures of Photovoltaic Modules," in "PHOTOVOLTAIC POWER
SYSTEMS PROGRAMME," IEA, T13-01:2014, 2014. [Online]. Available:
https://www.researchgate.net/publication/274717701_Review_of_Failures_of_Photovoltaic
_Modules

[56]   D. Ji, C. Zhang, M. Lv, Y. Ma, and N. Guan, "Photovoltaic Array Fault Detection by Automatic
Reconfiguration," *Energies,* vol. 10, p. 699, 05/16 2017, doi: 10.3390/en10050699.

[57]   B. Hashemi, S. Taheri, A.-M. Cretu, and E. Pouresmaeil, "Systematic photovoltaic system
power losses calculation and modeling using computational intelligence techniques," *Applied
Energy,* vol. 284, p. 116396, 2021/02/15/ 2021, doi:
https://doi.org/10.1016/j.apenergy.2020.116396.

[58]   Y. el basri, M. Bressan, L. Seguier, H. Alawadhi, and C. Alonso, "A proposed graphical
electrical signatures supervision method to study PV module failures," *Solar Energy,* vol. 116,
pp. 247-256, 06/30 2015, doi: 10.1016/j.solener.2015.02.048.

[59]   EnergySage. "Most efficient solar panels: solar panel cell efficiency explained." EnergySage.
https://news.energysage.com/what-are-the-most-efficient-solar-panels-on-the-market/
(accessed 01.11, 2021).

[60]   L. W. Thong, S. Murugan, P. K. Ng, and S. Chee, "Analysis of Photovoltaic Panel Temperature
Effects on its Efficiency," presented at the Conference: 2nd International Conference on
Electrical Engineering and Electronics, Ho Chi Minh, Vietnam, 2016.

[61]   SeNorge. "Nysnø." www.senorge.no. senorge.no (accessed 07.02, 2022).

[62]   U. Faculty of Engineering and Science, "OUTDOOR PV LAB J5, UIA GRIMSTAD," Engineering
Sciences, UiA, 2018.

[63]   MathWorks. "Partial Shading of a PV Module." MathWorks.
https://se.mathworks.com/help/physmod/sps/ug/partial-shading-of-a-pv-
module.html#d123e52519 (accessed 02.02, 2022).

[64]   R. Pfister and M. Schneebeli, "Snow accumulation on boards of different sizes and shapes," *Hydrological Processes - HYDROL PROCESS,* vol. 13, pp. 2345-2355, 10/01 1999, doi: 10.1002/(SICI)1099-1085(199910)13:14/153.0.CO;2-N.

[65]   C. W. Hansen and B. H. King, "Determining Series Resistance for Equivalent Circuit Models of a PV Module," *IEEE Journal of Photovoltaics,* vol. 9, no. 2, pp. 538-543, 2019, doi: 10.1109/JPHOTOV.2018.2883703.

[66]   Z. Song *et al.*, "An Effective Method to Accurately Extract the Parameters of Single Diode Model of Solar Cells," (in eng), *Nanomaterials (Basel, Switzerland),* vol. 11, no. 10, p. 2615, 2021, doi: 10.3390/nano11102615.

[67]   V. Chernov, J. Alander, and V. Bochko, "Integer-based accurate conversion between RGB and HSV color spaces," *Computers & Electrical Engineering,* vol. 46, pp. 328-337, 2015/08/01/ 2015, doi: https://doi.org/10.1016/j.compeleceng.2015.08.005.

[68]   C. Kanan and G. W. Cottrell, "Color-to-Grayscale: Does the Method Matter in Image Recognition?," *PLOS ONE,* vol. 7, no. 1, p. e29740, 2012, doi: 10.1371/journal.pone.0029740.

[69]   C. Huang, X. Li, and Y. Wen, "AN OTSU image segmentation based on fruitfly optimization algorithm," *Alexandria Engineering Journal,* vol. 60, no. 1, pp. 183-188, 2021/02/01/ 2021, doi: https://doi.org/10.1016/j.aej.2020.06.054.

[70]   K. Zidek and A. Hošovský, "Image thresholding and contour detection with dynamic background selection for inspection tasks in machine vision," *International Journal of Circuits, Systems and Signal Processing,* vol. 8, pp. 545-554, 01/01 2014.

[71]   C. Olalla, M. N. Hasan, C. Deline, and D. Maksimovic, "Mitigation of Hot-Spots in Photovoltaic Systems Using Distributed Power Electronics," *Energies,* vol. 11, p. 726, 03/23 2018, doi: 10.3390/en11040726.

[72]   K. Müller, H. Toft Larsen, and G. Sojer, "Snøomvandling," Norges vassdrags- og energidirektorat, NVE, 2020. Accessed: 22.03. [Online]. Available: https://publikasjoner.nve.no/faktaark/2020/faktaark2020_01.pdf

[73]   E. E. Stigter *et al.*, "The Importance of Snow Sublimation on a Himalayan Glacier," (in English), *Frontiers in Earth Science,* Original Research vol. 6, 2018-August-24 2018, doi: 10.3389/feart.2018.00108.

[74]   T. Huld *et al.*, "A power-rating model for crystalline silicon PV modules," *Solar Energy Materials and Solar Cells - SOLAR ENERG MATER SOLAR CELLS,* vol. 95, pp. 3359-3369, 12/01 2011, doi: 10.1016/j.solmat.2011.07.026.

[75]   I. PVPS, "Qualification of Photovoltaic (PV) Power Plants using Mobile Test Equipment," in "Task 13: Performance, Operation and Reliability of Photovoltaic Systems," ISBN 978-3-907281-12-3, 2021. Accessed: 03.05. [Online]. Available: https://iea-pvps.org/key-topics/qualification-of-pv-power-plants-using-mobile-test-equipment/

[76]   A. T. E. Corp. "TDI Power MCL488 3500W Multi-Channel Loads." ATEC. https://www.atecorp.com/atecorp/media/pdfs/data-sheets/tdipowermcl488_specs.pdf (accessed 15.05, 2022).

[77]   K. Zonen. "Kipp & Zonen Instruction Manual CMP Series." https://s.campbellsci.com/documents/us/manuals/kippzonen_manual_cmp-series.pdf (accessed 15.05, 2022).

[78]   C. Scientific. "110PV-L: Surface-Mount Thermistor." Campbell Scientific. https://www.campbellsci.com/110pv (accessed 15.05, 2022).

[79]   C. Reise, B. Müller, D. Moser, G. Belluardo, and P. Ingenhoven, "Task 13: Uncertainties in PV System Yield Predictions and Assessments," IEA, 2018. Accessed: 10.05. [Online]. Available: https://www.researchgate.net/publication/324703099_Task_13_Uncertainties_in_PV_System_Yield_Predictions_and_Assessments

[80]   M. Issa Faye and Ababacar Ndiaye and Elkhadji, "Influence of the Incidence Angle Modifier and Radiation as a Function of the Module Performance for Monocrystalline Textured Glass and No Textured in Outdoor Exposed," in *Solar Cells*, E. Ahmed Mourtada Ed. Rijeka: IntechOpen, 2021.

Appendices

Appendix A.1

MATLAB Simulink bypass diode parameter window.
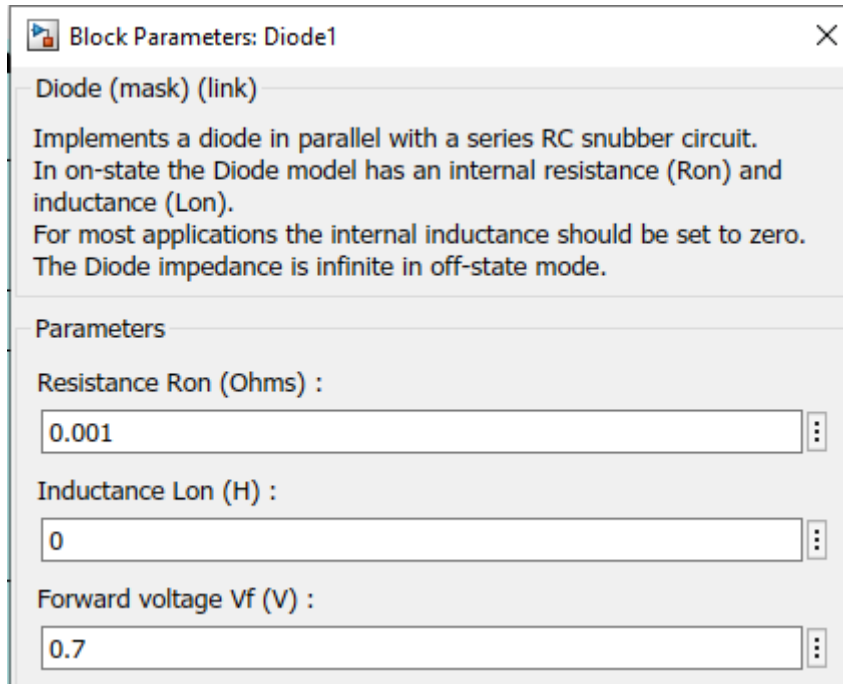
Appendix A.2

Modelled IV and PV-curves for MATLAB Simulink model validation, Q-Cells A10156 PV module.

Modelled and recorded curves for Q-Cells A10156 module on 23/03/15 at 12:31

Modelled and recorded curves for Q-Cells A10156 module on 05/03/16 at 10:46
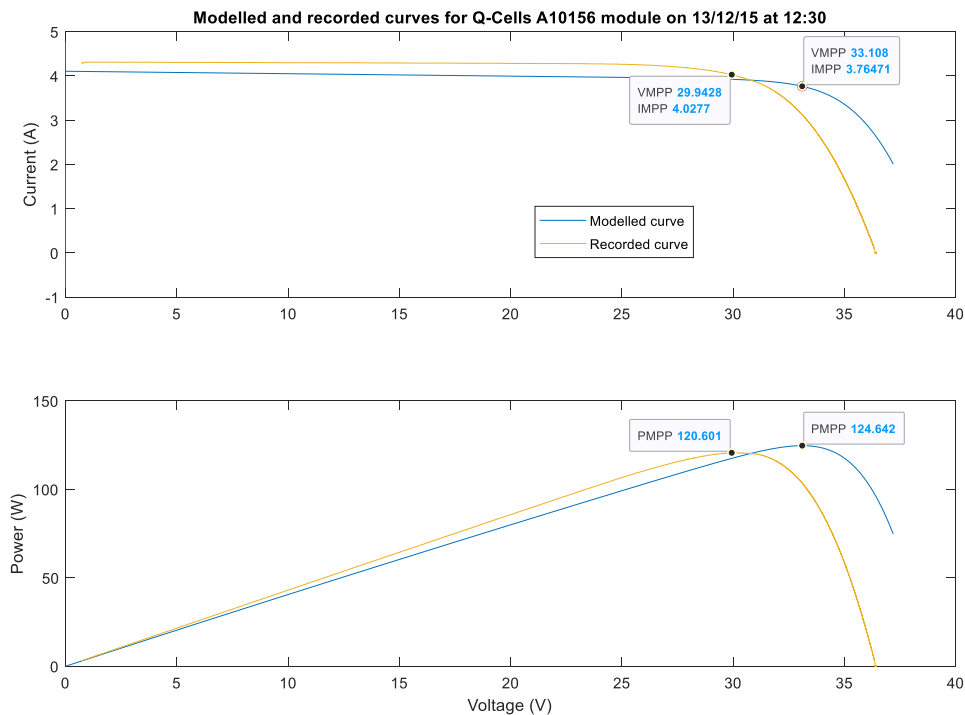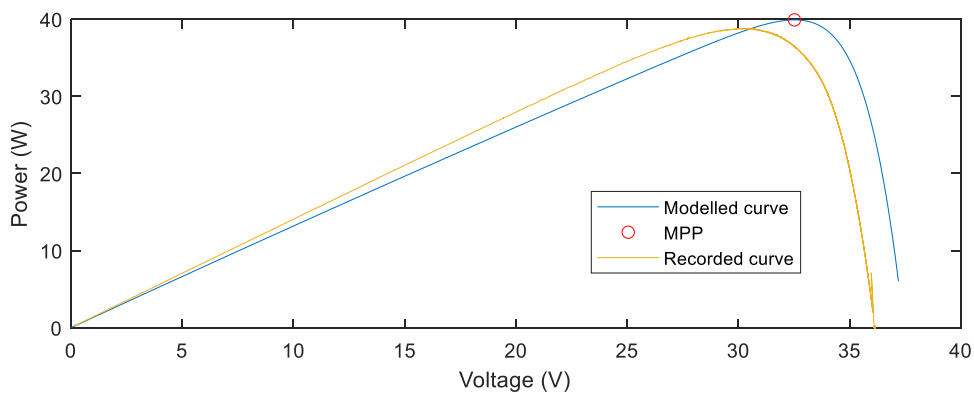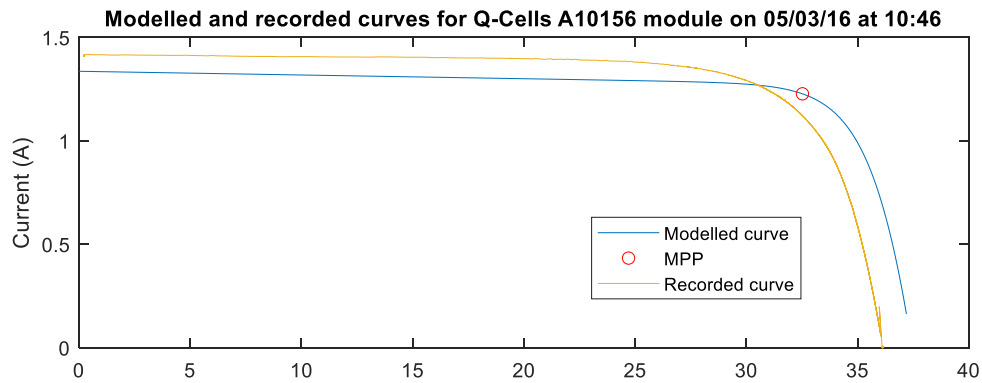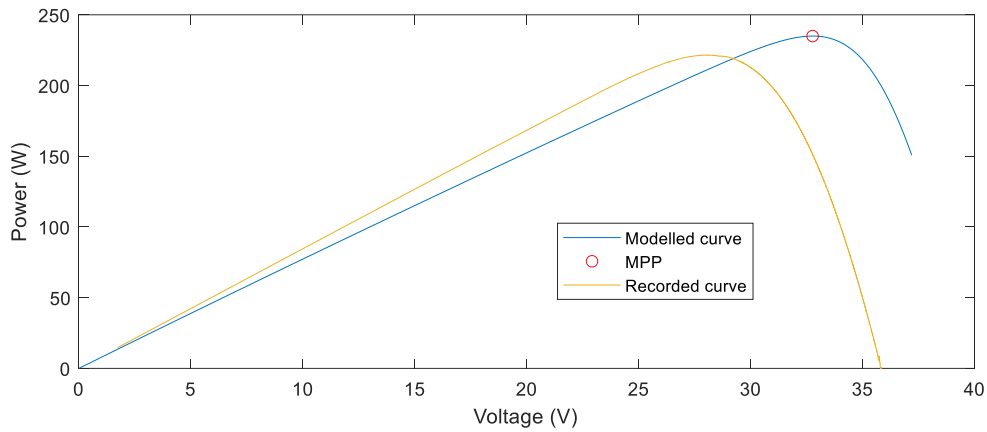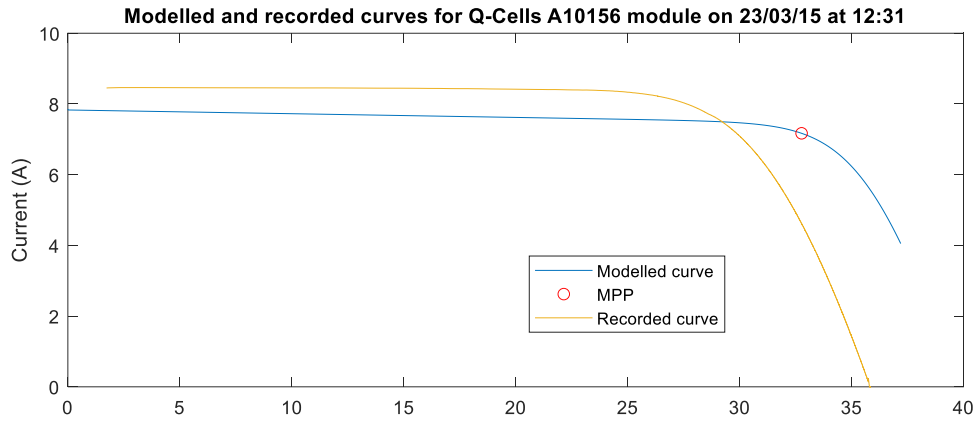
Appendix A.3

Modelled IV and PV-curves for MATLAB Simulink model validation, TITAN PV module.

Modelled and recorded curves for TITAN module on 13/12/15 at 14:30

Modelled and recorded curves for TITAN module on 02/04/15 at 13:09

Modelled and recorded curves for TITAN module on 13/12/15 at 12:30
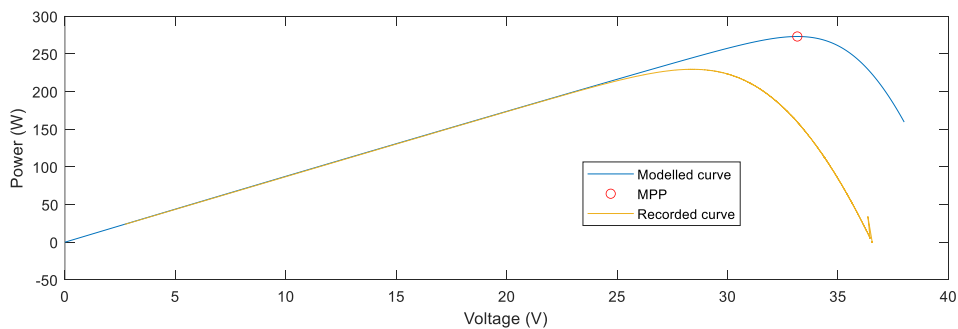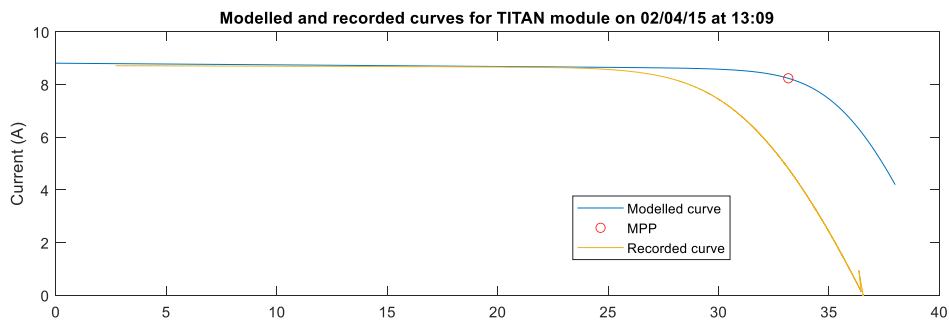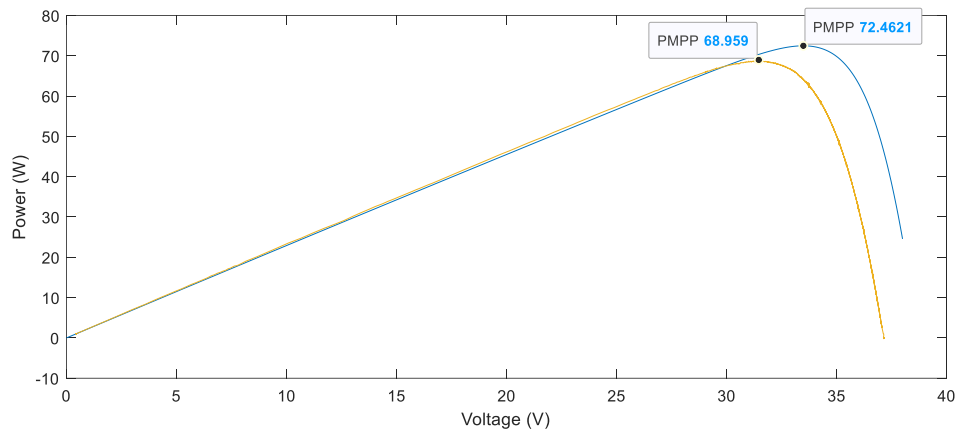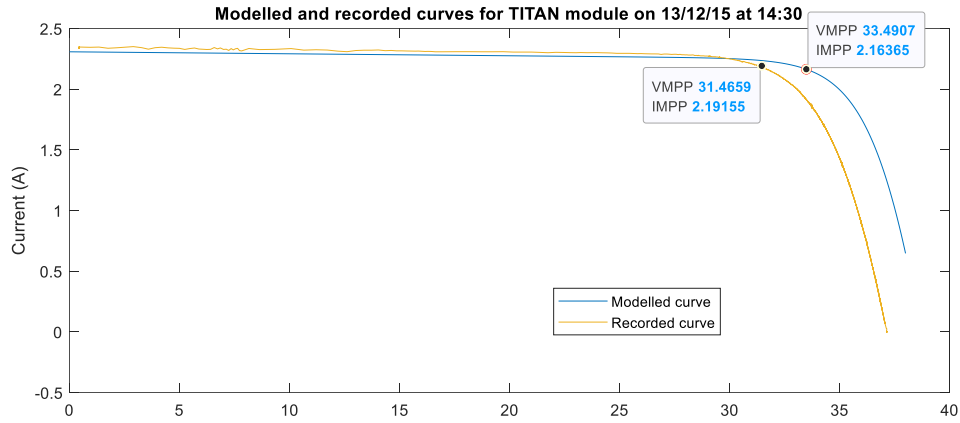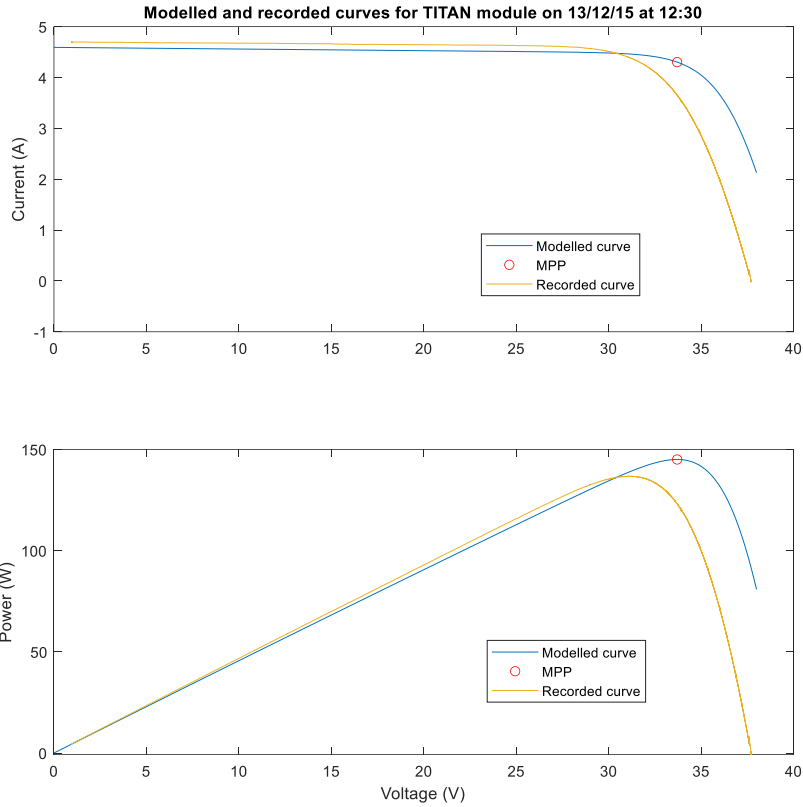
Appendix A.4

Modelled IV and PV-curves for MATLAB Simulink model validation, SunTech 422 PV module.

Modelled and recorded curves for SunTech 422 module on 18/01/16 at 12:45

Modelled and recorded curves for SunTech 422 module on 16/12/17 at 09:20

Modelled and recorded curves for SunTech 422 module on 08/03/16 at 14:31

Modelled and recorded curves for SunTech 422 module on 02/04/15 at 13:09
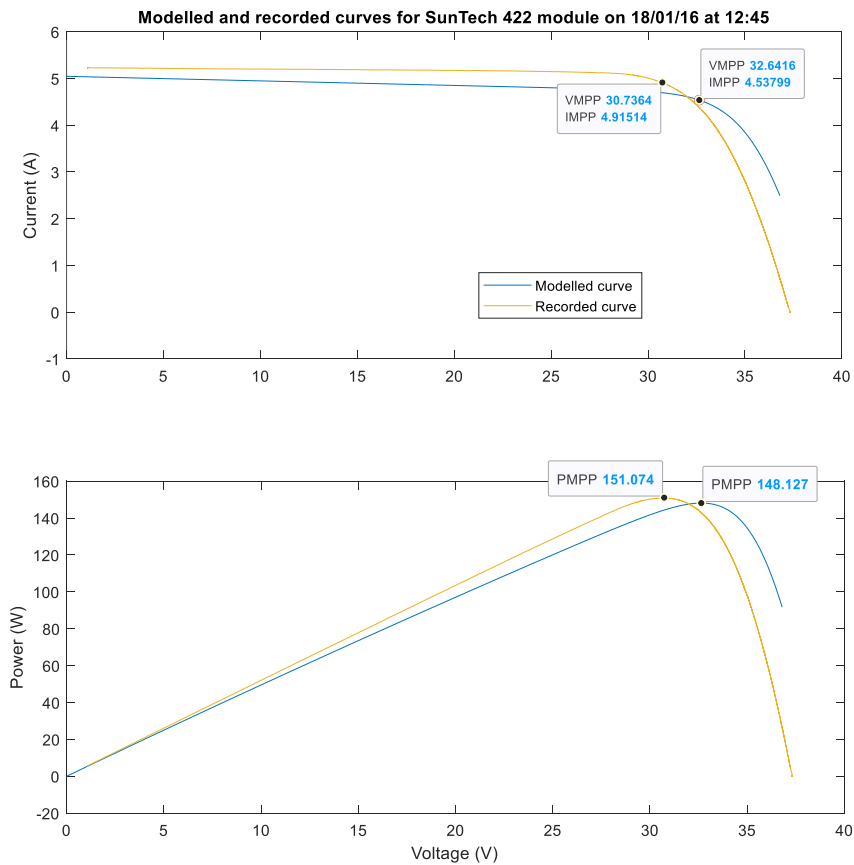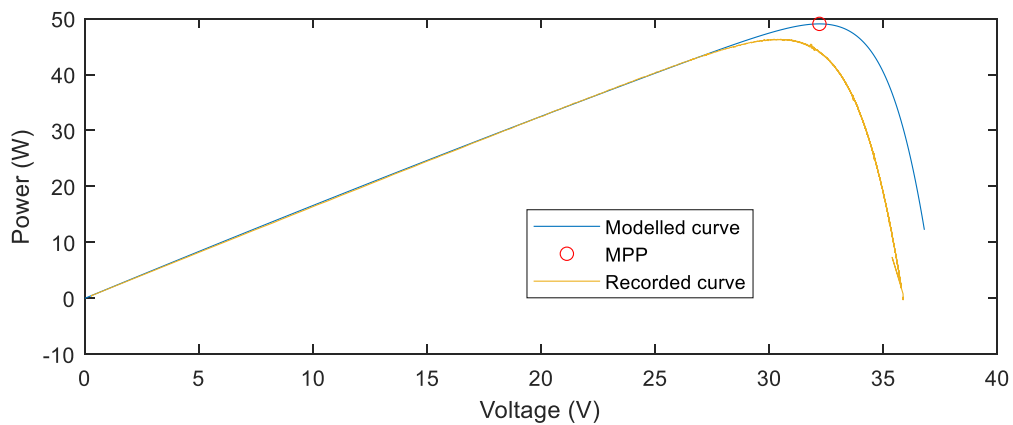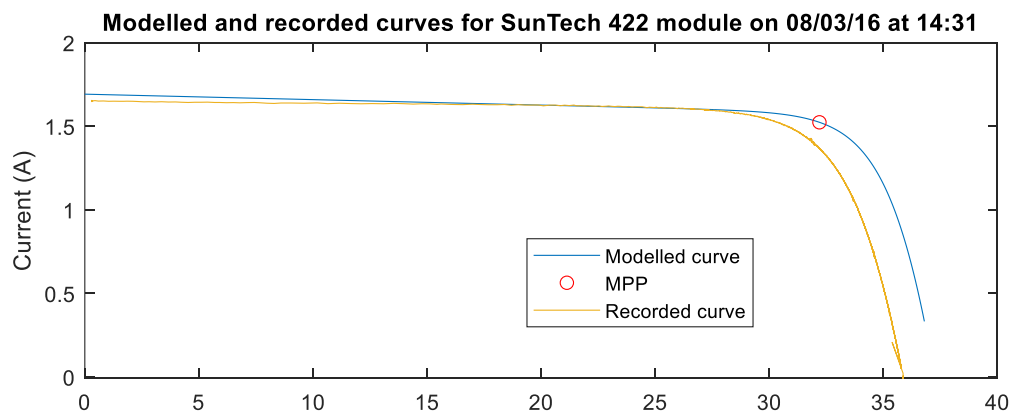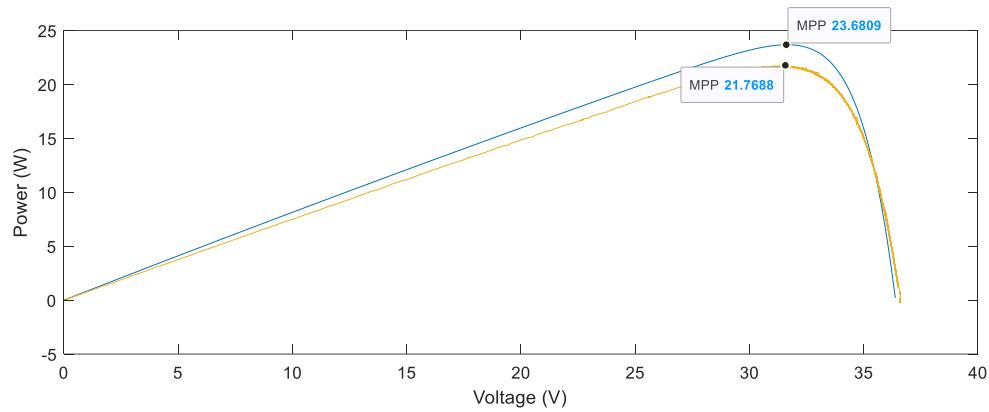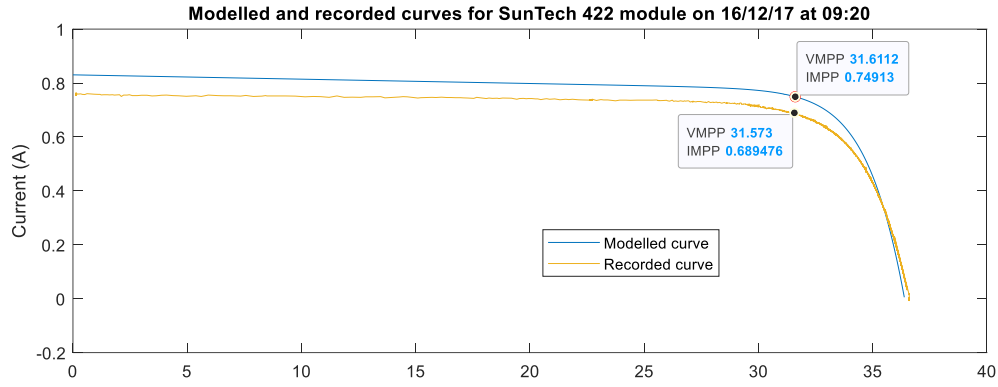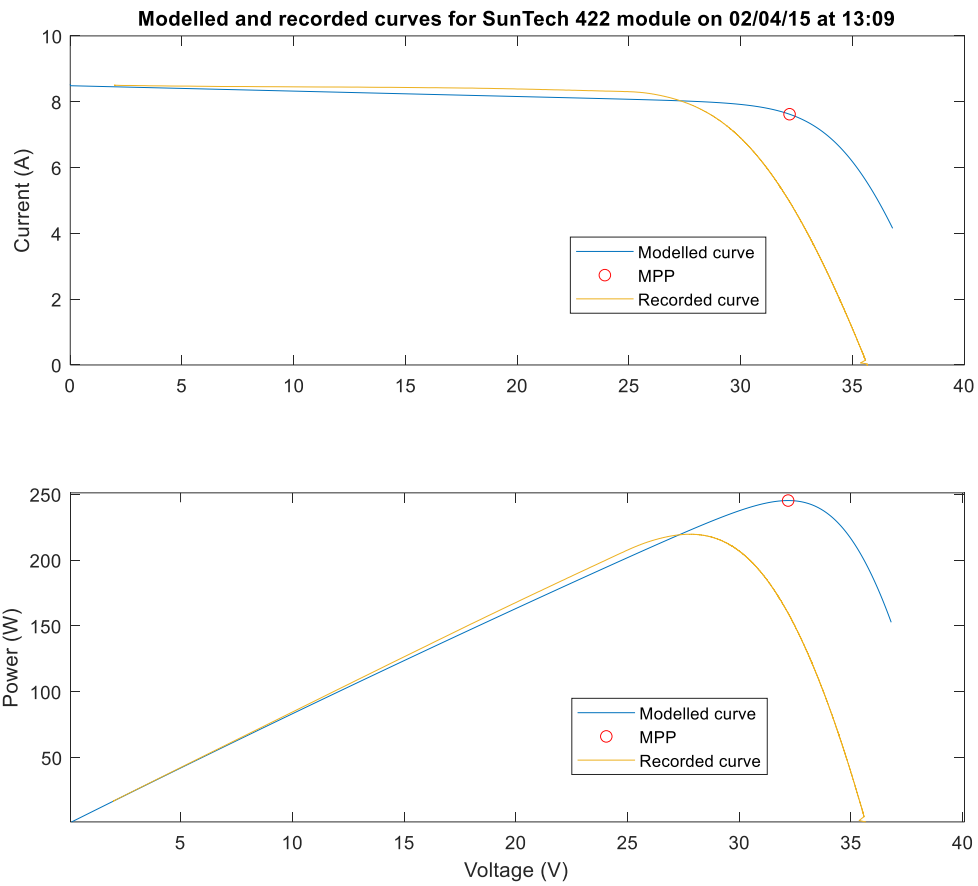
Appendix A.5

PV modules under different snow cover conditions for correlating snow depth and power loss.

22/01/2015 – 09:44

Q.CELLS A10156

19/01/2015 – 11:56

26/03/2015 – 13:10

23/01/2016 – 12:00
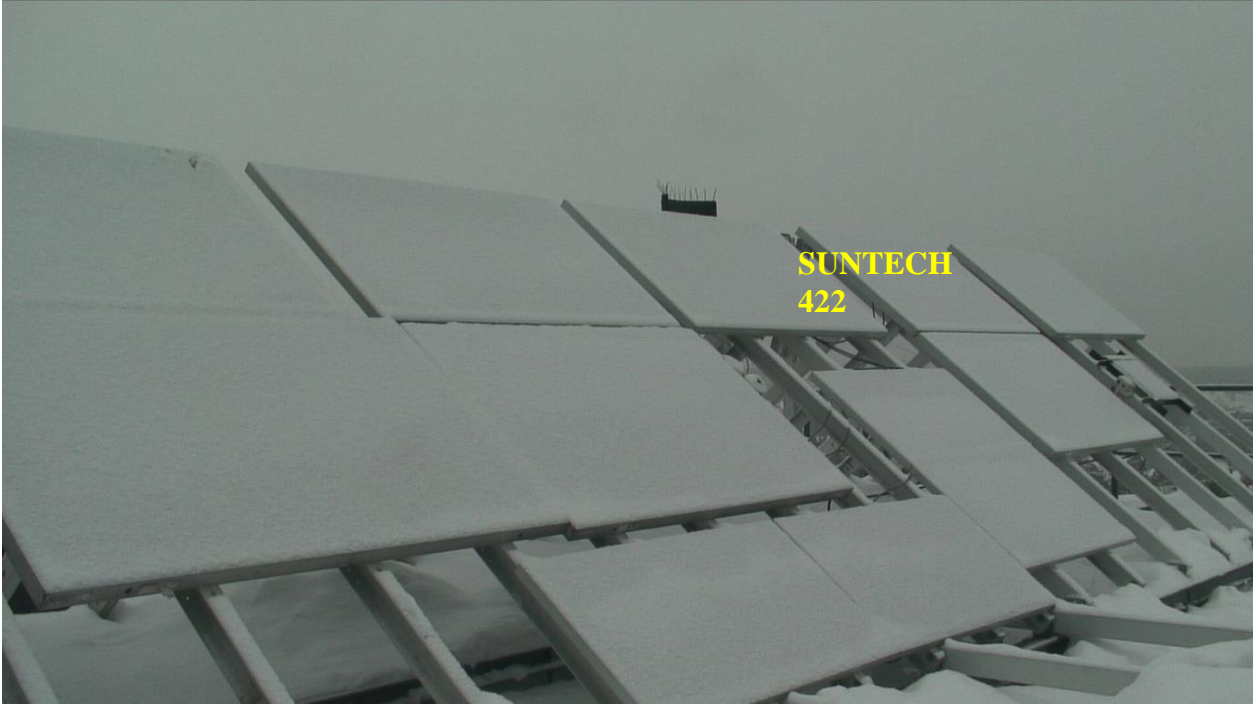
07/03/2016 – 09:00
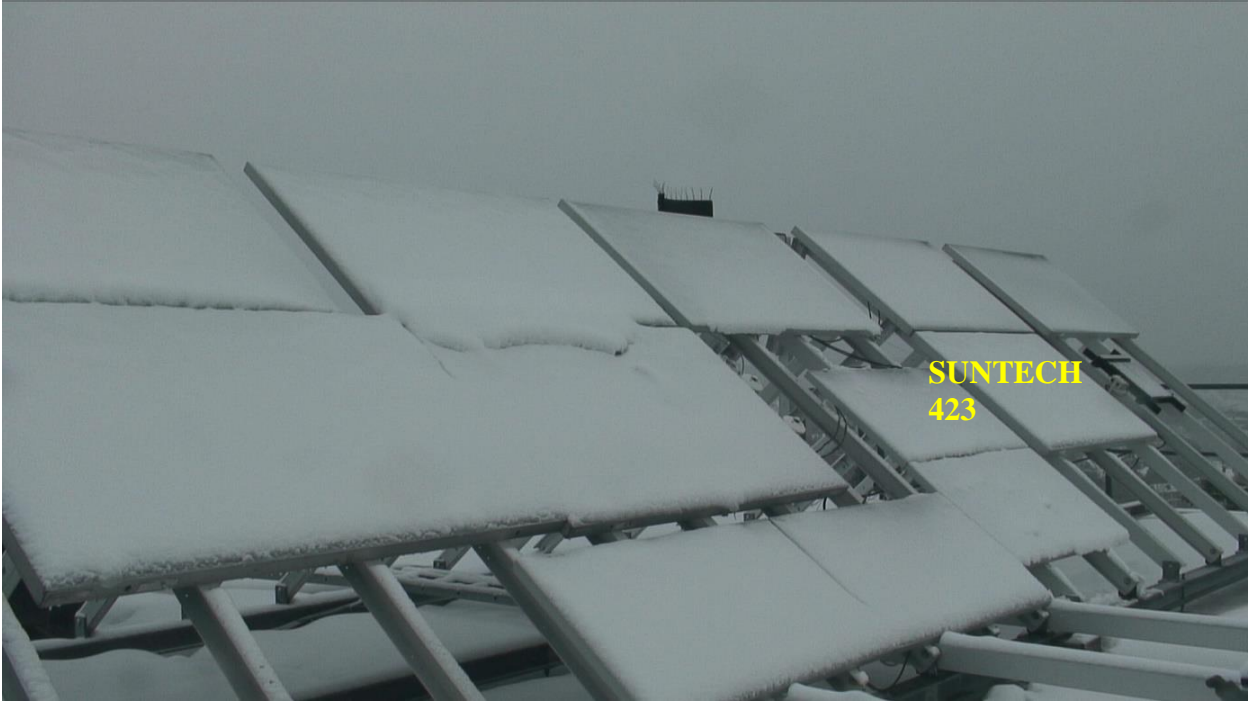
Appendix A.6

Modelling of uniform snow cover, simulated cases.

17/01/2016 – 12:00

11/12/2017 – 14:30. SunTech 433 with 13% irradiance.

11/12/2017 – 14:30. SunTech 433 with 13% irradiance.
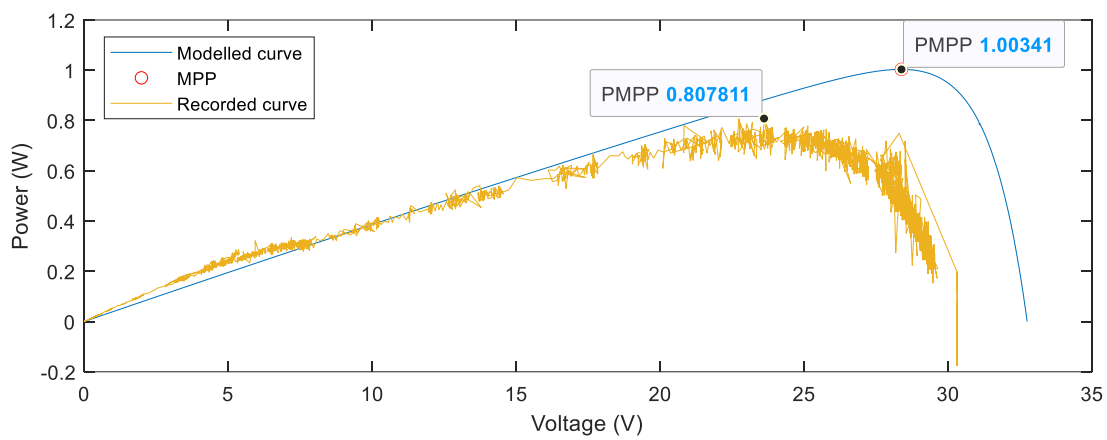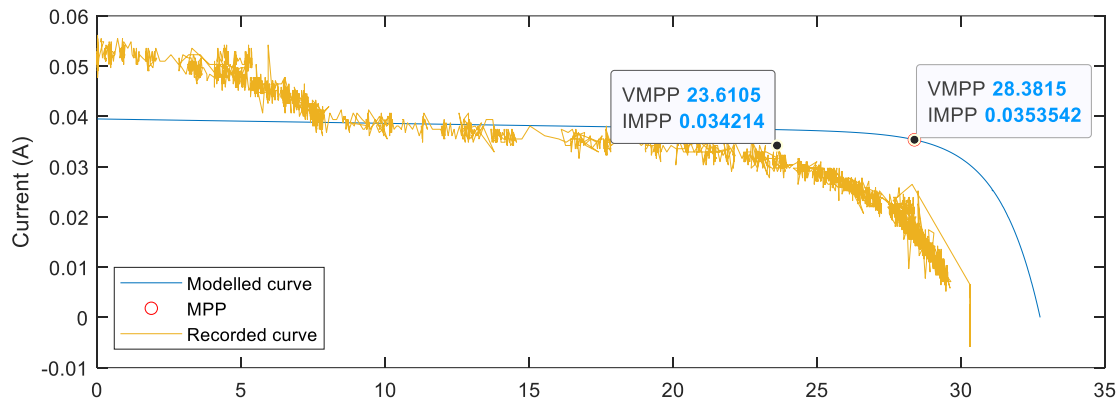
12/12/2017 – 10:00. SunTech 423 with 4% irradiance.

12/12/2017 – 10:00. SunTech 423 with 4% irradiance.
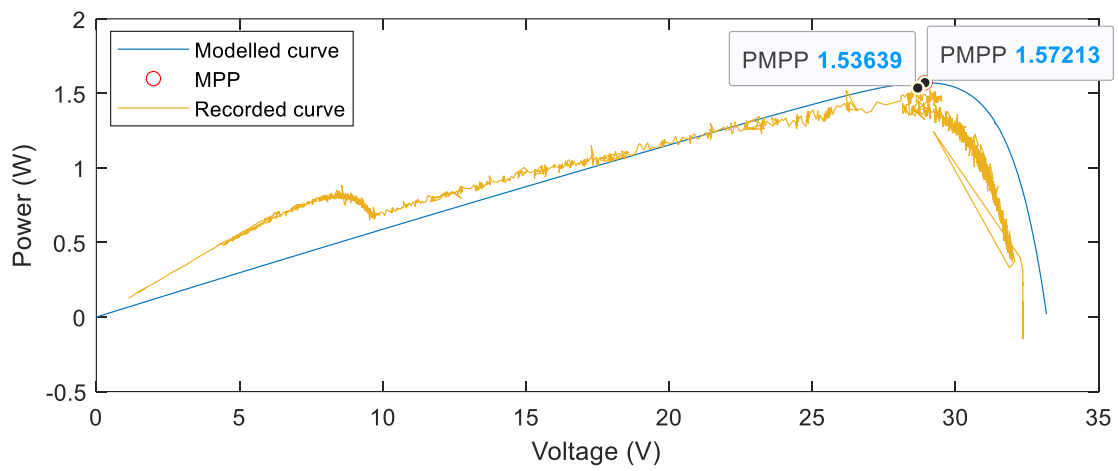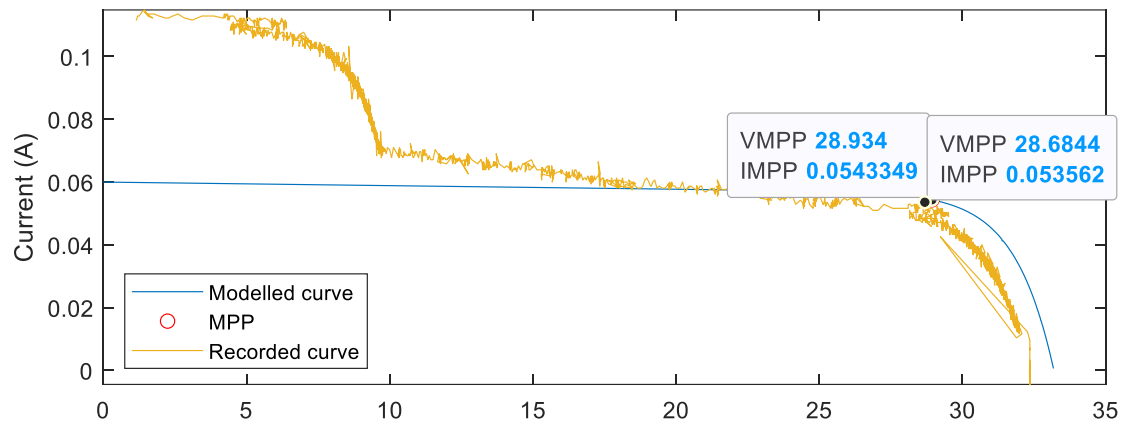
21/01/2015 – 14:20. TITAN with 10% irradiance.

21/01/2015 – 14:20. TITAN with 10% irradiance
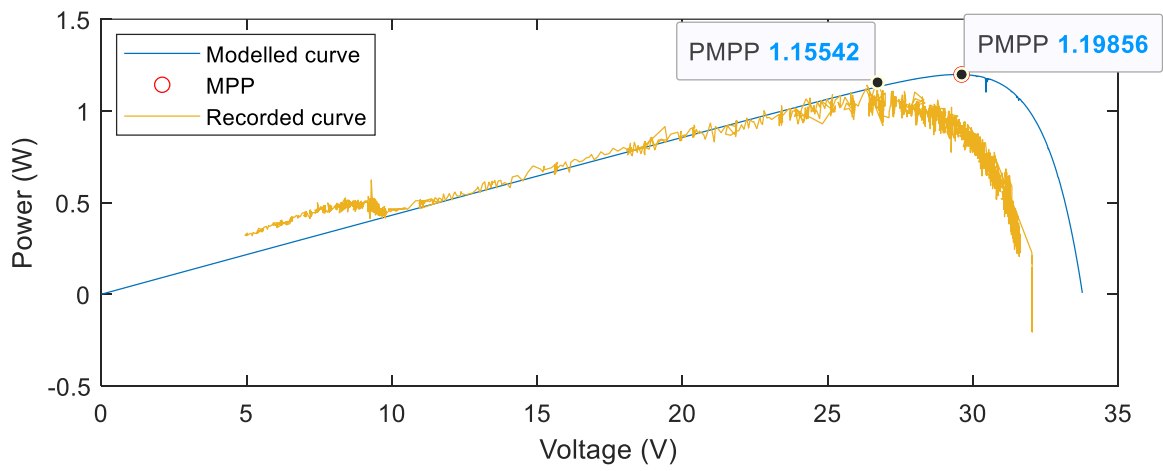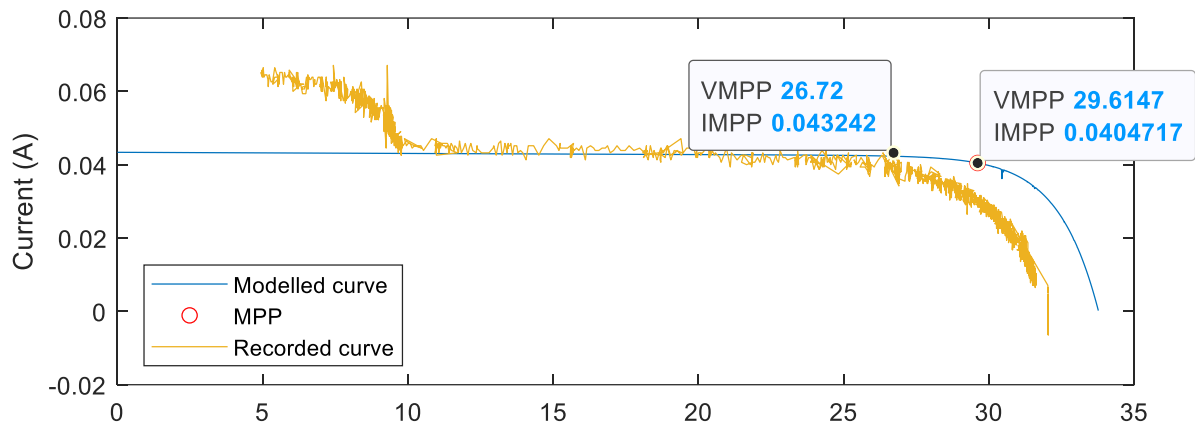
07/03/2016 – 09:40. SunTech 422 with 20% irradiance.

07/03/2016 – 09:40. SunTech 422 with 20% irradiance.
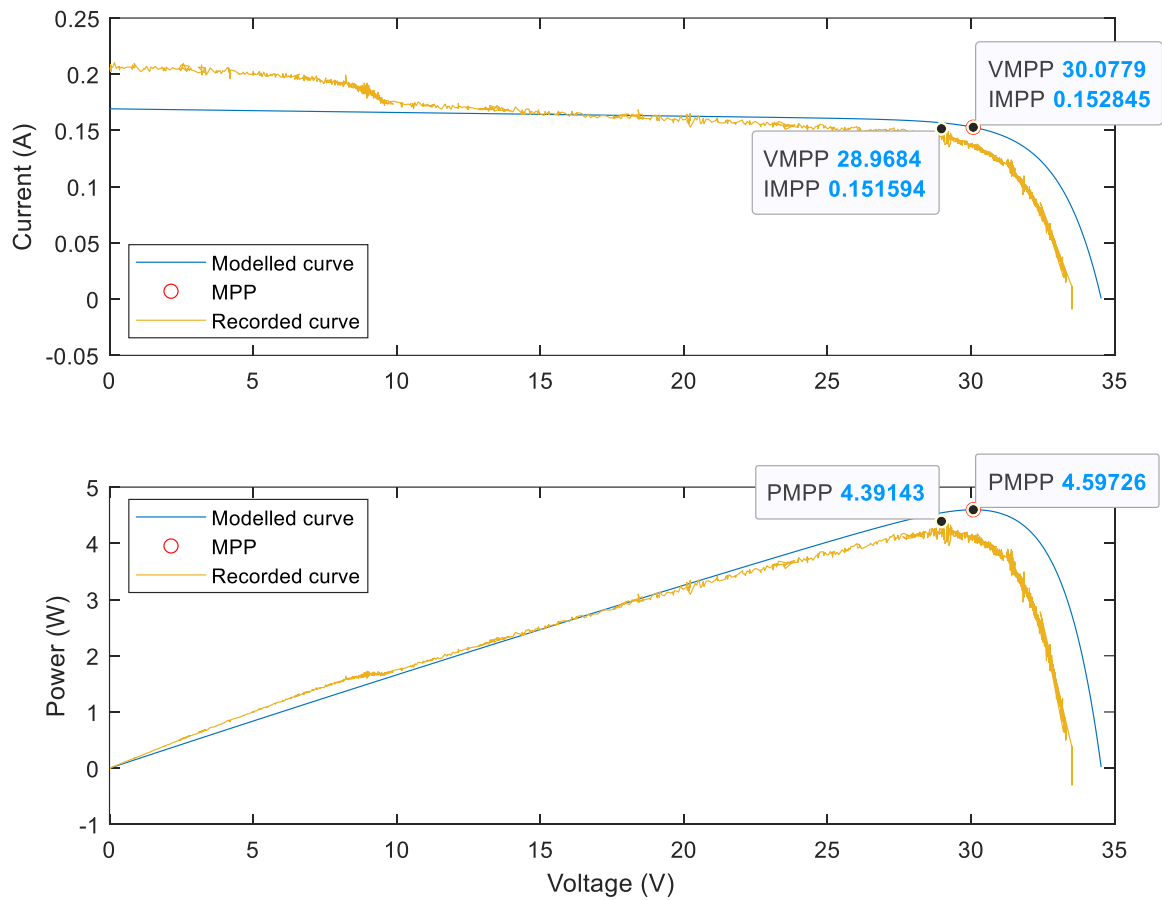
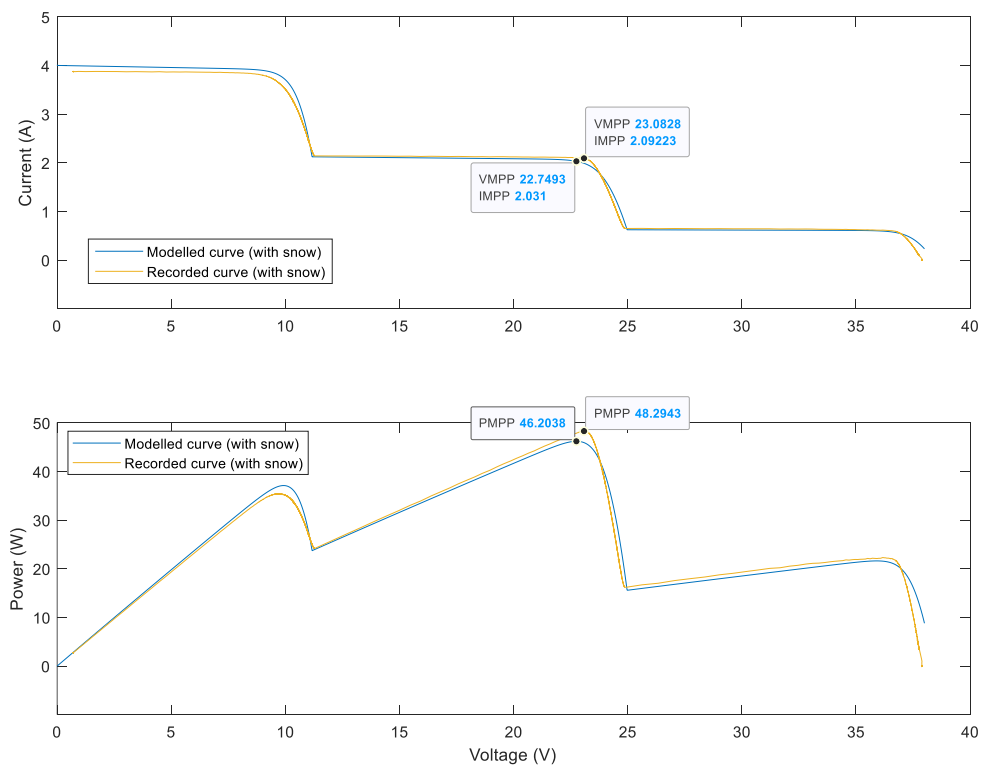03/03/2016 – 08:56. SunTech 433 with 15% irradiance.

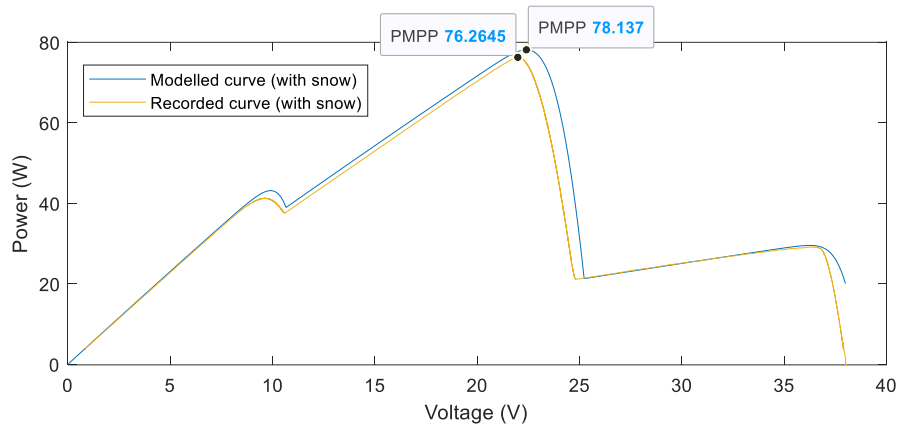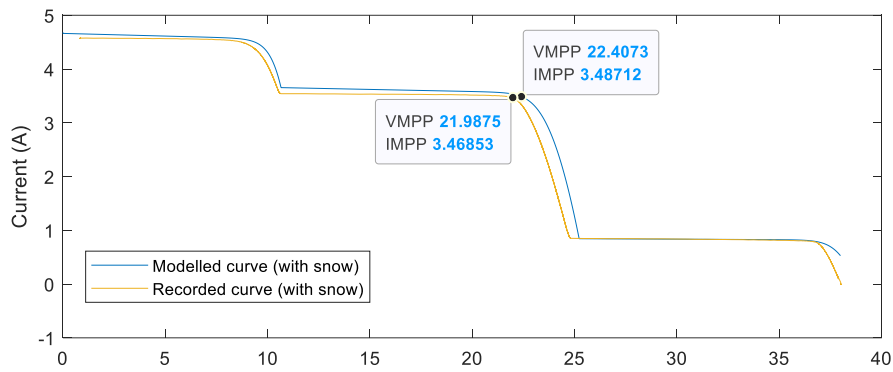03/03/2016 – 08:56. SunTech 433 with 15% irradiance.
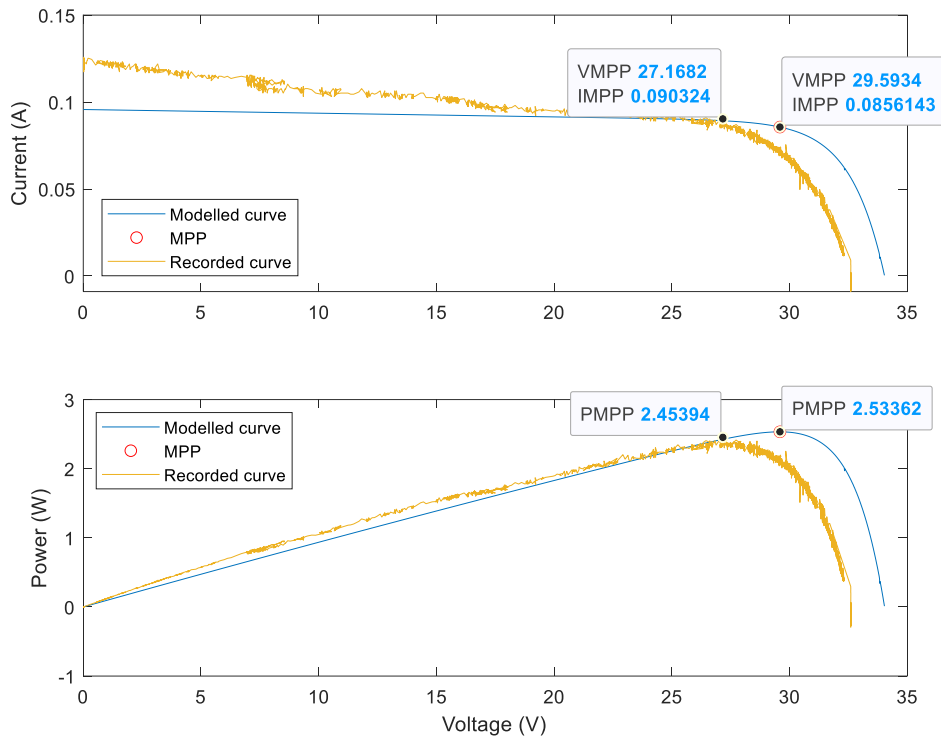
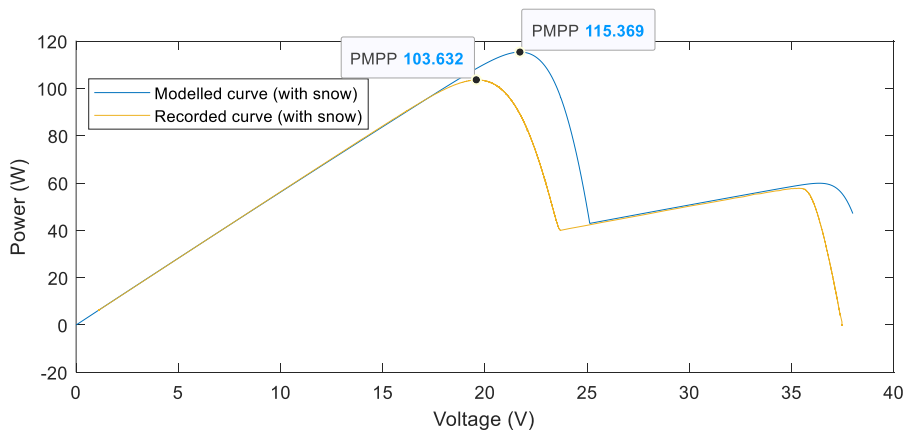**Appendix A.6**

Modelling cases with partial snow cover.
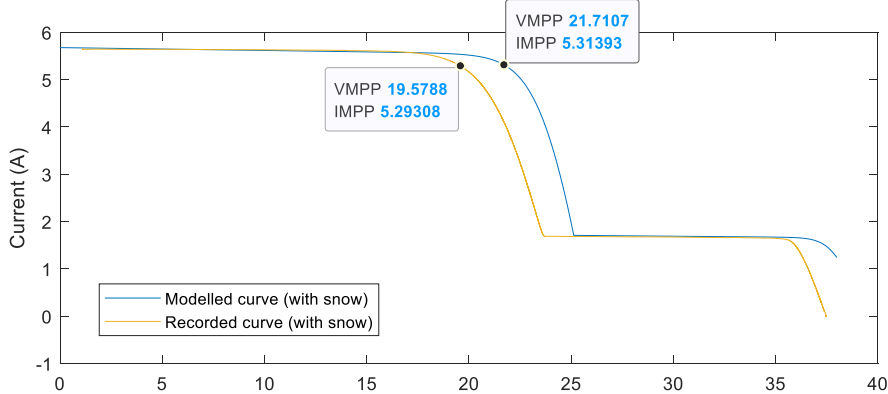
TITAN module 08:16. 2015 27 March

TITAN module 08:39 2015 27. March

TITAN Module 09:21. 2015 27. March

5.12 - Estimating partial snow cover on different PV modules using image analysis.

27/03/2015 – 08:10

23/01/2015 – 10:00

25/04/16 – 13:11

17/01/2016 – 12:42

Appendix A.8

Importing and converting module image.

```
%%Image conversion

I = imread('maskedimage.jpg'); %Read image

HSV = rgb2hsv(I); %Convert to HSV

GR = rgb2gray(HSV); %Convert to Greyscale

BW = imbinarize(GR); %Binarize image

figure
imshowpair(I,BW,'montage') %Plot image
```

Appendix A.9

Applying the created 60-cell mask to estimate snow cover percentage.

```
%%Estimating 60 cell/string based snow cover

I = imread('image15-01-23_10-00-16-29.jpg'); %Read image

%%Load the created 60-cell mask for the relevant PV module

load('BW_60CELLS_MASK_A10156.mat')

%%Apply the mask on the RGB image, and crop image of the PV module

maskedRgbImage = bsxfun(@times, I, cast(BW_60CELLMASK_A10156, 'like', I))

%%Save new image as jpg file.

imwrite(maskedRgbImage, 'maskedimage.jpg')

%%Import the newly cropped and masked RGB format image

I_mask = imread('maskedimage.jpg')

HSV_mask = rgb2hsv(I_mask); %Convert to HSV

GR_mask = rgb2gray(HSV_mask); %Convert to Greyscale

BW_mask = imbinarize(GR_mask); %Binarize image

%%Plotting the original and binarized image side by side.
figure
imshowpair(I_mask,BW_mask,'montage') %Plot image
```